Stony Brook University

The role of the transcription machinery in the remodeling of the promoter-proximal nucleosomes in *Saccharomyces cerevisiae*

A Dissertation Presented

by

Michael Tramantano

to

The Graduate School

in Partial Fulfillment of the

Requirements

for the Degree of

Doctor of Philosophy

in

Molecular and Cellular Biology

Stony Brook University

December 2016

Stony Brook University

The Graduate School

Michael Tramantano

We, the dissertation committee for the above candidate for the

Doctor of Philosophy degree, hereby recommend

acceptance of this dissertation.

Ed Luk, Ph.D. – Dissertation Advisor
Assistant Professor of Biochemistry and Cell Biology

Nancy Hollingsworth, Ph.D. – Chairperson of Defense
Distinguished Professor of Biochemistry and Cell Biology

Rolf Sternglanz, Ph.D.
Distinguished Professor Emeritus of Biochemistry and Cell Biology

Bruce Futcher, Ph.D.
Professor of Molecular Genetics and Microbiology

Caryn E. Outten, Ph.D. – Outside Member
Associate Professor of Biochemistry and Molecular Biology
University of South Carolina

This dissertation is accepted by the Graduate School

Charles Taber

Dean of the Graduate School

Abstract of the Dissertation

The role of the transcription machinery in the remodeling of the promoter-proximal nucleosomes in *Saccharomyces cerevisiae*

by

Michael Tramantano

Doctor of Philosophy

in

Molecular and Cellular Biology

Stony Brook University

2016

Approximately 147 base pairs of DNA wraps almost two turns around a protein core comprised of two copies of each H2A, H2B, H3 and H4 histones to form a nucleosome—the fundamental packaging unit of chromatin. In *Saccharomyces cerevisiae,* nucleosomes are organized along the genome in a closely spaced and non-random manner. This compact structure blocks assembly of the transcription machinery and thus is refractory to gene expression. Surrounding the promoters of most genes, a wider nucleosome depleted region (NDR), maintained in part by the activities of chromatin remodelers, serves as the platform for assembly of the transcription preinitiation complex (PIC). The nucleosome immediately downstream of the NDR, termed +1, covers the transcription start site (TSS) and is frequently assembled with the histone variant H2A.Z instead of H2A. The histones at the +1 nucleosome position turnover rapidly at both actively and infrequently transcribed genes, suggesting constitutive chromatin remodeling allows the PIC to engage the TSS. We hypothesize that the

H2A.Z nucleosome is recognized for disassembly to facilitate a rapid transcriptional response. The mechanism by which the +1 H2A.Z nucleosomes are removed is the central focus of my thesis.

Previous studies suggested that the PIC assembles immediately upstream of the +1 H2A.Z nucleosome. This idea led to the hypothesis that the transcription machinery itself functions as a chromatin remodeler that is responsible for ejecting the +1 nucleosome. To understand the contribution of the transcription machinery in the disassembly of the +1 H2A.Z nucleosome, I used conditional mutants to block PIC assembly. A quantitative ChIP-seq approach was developed that allows for detection of changes in global histone occupancy in order to measure H2A.Z levels genome-wide. Blocking PIC assembly resulted in the promoter-specific accumulation of H2A.Z at both active and infrequently transcribed genes, indicating the PIC is required for H2A.Z eviction. Previous reports have suggested that the ATP-dependent remodeling complex INO80 could play a role in H2A.Z eviction. However, I observed no change in global H2A.Z levels upon depletion of INO80. These findings suggest that the assembly of the PIC and/or its activity is required for the constitutive turnover of +1 H2A.Z nucleosomes.

Dedication Page

I dedicate this dissertation to my wife and parents for their constant support and unconditional love. Without them I would not be where I am today.

Table of Contents

List of Figures

List of Tables

List of Abbreviations

Δ(Z/A)	Δ(H2A.Z/H2A)
ΔA	ΔH2A.Z
ΔZ	ΔH2A.Z
1-NA-PP1	1-Naphthyl-PP1
A/T	adenine/thymine
AA	H2A/H2A nucleosome
Ac	acetyl
as	analog sensitive
Asf1	anti-silencing function 1
ATP	adenosine triphosphate
dATP	deoxyadenosine triphosphate
AZ	H2A/H2A.Z nucleosome
Bdf1	bromodomain factor 1
bp	base pairs
$CaCl_2$	calcium chloride
CHD	chromodomain helicase DNA-binding
ChIP	chromatin immunoprecipitation
CIP	calf intensitinal alkaline phosphatase
CPM	counts per million
cryo-EM	cryo-electron microscopy
CTD	C-terminal domain
CUTs	cryptic unstable transcripts
Cy3/5	cyanine 3/5

DAPI	4′,6-diamidino-2-phenylindole
DIC	differential interference contrast optics
DNase I	deoxyribonuclease I
DOC	deoxycholic acid
DTT	dithiothreitol
E. coli	*Escherichia coli*
EDTA	ethylenediamine tetraacetic acid
EGTA	ethylene glycol-bis(β-aminoethyl ether)-N,N,N',N'-tetraacetic acid
EtBr	ethidium bromide
exo	exonuclease
FACT	facilitates chromatin transcription
FRB	FKBP12-rapamycin-binding domain
FT	flow-through
GFP	green fluorescent protein
GTFs	general transcription factors
HEPES	4-(2-hydroxyethyl)-1-piperazineethanesulfonic acid
HFD	histone fold domain
HU	hydroxyurea
KCl	potassium chloride
KOAc	potassium acetate
KOH	potassium hydroxide
MNase	micrococcal nuclease
Mononucleosome	nucleosome monomer
mRNA	messenger RNA
NaCl	sodium chloride

NaN_3	sodium Azide
NaOAc	sodium acetate
Nap1	nucleosome assembly protein 1
NDR	nucleosome depletion region
NET-seq	native elongating transcript sequencing
NP-40	nonidet P-40
NuA4	nucleosome acetyltransferase of H4
OD	optical density
ORF	open reading frame
PAGE	polyacrylamide gel electrophoresis
PBS	phosphate-buffered saline
PCR	polymerase chain reaction
PI	protease inhibitor
PIC	preinitiation complex
PMSF	phenylmethylsulfonyl fluoride
Pol I	RNA Polymerase I
Pol II	RNA Polymerase II
Pol III	RNA Polymerase III
PVDF	polyvinylidene difluoride
qChIP	quantitative chromatin immunoprecipitation
qPCR	quantitative PCR
Rap1	repressor activator protein 1
RAP	rapamycin
RNase	ribonuclease
RP	ribosomal protein

rRNA	ribosomal RNA
RSC	chromatin structure remodeling
SAGA	Spt/Ada/Gcn5 acetyltransferase
SDS	sodium dodecyl sulfate
seq	sequencing
SF2	superfamily 2
SPT	suppressor of Ty
ssDNA	single stranded DNA
SUMO	small ubiquitin-related modifier
SUTs	stable unannotated transcripts
Swc	SWR1 complex subunit
SWI/SNF	SWItch/Sucrose Non-Fermentable
Tafs	TBP-associating factors
TBP	TATA-binding protein
TFIIX	transcription factor II X
tRNA	transfer RNA
TSS	transcription start site
UAS	upstream activation sequence
WT	wild type
YPD	yeast extract-peptone-dextrose
ZZ	H2A.Z/H2A.Z nucleosome

Acknowledgments

I want to take this opportunity to acknowledge the many people who have helped me along my path and made this dissertation achievable. I am overwhelmingly grateful to every one of them for the constant support they gave me throughout my graduate studies.

First and foremost, I want to thank my dissertation advisor Professor Ed Luk. I was very lucky to have Ed as my mentor. He was a patient teacher and taught me all the technical skills I needed to succeed at the bench. Whenever I encountered a problem in the lab he would make time to sit down with me and go over the issues. His advice was always very insightful and without his guidance this Ph.D. would not have been possible. I especially want to thank him for his advice on scientific writing and presenting. He taught me how to present complex scientific ideas to an audience in a way that can be understood by everyone. Ed not only provided me with valuable advice on research but in life as well. I feel honored to be his first student and hope to as great a scientist as him someday.

I also want to thank my committee members: Professor Nancy Hollingsworth, Professor Bruce Futcher, Professor Rolf Sternglanz and Professor Caryn Outten. They donated their time and expertise to make sure my research was focused and headed in a productive direction. I was fortunate enough to have a committee comprised of members with differing expertise and who were all at different stages in their careers. This made for very insightful and helpful discussions during committee meetings. I would especially like to acknowledge Nancy, Rolf and members of the Hollingsworth lab who all provided me with tremendous advice during our joint group meetings.

I would also like to thank the past and present members of the Luk lab: Lu Sun, Christy Au, Chitra Mohan, Daniel Labuz, Lihong Wan, and Karole D'Orazio for all their helpful conversations, both professional and personal. I want to especially acknowledge Lu Sun, Christy Au, Daniel Labuz, Chen Shen, Mindy Chou and Zhimin Liu who helped in generating data for my dissertation and have consented to allow me to use to their contributions. I also want to thank the Molecular and Cellular Biology Program at Stony Brook University, especially Professor Wali Karzai, Carol Juliano and Joann DeLucia-Conlon for being extremely helpful to me throughout my studies.

Lastly, I want to thank my family for their overwhelming love and support. My parents, Charlie and Laura, have provided me with everything I needed to succeed in life. Without their encouragement and support I would not be the person I am today. My brother Marc, who has always been someone I can talk to about anything. Most importantly, I want to recognize my wife Alicia, who is the kindest, most amazing and understanding person in the world. I am eternally grateful for the tremendous love and support she has shown to me throughout my Ph.D. Without her constant belief in me, none of this would have been possible.

Publications

Tramantano M, Sun L, Au C, Labuz D, Liu Z, Chou M, Shen C, Luk E (2016) Constitutive turnover of histone H2A.Z at yeast promoters requires the preinitiation complex. eLife 5: e14243. http://dx.doi.org/10.7554/eLife.14243

Data access:

Tramantano M, Sun L, Au C, Labuz D, Liu Z, Chou M, Shen C, Luk E (2016) Data from: Constitutive turnover of histone H2A.Z at yeast promoters requires the preinitiation complex. Dryad Digital Repository. http://dx.doi.org/10.5061/dryad.dj782

Chapter One: Background

1. Nucleosome and chromatin structure

To fit its DNA inside a nucleus, the genome of a eukaryotic cell is organized into a highly ordered structure called chromatin that consists of DNA, histone proteins and other DNA associating factors. The basic repeating unit of chromatin is the nucleosome, which is comprised of 147 base pairs (bp) of DNA wrapped in ~1.7 left-handed turns around a histone octamer core containing two copies of the H2A, H2B, H3, and H4 histones (Luger et al., 1997). A hierarchy of histone-histone and histone-DNA interactions stabilizes the nucleosome structure (Luger et al., 1997). The octameric histone core consists of two pairs of heterodimers: H3 with H4 and H2A with H2B. Each of these heterodimers is held together through a 'handshake' conformation between the two conserved histone fold domains (HFDs) in the histone pair (**Figures 1-1A** and **1-1B**) (Luger, 2001). The two H3-H4 dimers lie closely within the core of the nucleosome and interact more extensively with each other than the two H2A-H2B dimers to form a disc-like H3-H4 tetramer [designated as $(H3\text{-}H4)_2$] (**Figures 1-1C**). This H3-H4 tetramer is flanked by two H2A-H2B dimers to complete the octamer (**Figure 1-1D**). Within the nucleosome the two H2A-H2B dimers and the $(H3\text{-}H4)_2$ tetramer are organized into a globular structure with twofold symmetry. The symmetry axis that passes through the midpoint of the DNA is termed the nucleosomal dyad (Bowman, 2010) (**Figure 1-1D**). The DNA wrapped around the octamer makes 14 minor groove contacts with the histones, three with each histone pair and additional H3 contacts near the entry-exit sites (Luger, 2001; Luger et al., 1997) (**Figures 1-1E** and **1-1F**).

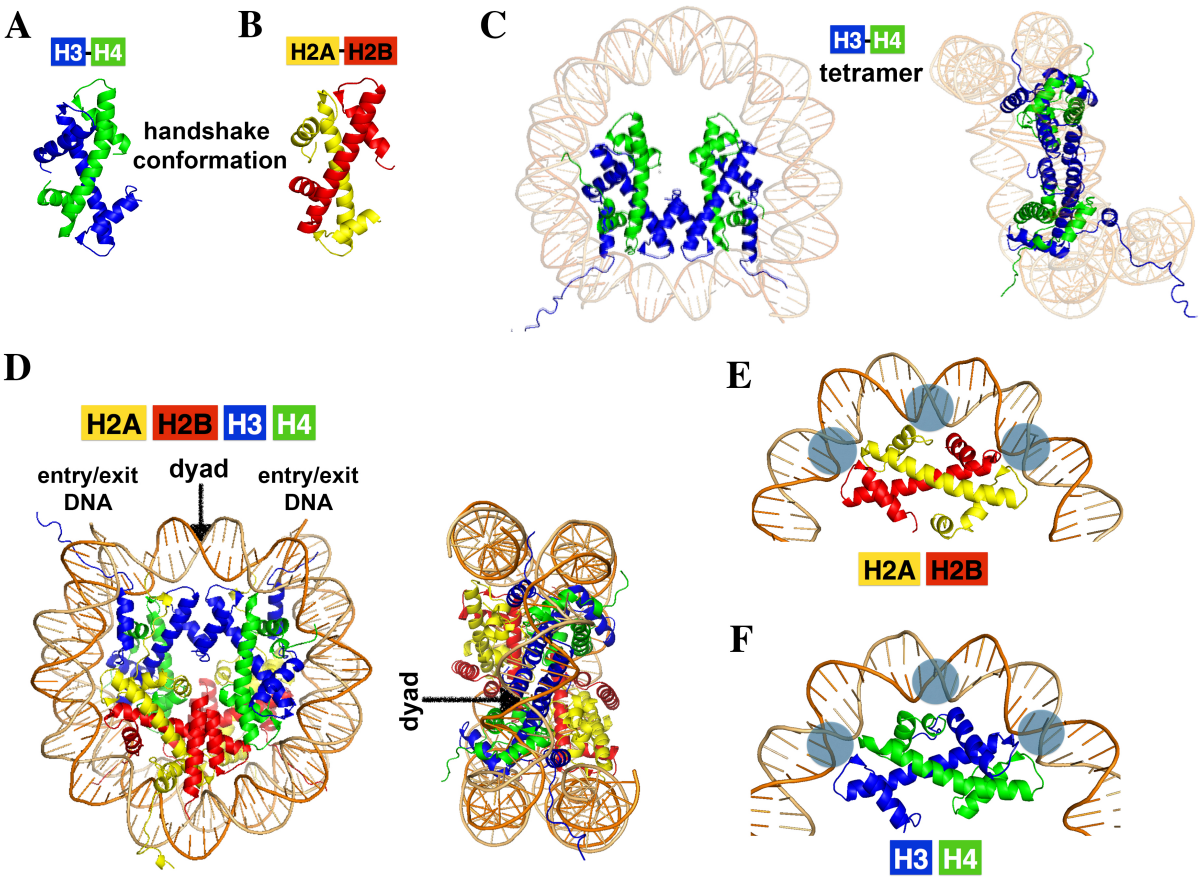

Figure 1-1. **The structure of the nucleosome is stabilized by histone-histone and histone-DNA interactions.** (**A**, **B**) The conserved histone fold domains in the H3-H4 dimer, shown in (**A**), and the H2A-H2B dimer, shown in (**B**), interact to form a handshake motif that stabilizes the structure of the heterodimers. (**C**) Two H3-H4 heterodimers form a four-helix bundle to give rise to an $(H3\text{-}H4)_2$ tetramer. On the right, the structure is rotated to highlight the disc-like shape of $(H3\text{-}H4)_2$. Nucleosomal DNA is shown in the background as a reference. (**D**) The crystal structure of the canonical nucleosome (Luger et al., 1997); entry/exit points of the DNA and the nucleosomal dyad (*black arrow*) are indicated. (**E, F**) Each histone pair makes three minor groove contacts with the nucleosomal DNA (highlighted with *blue circles*), which stabilize the nucleosome structure. The H2A-H2B histone-DNA contacts are shown in **E** and the H3-H4 DNA contacts are shown in **F**. H2A polypeptide is in *yellow*, H2B in *red*, H3 in *blue*, and H4 in *green*. All protein structures were adapted from (Luger et al., 1997).

The formation of chromatin is generally inhibitory to transcription. For example, previous *in vitro* studies have shown that packaging promoter DNA into nucleosomes prevents the binding of RNA Polymerase II (Pol II) and activation of gene expression (Knezetic and Luse, 1986; Lorch et al., 1987). These results suggest that gene expression requires the promoter to be relatively free of nucleosomes and accessible to binding by the transcription machinery. Furthermore, experiments that induced nucleosome loss at yeast promoters *in vivo* led to aberrant gene activation (Han and Grunstein, 1988). Therefore, accurate gene expression is dependent, at least in part, on the formation of a proper chromatin structure that allows for the convergence of the transcription machinery at promoters, while blocking other non-specific sites that could lead to erroneous transcriptional initiation.

2. Eukaryotic transcription and chromatin dynamics

To understand how chromatin structure is remodeled to facilitate gene expression it is first important to look at how the transcription machinery assembles and initiates on naked DNA. For a typical gene, transcription initiation begins with the binding of activators to sequence specific DNA elements called upstream activating sequences (UASs) (Hahn and Young, 2011). The activation domain of the activator then recruits co-activators, such as the mediator complex, which in turn helps recruit the transcription machinery (Allen and Taatjes, 2015; Hahn and Young, 2011) (**Figure 1-2**). After activator and co-activator binding, TATA-binding protein (TBP) is recruited to the promoter and binds through interaction with the minor groove of the TATA or TATA-like element causing the DNA to bend almost 90 degrees (Hahn, 2004; Kim et al., 1993) (**Figure 1-2**). At many promoters, TBP can be found as a component of the

transcription factor IID (TFIID) complex or the Spt/Ada/Gcn5 acetyltransferase (SAGA) complex (Hahn and Young, 2011). The general transcription factors (GTFs) TFIIA, TFIIB, TFIIE, TFIIH, TFIIF and Pol II are then recruited to the promoter forming the mature preinitiation complex (PIC) (Grünberg and Hahn, 2013) (**Figure 1-2**). At this point, the PIC is considered to be in the 'closed' conformation as the promoter DNA remains in the duplex form. The TFIIH DNA translocase subunit, Ssl2, then hydrolyzes ATP or dATP in an attempt to track away from the PIC, but because TFIIH movement is constrained through interaction with other PIC components, this activity results in the twisting and reeling of the downstream DNA into the PIC (Fishburn et al., 2015) . With TBP and the other general transcription factors bound tightly to the DNA at one end of the promoter and TFIIH twisting DNA at the other, the DNA unwinds or melts within the PIC creating a ~15 bp 'bubble' (Grünberg et al., 2012) (**Figure 1-2**). The single-stranded DNA template strand descends into the activation cleft of Pol II leading to the formation of the 'open complex' (Murakami et al., 2013) (**Figure 1-2**). More recent evidence suggests that the yeast open complex scans the template DNA for the transcription start site (TSS) and further scrunches up as much as 85 bp of DNA inside the open complex before committing to elongation (Fazal et al., 2015). After open complex formation the kinase domain of TFIIH phosphorylates the C-terminal domain (CTD) of Pol II resulting in promoter escape and productive elongation (Wong et al., 2014) (**Figure 1-2**). Upon promoter escape the elongating polymerase sheds most of the transcription factors required for initiation.

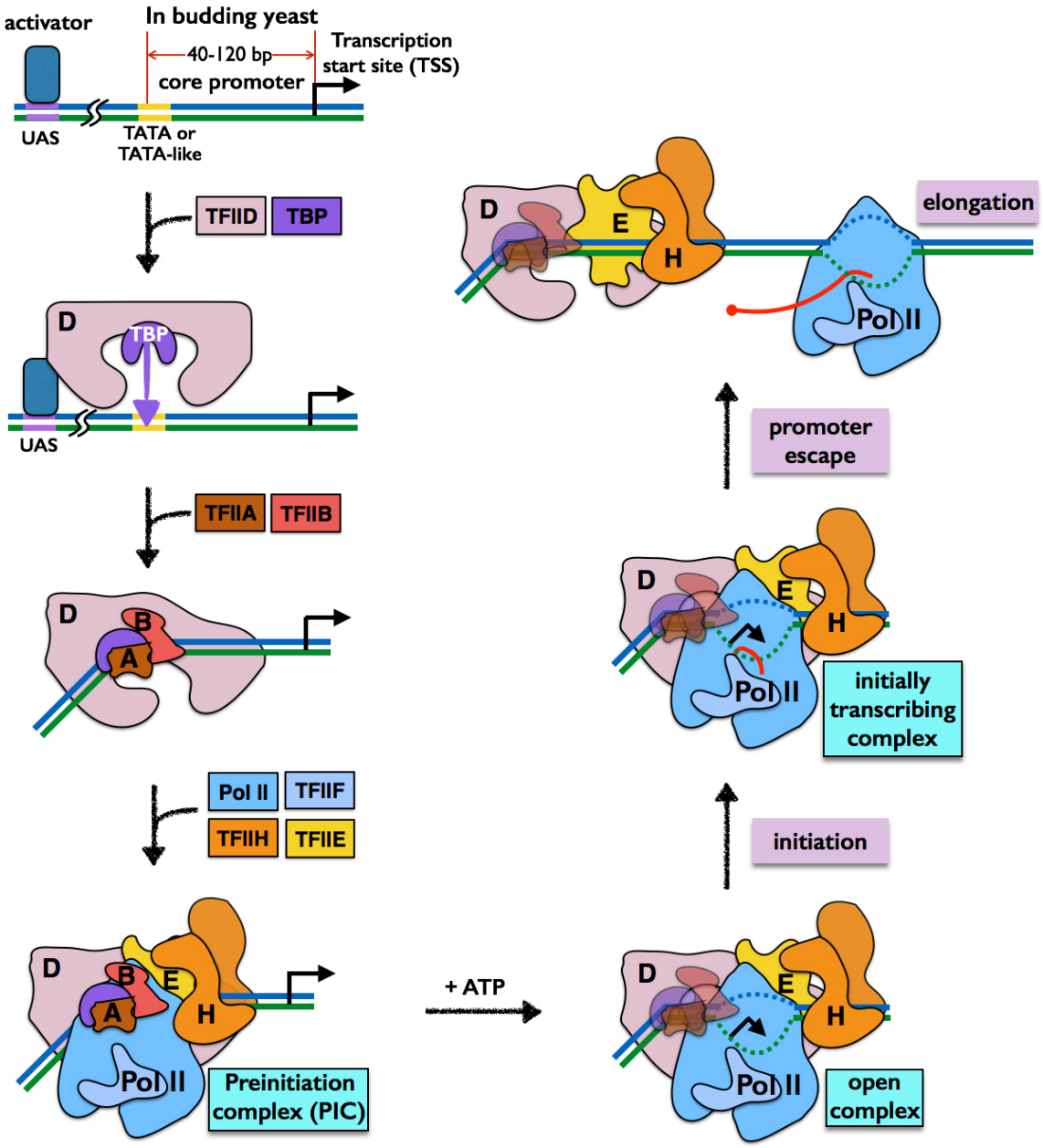

Figure 1-2. Assembly of the preinitiation complex (PIC) and promoter opening during transcription initiation. Depicted is a schematic representation of the stepwise model for the assembly of the PIC and transcription initiation. The *green* and *blue lines* represent the template strand and coding strand, respectively. The *purple region* of the promoter is the upstream activating sequence (UAS), which is bound by the transcriptional activator, and the *yellow region* is the TATA element, which is bound by TBP (shown in a complex with TFIID). In budding yeast, the TATA element is located 40 – 120 bp upstream of the transcription start site (*bent black arrows*). After PIC assembly, TFIIH hydrolyzes ATP to form the open complex. Nascent RNA is indicated as a *red line*. When the nascent RNA chain reaches ~10 – 15 nucleotides, Pol II leaves behind the general transcription factors and enters elongation (Hahn and Young, 2011). Structure of the PIC is modeled from (Murakami et al., 2013). ATP: adenosine triphosphate; Pol II: RNA Polymerase II; UAS: upstream activating sequence.

Transcription in eukaryotes, however, does not occur on naked DNA but in the presence of chromatin. Previous *in vitro* experiments have demonstrated that the wrapping of promoter DNA around histones in a nucleosome inhibits initiation of transcription by preventing transcription factors and Pol II from accessing the DNA (Knezetic and Luse, 1986; Lorch et al., 1987; Williamson and Felsenfeld, 1978). Therefore, chromatin must be remodeled to allow for the assembly of the PIC at promoters and initiation of transcription (**Figure 1-3**).

One way in which the chromatin architecture is modified to allow transcription factors to access genomic DNA is by eviction of histones from the nucleosome (**Figure 1-3A**). In fact, the chromatin in and around the promoters in yeast is highly dynamic in that the histones are reversibly taken apart during gene activation and reassembled during gene repression (Rando and Winston, 2012). This type of histone remodeling process can be catalyzed by ATP-dependent chromatin remodelers that are known to disrupt histone-DNA contacts within the nucleosome and unwrap the DNA from the octamer (Cairns, 2007). The disassembly process can occur in distinct stages leading to the formation of sub-nucleosomal structures that do not contain all eight histone proteins (Rhee et al., 2014; Saha et al., 2006) (**Figure 1-3A**). Since the H2A-H2B dimers are located near the outside of the nucleosome (**Figure 1-1D**), DNA unwrapping is predicted to destabilize the flanking H2A-H2B dimers first (Luger et al., 1997). Further unwrapping removes the $(H3\text{-}H4)_2$ tetramer, leading to complete disassembly of the nucleosome (**Figure 1-3A**).

Another way for transcription factors to access the DNA is by repositioning the histone octamer from one genomic location to an adjacent position in a process called sliding (Clapier and Cairns, 2009) (**Figure 1-3B**). Similar to eviction, the sliding of histones exposes DNA sites that were previously occluded within the nucleosome (**Figure 1-3B**). This type of remodeling is

facilitated by ATP-dependent remodelers that can catalyze the regulated disruption and reformation of histone-DNA contacts, thereby propagating the DNA along the histone octamer and effectively changing the position of the octamer on the DNA while leaving the histone core intact (Bowman, 2010; Narlikar et al., 2013).

In addition, nucleosomes can be remodeled by the replacement of canonical histones with histone variants (Weber and Henikoff, 2014) (**Figure 1-3C**). This histone exchange reaction involves the targeted removal of a histone pair within a nucleosome or complete disassembly of the nucleosome followed by the insertion of the variant histone or reassembly of the nucleosome with the variant (**Figure 1-3C**). Histone variants are expressed constitutively throughout the cell cycle and incorporated into nucleosomes in a replication-independent manner (Weber and Henikoff, 2014). The incorporation of histone variants can alter the biophysical properties of the nucleosome and each histone variant is typically linked with a specific biological process (Venkatesh and Workman, 2015). However, exactly how histone exchange facilitates transcription is controversial (see below).

Finally, the covalent attachment of chemical moieties (such as acetyl, methyl, and phosphate groups) or small proteins (such as ubiquitin and the SUMO protein) onto histones by histone modifying enzymes can have a major impact on transcriptional regulation (Bannister and Kouzarides, 2011; Nathan et al., 2006). These modifications are reversible and can influence transcription through two major mechanisms: 1) the disruption of the histone-DNA / histone-histone contacts leading to a change in nucleosome stability and/or 2) the recruitment of chromatin remodelers or transcription factors to the nucleosome bearing the modifications (Kouzarides, 2007). For example, the addition of acetyl (Ac) groups can neutralize the positive charge of the histone, thereby destabilizing the histone-DNA interaction (Li et al., 2007). One

such modification is H3K56Ac which is present at promoters and destabilizes nucleosomes to facilitate histone turnover (Neumann et al., 2009; Rufiange et al., 2007; Venkatesh and Workman, 2015). In addition, some transcription factors and chromatin remodelers contain bromodomain modules that can recognize and bind to histone acetylation marks. During gene activation, acetylation of promoter nucleosomes helps to recruit and stabilize the transcription machinery (Jiang and Pugh, 2009a).

Transcription can also be regulated by histone chaperones, which are highly acidic proteins that can bind to and store free histones (Venkatesh and Workman, 2015). Histone chaperones act as chromatin architects and regulate transcription by facilitating nucleosome assembly, histone eviction, and histone exchange. For example, the promoter specific acetylation of H3K56 by the Rtt109 histone acetyltransferase requires the histone chaperone Asf1 (Rando and Winston, 2012). In addition, the histone chaperones FACT and Spt6 interact with Pol II and are responsible for altering the nucleosome structure to facilitate passage of Pol II during elongation and reassembling the nucleosome in its wake (Belotserkovskaya et al., 2003; Rando and Winston, 2012).

Collectively, these so-called chromatin remodeling activities can dramatically alter the chromatin architecture and play major roles in the regulation of transcription. This study focuses on what contributions the transcription machinery itself has on the dynamic chromatin remodeling processes at the promoter.

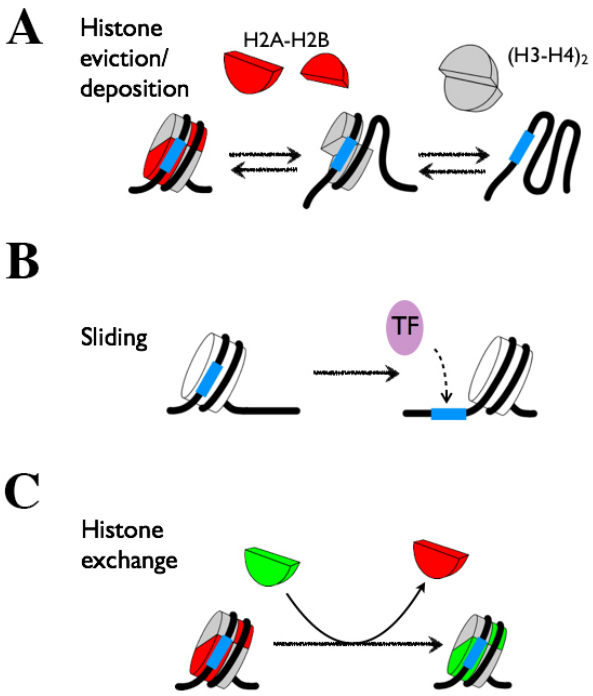

Figure 1-3. ATP-dependent remodelers can modify chromatin structure in multiple ways to expose or cover DNA regulatory elements. (**A**) Remodelers evict histone pairs from the nucleosome to uncover transcription factor (TF) binding sites on the DNA, indicated in *blue.* Reversely, remodelers can cover binding sites by depositing histones onto the DNA during nucleosome assembly. (**B**) Remodelers slide nucleosomes and thus reposition the histone octamer on the genome. Depending on the direction of sliding, this can expose or cover DNA sequence elements. (**C**) Remodelers replace canonical histones in the nucleosome with variant histones. H2A-H2B dimers are shown as *red half circles*, $(H3\text{-}H4)_2$ tetramers as two *gray half circles*, and histone variant dimers as *green half circles*. Transcription factor is shown as a *purple oval.* TF: transcription factor

3. Genomic approaches used to study chromatin organization in yeast

To better understand gene regulation, we need to understand how nucleosomes are organized around the promoter and identify sites of high histone dynamics. Two common approaches have been used to understand chromatin organization and dynamics in eukaryotes: micrococcal nuclease (MNase)-seq (**Figure 1-4**) and chromatin immunoprecipitation (ChIP)-seq. These approaches take advantage of the fact that nucleosomal DNA is more resistant to digestion by endonucleases, such as DNase I and MNase, than the naked DNA found at linker regions (i.e. the stretch of DNA between two nucleosomes) (Hughes and Rando, 2014). MNase in particular has been widely used for determining nucleosome position and occupancy because of its strong preference for linker DNA over nucleosomal DNA (Zhang and Pugh, 2011) (**Figure 1-4A**). As a result, intact nucleosome monomers (or mononucleosomes) with well-defined DNA length, corresponding to the regions wrapped around the octameric histone core, can be extracted after controlled MNase digestion (**Figure 1-4A**). When the associating DNA of a collection of mononucleosomes is extracted and the sequence information of the DNA fragments is mapped by genomic approaches, such as tiling microarrays or deep sequencing, the coverage/counts of the DNA reads can be used to infer nucleosome position and occupancy (i.e. nucleosomal density) (Lieleg et al., 2014) (**Figure 1-4B**). In addition, when this technique is used in combination with chromatin immunoprecipitation (ChIP), it can be used to determine the occupancy and position of a particular histone modification or histone variant along the genome (Zhang and Pugh, 2011). Specifically, this approach requires the use of an antibody directed against a specific histone mark on the MNase generated mononucleosomes, thereby enriching for the associated DNA that will subsequently be quantified by microarrays or deep sequencing (Lieleg et al., 2015).

The budding yeast, *Saccharomyces cerevisiae,* is an ideal model organism to study chromatin regulation for several reasons. First, yeast culture is quite homogenous when compared to other cell lines (Zhang and Pugh, 2011). This fact means that the genomic information generated from a population of cells is representative of the organism. As such, the mononucleosomal DNA fragments from individual cells contribute collectively to generate sequencing data that can be amplified into patterns along the genome. By contrast, these patterns may be obscured in a heterogeneous cell mixture because nucleosome position and occupancy may vary drastically from cell to cell. Second, the relatively small genome size means that a specific number of deep sequencing reads can cover the same genomic region more times in yeast than in other model organisms with larger genomes. The more times the same region is covered the "deeper" the sequencing and more reliable the data. Third, yeast has only two copies of the canonical histone genes and one copy of each histone variant gene (Eriksson et al., 2012; Talbert and Henikoff, 2010). By contrast, mammals have 10-20 genes encoding each of the core histone proteins (Marzluff et al., 2002). Therefore, it is simpler to mutate or tag specific histone genes in yeast than it is in higher eukaryotes. Lastly, many powerful tools are available for genetic manipulation in yeast. In particular, there are several strategies for conditionally inactivating a target gene (Haruki et al., 2008; Nishimura and Kanemaki, 2014). Given that many chromatin regulators are required for viability, the ability to generate conditional depletion mutants is invaluable for the study of chromatin remodeling processes.

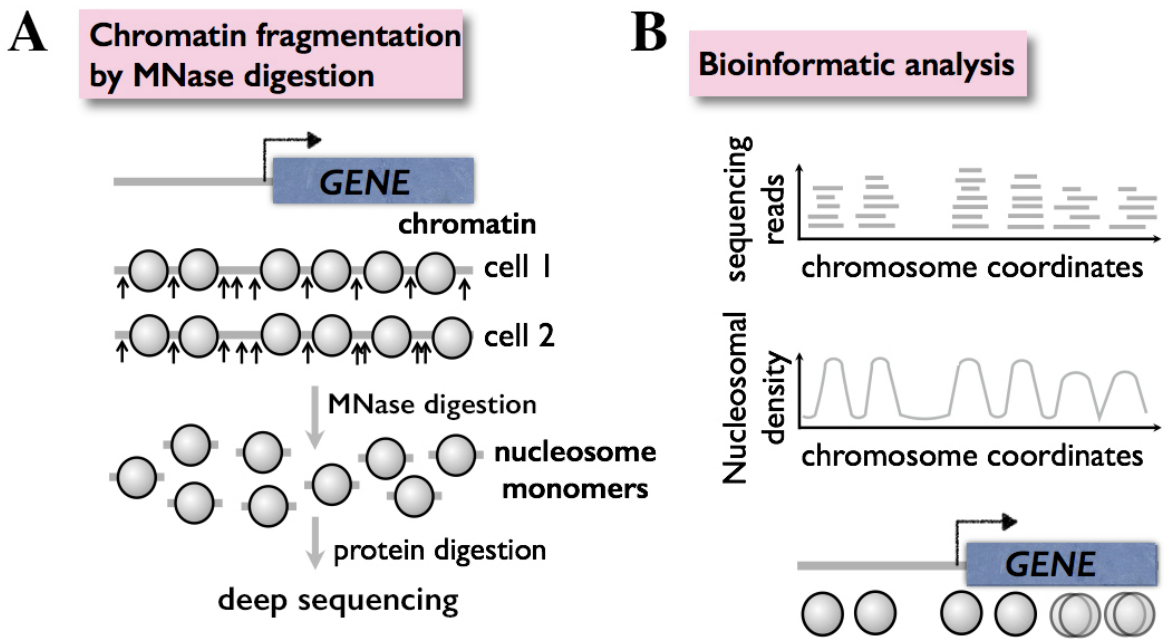

Figure 1-4. Overview of MNase-seq technique. Micrococcal nuclease (MNase)-seq data provides population averages from a large number of cells to determine chromatin organization genome-wide. (**A**) Chromatin is prepared from cells that have been fixed with formaldehyde, which will freeze the existing protein-protein and protein-DNA interactions and preserve the *in vivo* chromatin state (Zhang and Pugh, 2011). Chromatin is then fragmented with MNase, which will preferentially digest the linker DNA between nucleosomes, to release nucleosome monomers (or mononucleosomes). The histones are digested and the associating DNA is then mapped by deep sequencing. (**B**) Bioinformatics is used to infer nucleosome density from the mapped sequencing reads. Genomic areas with high nucleosomal density will have a greater number of sequencing reads and vice-versa. The *gray line* and *blue-gray rectangle* represent the promoter DNA and open reading frame of the gene, respectively. The *large black arrow* in front of the *GENE* indicates the transcription start site. Gray circles represent nucleosomes. *Small black arrows* indicate the preferentially cut sites for MNase digestion.

4. Chromatin architecture in and around yeast promoters

Previous genome-wide studies in yeast have led to several major conclusions. First, nucleosomes are organized in a non-random fashion along the yeast genome (Yuan et al., 2005). For example, nucleosomes are tightly packed within the gene coding regions forming uniformly spaced nucleosomal arrays, with an average linker length of ~20 bp (Lee et al., 2007; Mavrich et al., 2008). By contrast, nucleosome spacing at regulatory regions such as promoters, replication origins, and enhancers is much wider (Eaton et al., 2010; Heintzman et al., 2007; Yuan et al., 2005) (**Figure 1-5A**). These nucleosome depleted regions or NDRs are also known as hypersensitivity sites as they are highly prone to nuclease digestion (Almer and Hörz, 1986; Wu, 1980). Formation of the chromatin array structure, as well as the NDRs, is dependent on both intrinsic DNA sequence and enzymatic activities, discussed below.

Second, a strongly positioned nucleosome, called the +1 nucleosome, is generally associated with the start of most genes (Jiang and Pugh, 2009b). Strong positioning means the +1 nucleosome is consistently present at the same genomic location in a population of cells. At promoters, the +1 nucleosome is defined as the nucleosome immediately downstream of the TSS (Albert et al., 2007; Mavrich et al., 2008) (**Figure 1-5**). For most genes, an 80-200 bp NDR is present upstream of the +1 nucleosome. Since the TSS is usually located 10-15 bp inside the promoter-proximal edge of the +1 nucleosome, this structure is expected to prevent the transcription machinery from engaging the TSS (Jiang and Pugh, 2009b). Therefore, disassembly of the +1 nucleosome likely represents an important molecular step in transcriptional regulation. The +1 nucleosome is also enriched for specific histone modifications, such as H3K56Ac, and the histone variant H2A.Z (Li et al., 2007; Raisner et al., 2005) (**Figure 1-5**). Both of these nucleosome modifications are associated with chromatin sites

with fast histone turnover and have been implicated in facilitating disassembly of the +1 nucleosome *in vivo* (Rufiange et al., 2007; Zhang et al., 2005).

Finally, signals from nucleosomes located downstream of the +1 nucleosome are progressively fuzzier, meaning these nucleosomes have more variable positioning within a cell population and/or that there is a lower histone density at these locations. One hypothesis for this phenomenon, called statistical positioning, is that the strongly positioned +1 nucleosome acts as a reference and forms a barrier against which subsequent nucleosomes are packed, resulting in a uniform positioning that decays at farther distances (**Figure 1-5**) (Mavrich et al., 2008).

While the majority of genes in yeast have the 'stereotypical' chromatin architecture described above, there is considerable variability in the organization of nucleosomes among genes. In fact, the chromatin architecture at yeast promoters can be subdivided into two broad classes: open promoters and covered promoters (Hughes and Rando, 2014) (**Figure 1-5**). Open promoters are typically associated with housekeeping genes (~80% of protein-coding genes), such as the ribosomal protein (RP) genes (Rando and Winston, 2012). These genes are regulated by TFIID, have promoters that contain a well-defined NDR and do not contain a strong consensus TATA box (Basehoar et al., 2004; Newman et al., 2006) (**Figure 1-5A**). By contrast, covered promoters are associated with stress responsive genes (~20% of protein-coding genes), such as the *PHO5* and *GAL1-10* genes, which are typically transcribed at low levels and induced in response to various growth and stress conditions. These genes are regulated by the Spt/Ada/Gcn5 acetyltransferase (SAGA) complex, characterized by "bursty" expression and contain a strong consensus TATA sequence (Rando and Winston, 2012) (**Figure 1-5B**). Since the chromatin structure at covered promoters is not as nucleosome depleted as open promoters they tend to be more dependent on chromatin remodeling activities (Rando and Winston, 2012).

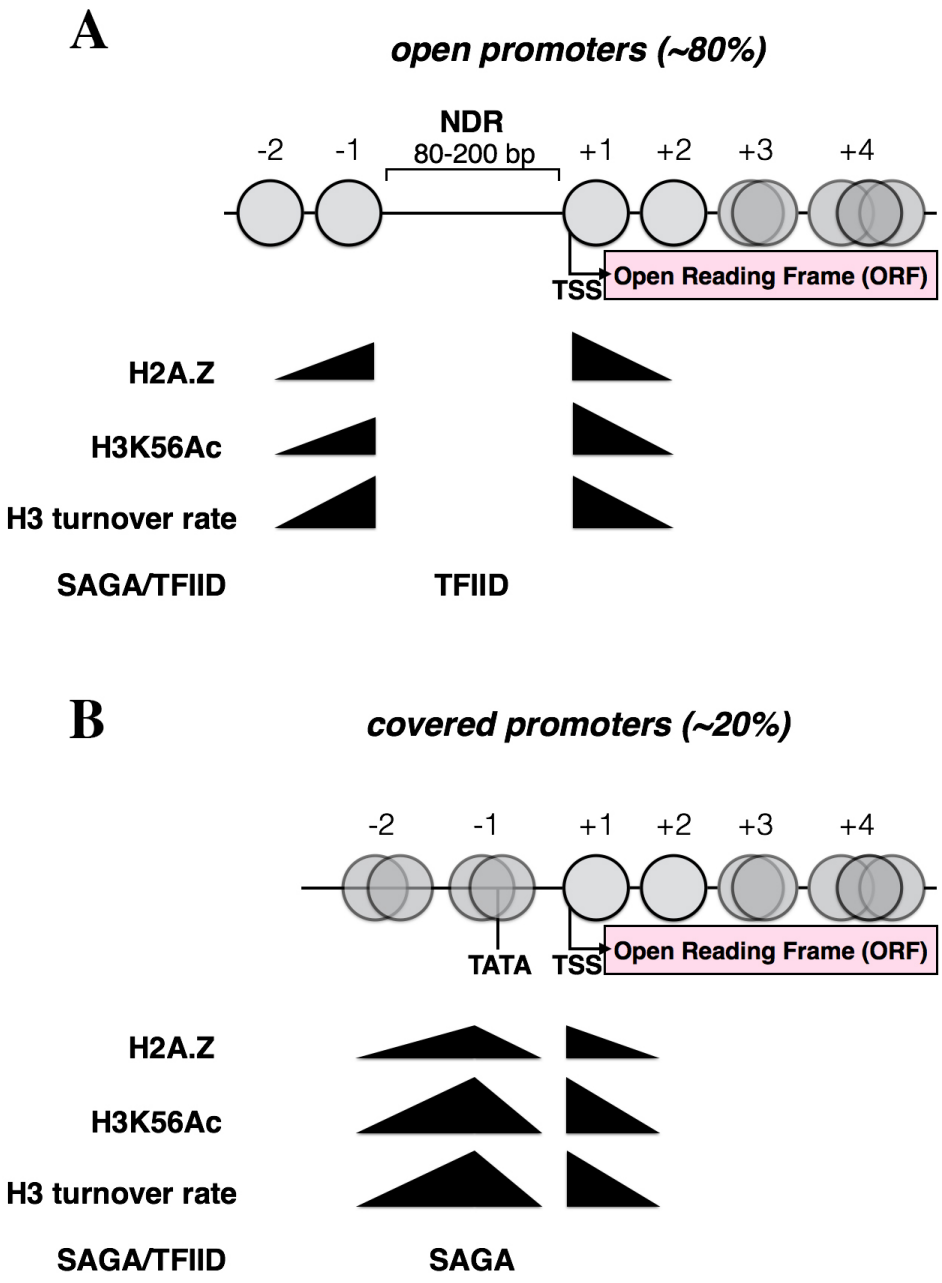

Figure 1-5. Chromatin architecture at budding yeast promoters. The chromatin structure of open promoters, shown in (**A**), and covered promoters, shown in (**B**), which represent ~80% and ~20% of protein-coding genes, respectively (Rando and Winston, 2012). Gray circles represent nucleosomes. The 'shifting' gray circles indicate these nucleosomes display variable positioning at different promoters as well as within the same promoter in a population of cells. Triangles depict the relative levels of H2A.Z, H3K56Ac, and rate of H3 turnover (Albert et al., 2007; Dion et al., 2007; Raisner et al., 2005; Rufiange et al., 2007; Zhang et al., 2005). H2A.Z is less enriched at covered promoters (**B**) than open promoters (**A**). Numbers above nucleosomes represent their positions relative to the transcription start site. NDR: nucleosome depleted region; TSS: transcription start site; SAGA: Spt/Ada/Gcn5 acetyltransferase

5. The function of the NDR and the mechanism of its formation

The specific organization of nucleosomes within the genome creates chromatin arrays that are tightly spaced over the gene coding regions and NDRs at promoters that expose DNA elements for transcription factor binding. In a way chromatin functions as a molecular filter that prevents non-specific binding while focusing the recruitment of the transcription machinery to *bona fide* promoter sites. Mutations that affect the position and density of nucleosome organization can negatively impact the accuracy of transcriptional start site selection and induction response (Rando and Winston, 2012). For example, a previous study showed that inactivation of the histone chaperones *SPT6* or FACT in yeast, which leads to global histone depletion, causes aberrant transcription initiation from within the open reading frame of genes (Kaplan, 2003) (**Figure 1-6A**, middle). This result suggests that perturbation of the normal density of open reading frame nucleosomes by histone depletion can expose previously blocked or 'cryptic' promoter elements. Another study showed the ATP-dependent remodeler Isw2 is required to push or slide the +1 nucleosomes towards the NDR. Deletion of *ISW2* led to widening of the NDR and an increase in the inappropriate expression of both sense and antisense transcripts emanating from the widened NDR (Whitehouse et al., 2007) (**Figure 1-6A**, bottom). Taken together, these data suggest that disruption of native nucleosome position and density can lead to transcriptional derepression and aberrant transcription initiation from cryptic start sites. Therefore, the proper formation and maintenance of chromatin architecture is crucial in directing the transcription machinery to assemble and initiate at the correct locations in the genome.

The NDR is the platform for transcription machinery assembly and therefore understanding how it is formed is central to the understanding of transcriptional regulation. The establishment and maintenance of the NDR appears to be the result of multiple forces. The

formation of the NDR at yeast promoters is influenced in part by DNA sequences that disfavor nucleosome formation. Promoter DNA is highly A/T-rich and it has been shown that long stretches of A/T nucleotides are refractory to nucleosome formation (Anderson and Widom, 2001; Drew and Travers, 1985). This is because A/T-rich DNA sequences intrinsically resist the distortion required to wrap around the histone octamer (Segal and Widom, 2009). However, DNA sequence alone is insufficient to establish the NDR on genomic DNA as previous studies showed that histone octamers reconstituted onto yeast genomic DNA only partially recapitulate the chromatin organization observed *in vivo* (Kaplan et al., 2009; Zhang et al., 2009). Specifically, the +1 nucleosome of the *in vitro* reconstituted chromatin is not as strongly positioned and the NDR is not as wide. In addition, the positioning of the nucleosomes within the gene body is completely unorganized. Taken together, these observations suggest that other factors are necessary for establishing the chromatin architecture *in vivo*. Indeed, the Pugh and Korber labs showed that adding yeast whole cell extract and ATP to *in vitro* reconstituted nucleosome arrays resulted in nucleosome positions that more accurately reflected the native chromatin architecture (Zhang et al., 2011). This result suggests that nucleosome positioning and NDR formation *in vivo* arises from a combination of DNA sequence determinants and ATP-dependent chromatin remodeling activity.

6. How the chromatin architecture at promoters regulates gene expression

The transcription machinery has to assemble at gene promoters in the context of chromatin and therefore the chromatin architecture in and around gene promoters has important roles in transcriptional regulation. One of the ways in which chromatin regulates the

transcription process is by preventing assembly of the PIC. This mode of regulation is exemplified by experiments conducted on the stress responsive genes, such as *PHO5* and *GAL1-10*, which have covered promoters (**Figures 1-5B** and **1-6B**). Within the promoter region of the *PHO5* gene, nucleosomes block the TATA element and one of the two Pho4 activator binding sites (Almer and Hörz, 1986; Reinke and Hörz, 2003) (**Figure 1-6B,** top). During gene activation in low phosphate (Pi), Pho4 binds to the exposed binding site located between two nucleosomes and recruits the histone acetyltransferase SAGA and the ATP-dependent chromatin remodeler SWI/SNF, which facilitate histone eviction, thereby exposing the second Pho4 site and TATA element (Barbaric et al., 2007) (**Figure 1-6B,** second from top). In addition, transcription is not required for this process as the loss of histones and subsequent chromatin opening still occurs even if the TATA element has been removed (Barbaric et al., 2007) (**Figure 1-6B**, middle). Similarly, studies examining the *GAL1-10* promoters observed nucleosomes positioned over the TATA element that are lost during gene induction in a manner that is dependent on the transcriptional activator Gal4 (Bryant et al., 2008; Lohr and Lopez, 1995). Importantly, histone depletion is not just a consequence of gene activation but appears to be directly regulating gene activation. For example, artifically stimulating nucleosome loss at the *PHO5* promoter causes abberant gene activation (Han and Grunstein, 1988) (**Figure 1-6B**, second from bottom). By contrast, hyperstabilizing the *PHO5* promoter nucleosome, by replacing the nucleosomal DNA with an exogenous DNA sequence that has a very high affinity for histones, prevents gene activation even in inducing conditions (Straka and Hörz, 1991) (**Figure 1-6B**, bottom). Taken together, these studies suggest chromatin changes precede and are required for gene expression.

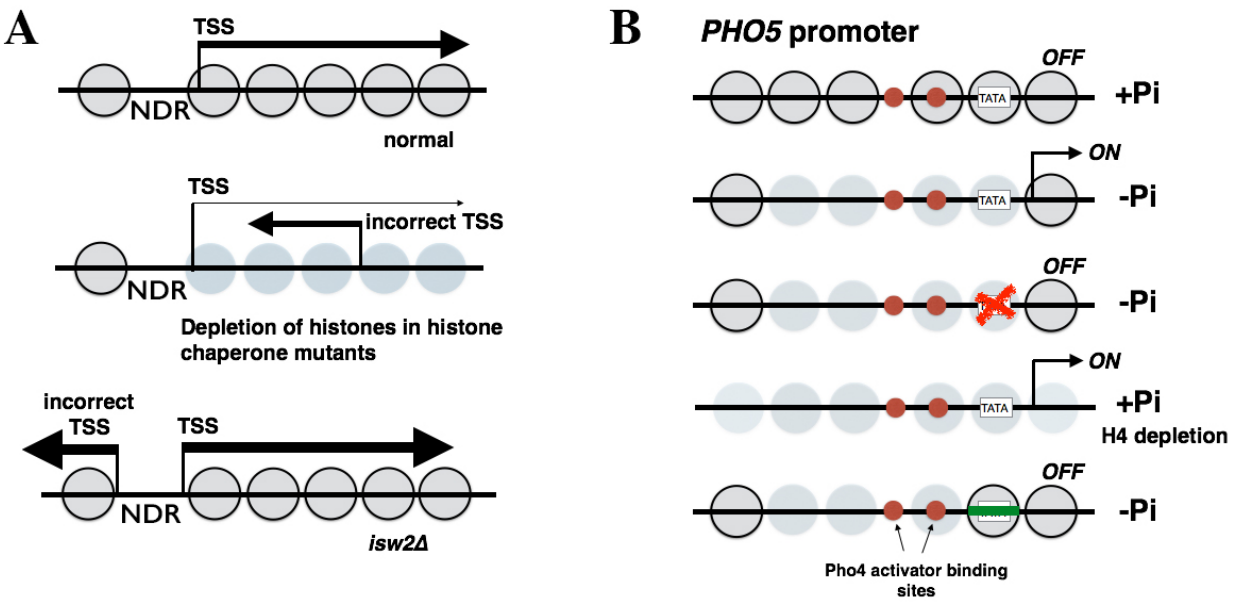

Figure 1-6. Chromatin structure regulates gene expression (**A**) Mutations that cause a change in nucleosome occupancy or position lead to incorrect transcription. *Top*: normal transcription. *Middle*: Depletion of histones leads to transcription initiation from 'cryptic' or hidden transcription start sites within the open reading frame of the gene (Kaplan, 2003). *Bottom*: Mutations that impact the position of promoter nucleosomes result in increase of transcription from the normal transcription start site as well as initiation from a cryptic start site (Whitehouse et al., 2007). (**B**) Removal of promoter nucleosomes is a crucial step in *PHO5* gene activation. *Top*: *PHO5* is OFF in high phosphate (+Pi) and nucleosomes are positioned over the TATA element and one of the two Pho4 activator binding sites (Almer and Hörz, 1986). *Second from top*: *PHO5* is ON in low phoshate (-Pi) and promoter nucleosomes are evicted (Reinke and Hörz, 2003). *Middle*: Deletion of the TATA element, which prevents *PHO5* from turning ON, still led to eviction of promoter nucleosomes in low phosphate (-Pi) (Barbaric et al., 2007). *Second from bottom*: Artificially stimulating nucleosome loss, with H4 depletion, led to *PHO5* turning ON even in high phosphate (+Pi) (Han and Grunstein, 1988). *Bottom*: Stabilizing the nucleosome positoned over the TATA element, using an exogenous DNA sequence, prevented *PHO5* from turning ON in low phosphate (-Pi) (Straka and Hörz, 1991). Gray circles represent nucleosomes. Faded gray circles indicates histone depletion. *Black arrows* indicate transcription start site. Thickness of arrows correlates with amount of transcription. *Red circles* are Pho4 activator binding sites. *Green line* represents an exogenous DNA sequence with high affinity for histones. NDR: nucleosome depleted region; TSS: transcription start site; Pi: Phosphate.

At genes where the promoter is more depleted of nucleosomes, such as open promoters, chromatin remodeling is likely regulating transcription at a step downstream of PIC assembly (**Figures 1-5A** and **1-2**). In yeast, the PIC assembles at a TATA element that is ~40-120 bp upstream of the TSS and occupies a ~60-90 bp footprint (Hahn and Young, 2011) (**Figure 1-2**). This suggests that the PIC can assemble at the NDR without disrupting the +1 nucleosome (Rhee and Pugh, 2012). In support of this hypothesis, the cryo-EM structure of yeast PIC suggests that it can coexist with the +1 nucleosome in its closed conformation (Murakami et al., 2013). After assembling at the promoter the PIC has to engage the TSS located within the +1 nucleosome. However, not much is known about how the +1 nucleosome affects this stage of transcription in yeast. A previous study using *Drosophila* cells demonstrated that chromatin bound Pol II stalls at the entry site of the +1 nucleosome more than any other position in the genome (Weber et al., 2014). This observation suggests that the +1 nucleosome is a major barrier to Pol II transcription *in vivo*. Interestingly, this barrier can be partially alleviated by the incorporation of the histone variant H2A.Z into the +1 nucleosome (Rudnizky et al., 2016; Weber et al., 2014). Therefore, at these genes transcription appears to be regulated by a combination of +1 nucleosomal density and H2A.Z levels. In the sections below, I will discuss how the unique histone dynamics of the +1 nucleosome may be playing a role in transcriptional regulation in yeast.

7. Nucleosomes at the +1 position are highly dynamic

The TSS in yeast is located ~13 bp inside the upstream border of the +1 nucleosome, making it inaccessible to the transcription machinery (Albert et al., 2007; Mavrich et al., 2008) (**Figure 1-5**). Therefore, the transition of the PIC to its open conformation, which involves the

melting of an ~15 bp region around the TSS, likely requires that this nucleosome be remodeled or disassembled. In support of this idea, the +1 nucleosome is subject to robust chromatin remodeling activities and its occupancy is contributed by a dynamic equilibrium caused by rapid nucleosome disassembly and reassembly (Jiang and Pugh, 2009a; Li et al., 2007; Rando and Winston, 2012). Two independent studies demonstrated that an inducible tagged version of histone H3 is incorporated at promoter-proximal nucleosomes more rapidly than nucleosomes within the open reading frame (Dion et al., 2007; Rufiange et al., 2007). Importantly, the promoter specific incorporation of histone H3 is observed at both active and infrequently transcribed genes suggesting that little or no transcription activity is required for H3 eviction. Since the $(H3\text{-}H4)_2$ tetramer is present at the core of the nucleosome, H3 turnover suggests complete disassembly and reassembly of the promoter-proximal nucleosomes.

In addition, one of the studies observed that the newly incorporated H3 at the +1 position is enriched for the H3K56Ac histone mark, suggesting that this modification may contribute to the turnover of H3 (Rufiange et al., 2007). Because this modification is located near the entry/exit site of the DNA on the histone octamers, it has been suggested that it plays a role in destabilizing the +1 nucleosome and making it easier to disassemble (Neumann et al., 2009).

8. Players involved in nucleosome dynamics in and around the promoters

One class of enzymes that might be contributing to histone dynamics at the promoter contains ATP-dependent chromatin remodelers. These enzymes utilize the energy of ATP hydrolysis to disrupt histone-DNA contacts and can mobilize histone octamers along the DNA or

evict histones from DNA (**Figure 1-3**). ATP-dependent remodelers are classified into four groups based on the sequence similarity of the ATPase domain, namely the ISWI-, CHD-, SWI/SNF- and INO80-families (Clapier and Cairns, 2009). ATP-dependent chromatin remodelers affect histone dynamics by catalyzing nucleosome sliding (the translational movement of the histone octamer along the DNA), nucleosome disassembly (the eviction of one or more histone pairs within a nucleosome), nucleosome reassembly (the regulated deposition of histone pairs onto the DNA to form a nucleosome), and histone exchange (replacing one type of histone with another within a nucleosome) (Cairns, 2007, 2009) (**Figure 1-3**). In yeast, these chromatin remodeling activities converge around the +1 nucleosome and play important roles in the formation and maintenance of the NDR and the turnover of histones at the +1 position (Hughes and Rando, 2014; Rando and Chang, 2009).

9. The histone variant H2A.Z is preferentially inserted into +1 nucleosomes (and is likely involved in histone turnover)

Another unique feature of the +1 nucleosome is that it is enriched for the histone variant H2A.Z (Albert et al., 2007; Guillemette et al., 2005; Jin et al., 2009; Li et al., 2005; Raisner et al., 2005; Zhang et al., 2005) (**Figure 1-5**). H2A.Z-containing nucleosomes are enriched at the +1 positions of the majority of yeast genes (two thirds), with the exception of the most highly transcribed genes, the very poorly transcribed genes, and those with covered promoters (Rando and Winston, 2012). H2A.Z is well conserved from yeast to humans and has ~60% sequence similarity with canonical H2A (Zlatanova and Thakar, 2008). Yeast that are mutant for the gene encoding H2A.Z (*HTZ1*) are viable but exhibit slow growth, sensitivity to genotoxic and

environmental stresses, and gene silencing defects (Kobor et al., 2004; Meneghini et al., 2003; Mizuguchi et al., 2004; Santisteban et al., 2000). *HTZ1* demonstrates genetic interactions with genes involved in transcription and chromatin remodeling, such as *SPT5, SPT16,* and genes encoding components of the SAGA, NuA4, and SWI/SNF complexes, implying a role for H2A.Z in gene activation (Krogan et al., 2003, 2004; Lin et al., 2008; Santisteban et al., 2011).

Given its enrichment at the +1 nucleosomes of most promoters, H2A.Z is expected to play a role in regulating the transcription process. However, despite being widely studied, the exact function of H2A.Z in transcription is still unclear and a subject of debate (Zlatanova and Thakar, 2008). H2A.Z has been proposed to be involved in activation of gene expression, more specifically in recruitment of the transcription machinery to the promoter. For example, experiments on the oleate-responsive genes observed that loss of H2A.Z prevents optimal recruitment of TATA-binding protein (TBP) during induction (Wan et al., 2009). Further, the C-terminal domain of H2A.Z has been shown to interact with Pol II (Adam et al., 2001). Other studies have shown that there is an inverse correlation between H2A.Z occupancy and transcription levels, suggesting that Pol II activity or chromatin remodeling activities associated with gene activation drive H2A.Z eviction (Li et al., 2005; Zanton and Pugh, 2006; Zhang et al., 2005). Surprisingly, global gene expression profiling studies showed that *htz1*Δ mutants exhibit only a very minor defect in steady state mRNA levels (with only 15 genes exhibiting a 2.0 fold increase or decrease in mRNA level) (Meneghini et al., 2003; Mizuguchi et al., 2004). This led to the hypothesis that the H2A.Z nucleosome at promoters is required for rapid induction of transcription but not the final steady state mRNA levels. Indeed, kinetic experiments showed that rapid induction of the *GAL1-10*, *PHO5*, cyclin genes and heat-shock genes requires H2A.Z (Dhillon et al., 2006; Santisteban et al., 2000; Venters et al., 2011; Zhang et al., 2005). The

observation that H2A.Z is preferentially lost from promoters over H2A during activation further supports this notion (Santisteban et al., 2000; Venters et al., 2011; Zhang et al., 2005). Taken together, these data suggest that the incorporation of H2A.Z at the +1 nucleosome position primes genes for activation, although the exact mechanism of how H2A.Z is evicted is still unclear.

One hypothesis is that H2A.Z containing nucleosomes are inherently unstable and therefore poised for disassembly (Guillemette et al., 2005; Zhang et al., 2005). However, studies attempting to address this hypothesis have produced contradictory results. For example, experiments testing the stability of reconstituted H2A.Z nucleosomes have been inconsistent, with some reports demonstrating a stabilizing role for H2A.Z (Park et al., 2004; Thambirajah et al., 2006) and others a destabilizing role (Abbott et al., 2001; Horikoshi et al., 2016). When crude chromatin from yeast is subjected to salt washes, H2A.Z dissociates from the chromatin at a lower salt concentration than H2A, suggesting that native H2A.Z nucleosomes are indeed unstable (Zhang et al., 2005). However, the concentration of salt required to disrupt H2A.Z nucleosomes (500 mM) is significantly higher than the physiological ionic strength (~150mM), making it unclear if salt sensitivity *in vitro* is relevant to nucleosome disassembly *in vivo*.

Studies on the stability of H2A.Z nucleosomes from vertebrates are further complicated by the fact that H2A.Z can be packaged with either the histone variant H3.3 or the canonical histone H3.1 (Weber and Henikoff, 2014). In metazoans, H3.3 is incorporated specifically at dynamic chromatin sites including promoters, enhancers and insulators; whereas H3.1 is found ubiquitously throughout the genome (Jin et al., 2009; Talbert and Henikoff, 2010). Experiments using native mononucleosomes prepared from avian and mammalian cells demonstrated that H2A.Z and H2A nucleosomes are more susceptible to salt-induced dissociation when packaged

with H3.3 than with H3.1 (Jin and Felsenfeld, 2007; Jin et al., 2009). However, this result is controversial as a different group recently showed that incorporation of H3.3 did not affect the thermal stability of H2A.Z nucleosomes *in vitro* (Horikoshi et al., 2016). Budding yeast have two H3 genes but both copies are more closely related to the metazoan H3.3 than H3.1 (Weber and Henikoff, 2014). Therefore, whether intrinsic instability of H2A.Z nucleosomes contributes to the turnover of +1 nucleosomes *in vivo* remains an open question. Alternatively but not exclusively, a chromatin remodeling enzyme could recognize H2A.Z within the +1 nucleosome and drive its disassembly.

10. How is H2A.Z inserted at the promoter +1 nucleosome?

The promoter-specific deposition of H2A.Z in yeast is catalyzed by the 14-polypeptide SWR1 complex, which is an ATP-dependent enzyme and a member of the INO80-family of chromatin remodelers (Kobor et al., 2004; Krogan et al., 2003; Mizuguchi et al., 2004). SWR1 is recruited to the promoter NDR via the DNA binding affinity of Swc2 for long stretches of nucleosome free DNA (Ranjan et al., 2013) (**Figure 1-7**). In addition, the recruitment of SWR1 to the promoter is facilitated by the Bdf1 subunit, which contains tandem bromodomains that bind the N-terminal tails of H3 and H4 that are acetylated on lysine residues (e.g. H3K9, H3K14, H4K5, and H4K12) (Raisner et al., 2005) (**Figure 1-7**). The post-recruitment activation of SWR1 requires the binding of both of its histone substrates, namely canonical H2A nucleosomes and H2A.Z-H2B dimers (Luk et al., 2010). After protein synthesis, H2A.Z forms a dimer with H2B that is immediately bound by one of several histone chaperones, such as Nap1, Chz1, or FACT (Luk et al., 2007). The H2A.Z-H2B dimer is then delivered to the SWR1 complex where

it is recognized by two acidic domains, one found in the core Swr1 subunit and the other in Swc2 (Hong et al., 2014; Luk et al., 2007; Wu et al., 2005) (**Figure 1-7**). The enzyme then catalyzes an ATP-dependent histone exchange reaction in which one of the two H2A-H2B dimers of the nucleosome is replaced by an H2A.Z-H2B dimer (Mizuguchi et al., 2004) (**Figures 1-3C** and **1-7**). Given that there are two copies of each histone in the nucleosome, SWR1 catalyzes the conversion of homotypic H2A/H2A nucleosomes (AA) to homotypic H2A.Z/H2A.Z nucleosomes (ZZ) by generating a heterotypic H2A/H2A.Z nucleosome (AZ) intermediate before the second H2A-H2B histone pair is replaced (Luk et al., 2010).

Interestingly, in a population of G1-arrested cells, the +1 nucleosomes are almost equally represented by the ZZ, AZ, and AA configurations (Luk et al., 2010). This suggests the SWR1-mediated histone exchange reaction is likely opposed by a histone eviction reaction that converts H2A.Z nucleosomes back to its H2A state. Therefore, the insertion of H2A.Z at the +1 nucleosomal position appears to be priming nucleosomes for disassembly. In support of this hypothesis, H3 turns over very rapidly at the +1 position of most genes, independent of transcription (Dion et al., 2007; Rufiange et al., 2007). How these H2A.Z containing nucleosomes at the promoter are disassembled is an important question that has yet to be answered and the central theme of my thesis.

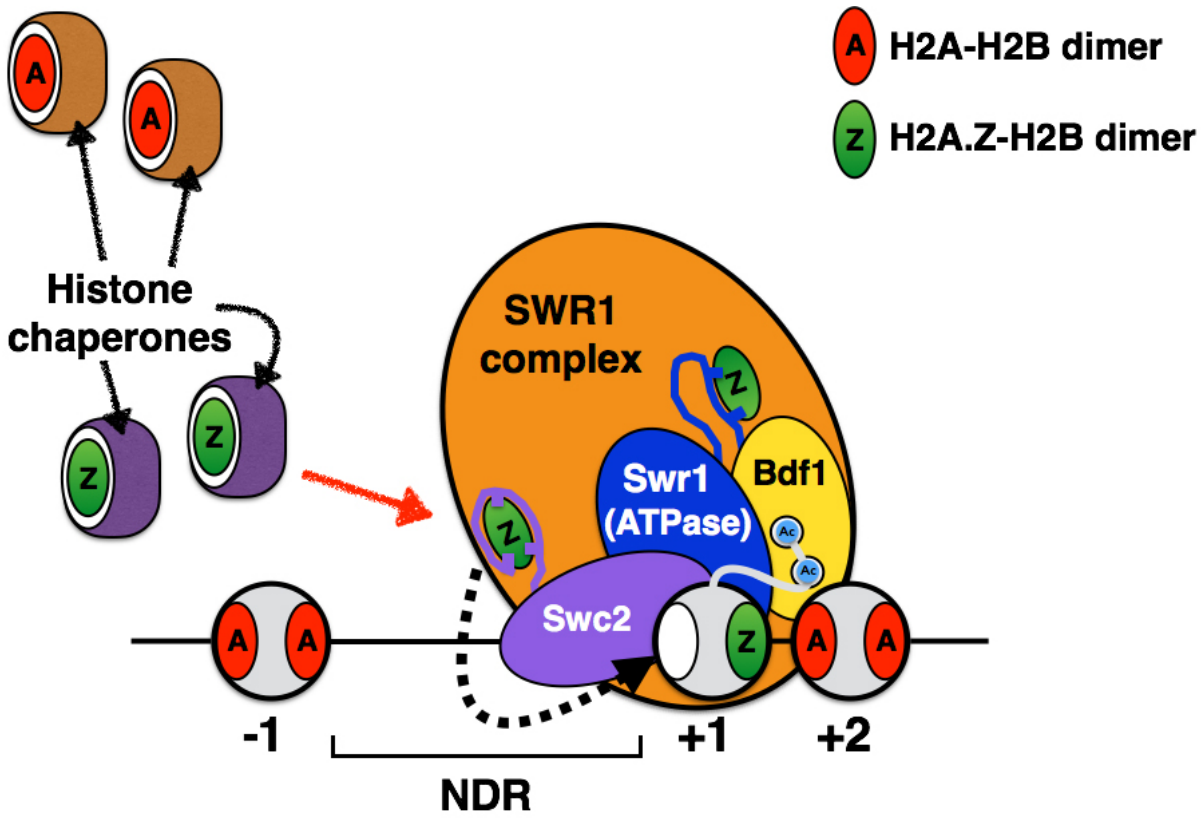

Figure 1-7. The ATP-dependent remodeler SWR1 catalyzes a histone exchange reaction depositing H2A.Z at the +1 nucleosomal position. H2A-H2B dimers (A) are shown in *red*, H2A.Z-H2B dimers (Z) in *green* and $(H3\text{-}H4)_2$ tetramers in *gray*. The N-terminal tails of histones H3 and H4 at the +1 position are depicted as a *gray* line and acetylated (Ac) lysine residues indicated with *light blue* circles. Other histone N-terminal tails and additional histone modifications were omitted for simplicity. Histone chaperones are indicated with *black arrows*: H2A-H2B chaperones are in *brown* and H2A.Z-H2B chaperones are in *purple*. The SWR1 complex is shown in *orange* with the Swc2 subunit in *light purple*, the Swr1 ATPase subunit in *blue*, and the Bdf1 bromodomain containing subunit in *yellow*. The acidic domains of Swc2 and Swr1 that contact H2A.Z-H2B dimers are shown as *purple* and *blue* lines, respectively. The *red arrow* represents the delivery of an H2A.Z-H2B dimer to the SWR1 complex by a histone chaperone. The *dashed black arrow* indicates histone exchange reaction in progress. Numbers under nucleosomes represent their position relative to the transcription start site, which is omitted for simplicity. NDR: nucleosome depleted region.

11. Potential mechanism for +1 H2A.Z nucleosome disassembly

How the H2A.Z containing +1 nucleosome is disassembled to allow for the PIC to engage the TSS is an important question related to the mechanism of transcriptional control. ATP-dependent remodelers are known to eject nucleosomes *in vivo* and *in vitro* (Lorch et al., 1999; Narlikar et al., 2002; Whitehouse et al., 1999; Yen et al., 2012). In addition, they are linked to chromatin opening at promoters during gene activation and therefore are potential candidates for H2A.Z eviction (Barbaric et al., 2007; Bryant et al., 2008). In this section, I will highlight several ATP-dependent remodelers that could play a role in H2A.Z eviction.

The INO80 complex has been reported to perform a reverse histone replacement reaction opposing the activity of SWR1 *in vitro* (Papamichos-Chronakis et al., 2011). The INO80 complex presumably can convert the homotypic ZZ nucleosome back to the AA form by replacing the nucleosomal H2A.Z-H2B dimers with H2A-H2B dimers (Papamichos-Chronakis et al., 2011). Consistent with this idea, deletion of *ARP5* and *INO80*, which encode critical subunits of the INO80 complex, results in global accumulation of H2A.Z (Papamichos-Chronakis et al., 2011; Yen et al., 2013). However, the *in vitro* histone replacement activity of INO80 is controversial as the data cannot be reproduced by other groups, including our own (Wang et al., 2016, Lihong Wan unpublished data). In addition, a recent ChIP-coupled microarray experiment demonstrated that H2A.Z levels at promoters in *ino80*Δ cells are unchanged compared to wild-type cells (Jeronimo et al., 2015). Therefore, what contribution INO80 has on eviction of H2A.Z *in vivo* remains an open question.

The SWI/SNF chromatin remodeler mediates promoter-specific nucleosome disassembly *in vivo* and therefore is a candidate for catalyzing +1 H2A.Z eviction (Brown et al., 2011; Bryant

et al., 2008; Gkikopoulos et al., 2009). SWI/SNF is recruited to the divergent *GAL1-10* promoters upon gene activation and is required to disassemble the promoter-proximal nucleosomes during gene activation (Bryant et al., 2008). In addition, an *in vitro* study showed that targeting the SWI/SNF complex to reconstituted nucleosome arrays can cause histone eviction (Gutiérrez et al., 2007). However, these experiments were performed in the presence of excess free DNA to act as a histone acceptor, which is non-physiological. Therefore, whether SWI/SNF can eject H2A.Z *in vivo* remains unknown. Unpublished data from Lu Sun in our lab has shown that conditional depletion of the SWI/SNF ATPase, Snf2, does not lead to H2A.Z accumulation at the +1 position, arguing against SWI/SNF being a general H2A.Z evictor.

RSC remodeler is another candidate that may play a role in H2A.Z eviction. Inactivation of RSC leads to encroachment of nucleosomes into the NDR, suggesting that RSC is involved in sliding histone octamers out of the NDRs or evicting histones from the promoter DNA entirely (Hartley and Madhani, 2009; Parnell et al., 2008; Yen et al., 2012). Consistent with the histone eviction model, *in vitro* experiments have shown that purified RSC, in the presence of ATP and excess amounts of histone chaperone Nap1, is capable of ejecting histones from reconstituted mononucleosomes (Lorch et al., 2006). However, one interpretation of this result is that RSC slides histone octamers off of the ends of the DNA templates. Therefore, whether RSC can eject H2A.Z from +1 nucleosomes *in vivo* is not known. Recent data from our lab showed that conditional depletion of Sth1, the catalytic subunit of RSC, leads to no change in relative H2A.Z levels at the +1 position, further arguing against RSC functioning as the H2A.Z evictor (unpublished data of Lu Sun).

Lastly, the remodeler Chd1 has been implicated in histone eviction at the *PHO5* gene promoter (Ehrensberger and Kornberg, 2011). Activation of the *PHO5* gene occurs under low

phosphate conditions and is accompanied by depletion of promoter nucleosomes. A biochemical study using reconstituted nucleosome arrays, bearing the promoter and open reading frame sequence of the *PHO5* gene, showed that Chd1 can stimulate histone eviction in the presence of the activator Pho4 and ATP (Ehrensberger and Kornberg, 2011). However, subsequent deletion of *CHD1* leads to only a slight reduction in *PHO5* expression *in vivo.* When *CHD1* and *ISW1* were both deleted, *PHO5* expression is completely abolished, suggesting that Chd1 works with ISW1 to remove nucleosomes and promote gene activation (Ehrensberger and Kornberg, 2011). However, *PHO5* is a stress responsive gene with unique transcriptional regulation, a smaller than average NDR and very low H2A.Z content at the +1 nucleosome (Rando and Winston, 2012) (**Figures 1-5B** and **1-6B**). Therefore, it is unclear how relevant the nucleosome disassembly activity of Chd1 is for H2A.Z eviction genome-wide.

Taken together, it is still unclear what factor(s) is responsible for the conversion of ZZ nucleosomes back to the AA nucleosomal state at the +1 positions. The goal of my thesis was to understand the role of the transcription machinery in the disassembly of +1 H2A.Z nucleosomes.

12. The transcription machinery could play an active role in the chromatin remodeling at promoter

My thesis work addresses the outstanding question of what factor(s) are responsible for driving the disassembly of +1 H2A.Z nucleosomes at promoters genome-wide. Given that the PIC is assembled at the NDR region adjacent to the +1 nucleosome, we hypothesized that the PIC plays an active role in disassembling or remodeling +1 H2A.Z nucleosomes (Murakami et

al., 2013; Rhee and Pugh, 2012). In support of this hypothesis, previous work has demonstrated that Pol II and the general transcription factors may play a direct role in chromatin remodeling. For example, a previous study showed that promoters with wider NDRs generally have higher general transcription factor occupancy, suggesting that the assembly of the PIC may be responsible for displacing nucleosomes to generate the NDR, either by histone eviction or nucleosome sliding (Venters and Pugh, 2009).

The elongation activity of Pol II has also been implicated in chromatin remodeling in that the native spacing of nucleosomes along yeast genes requires transcription (Hughes and Rando, 2014). An MNase-seq study found that inactivation of Pol II using the temperature sensitive allele *rpb1-1* led to an overall shift of nucleosomes away from the NDR within the gene body (Weiner et al., 2010). Specifically, it was reported that an overall relaxation of chromatin structure is associated with Pol II inactivation. As such, nucleosomes are repositioned to genomic locations that are more closely related to the preferred, intrinsic positioning sequence (Weiner et al., 2010). The *in vivo* result is in agreement with *in vitro* experiments demonstrating that an elongating Pol II can disassemble the histones in front of it and reassemble them in its wake (Hodges et al., 2009).

Taken together, these experiments suggest that the transcription machinery could function as chromatin remodeling factor and affect yeast chromatin structure genome-wide. Therefore, it would be interesting to know if the transcription machinery has a significant role in remodeling or disassembling +1 H2A.Z nucleosomes.

13. Proposed Histone Cycle model

I propose a "histone cycle" model to unify the promoter-specific H2A.Z dynamics. First, ATP-dependent remodelers, such as RSC and SWI/SNF, are recruited to the promoter region by sequence specific DNA-binding factors to establish the NDR (**Figure 1-8 –** *Step I*). Next, SWR1 is recruited to the NDR by its affinity for extended stretches of naked DNA and, to lesser extent, promoter-specific histone acetylation. SWR1 then sequentially converts canonical AA nucleosomes to AZ then ZZ nucleosomes (**Figure 1-8 –** *Step II-a* and *II-b*). A putative eviction process is responsible for disassembling the +1 H2A.Z nucleosomes allowing for transcription to occur (**Figure 1-8 –** *Step III red arrow*). After transcription and/or dissociation of the general transcription factors and Pol II, +1 nucleosomes are reassembled with canonical H2A histones and the cycle begins again (**Figure 1-8 –** *Step IV*). My thesis addressed the hypothesis that the transcription machinery is the major driving force for disassembly of +1 H2A.Z nucleosomes.

To test this hypothesis I conditionally depleted components of the transcription machinery and used a quantitative ChIP-seq (qChIP-seq) approach to probe for changes in H2A.Z (and H2A) occupancy genome-wide at base pair resolution. The goal was to determine what role, if any, the transcription machinery has in eviction of +1 H2A.Z nucleosomes when genes are preparing for transcription.

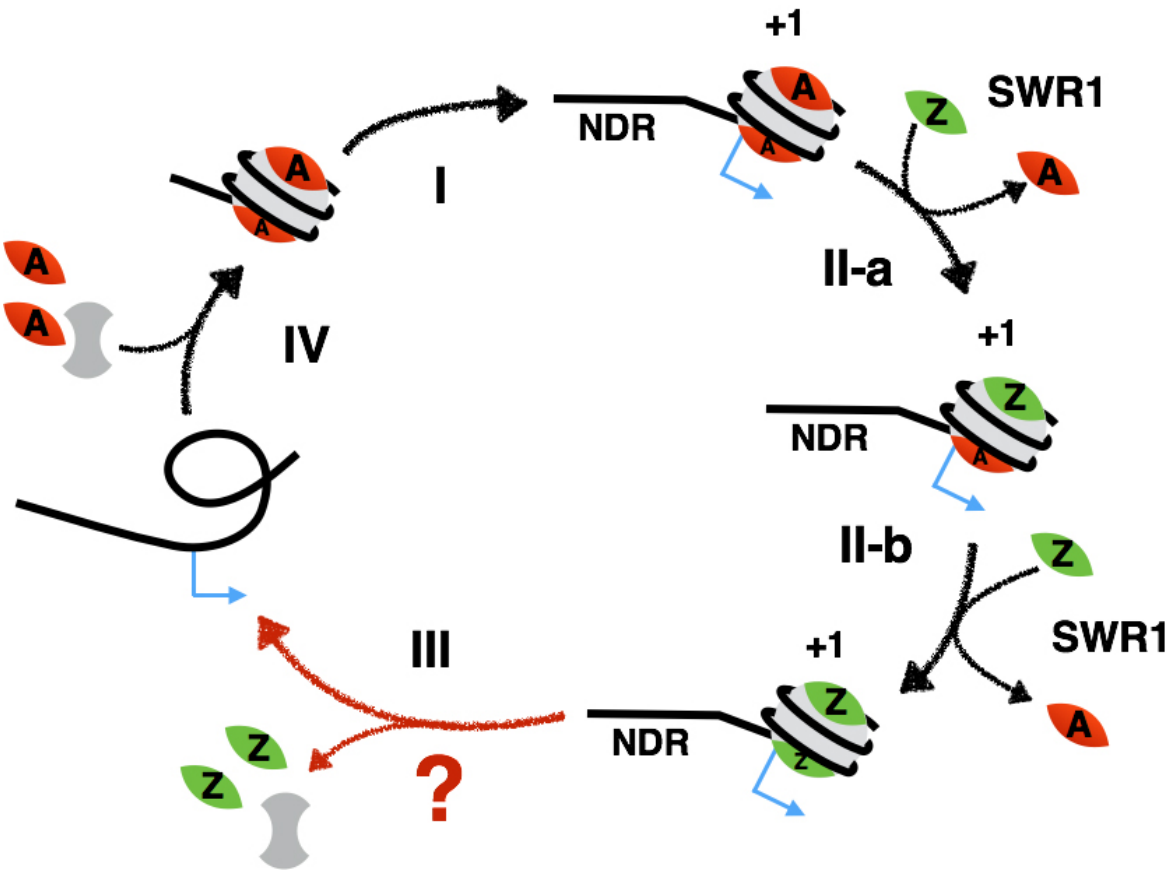

Figure 1-8. Proposed histone cycle model to account for histone dynamics of the +1 nucleosome. (Step I) ATP-dependent chromatin remodelers are recruited to promoters and create the NDR. (Steps II-a and II-b) SWR1 is recruited to NDRs and converts AA nucleosomes to ZZ nucleosomes at the +1 position. (Step III) The ZZ nucleosome is disassembled by an unknown mechanism, indicated by the *red arrows* and question mark. (Step IV) After transcription and/or dissociation of the transcription machinery, nucleosomes are reassembled at the promoter with canonical histone H2A. H2A-H2B dimers (A) are in *red*, H2A.Z-H2B dimers (Z) in *green* and $(H3\text{-}H4)_2$ tetramers in *gray*. The *blue arrows* indicate the position of the transcription start site. Histone chaperones are omitted for simplicity. NDR: nucleosome depleted region.

Chapter Two: Constitutive turnover of histone H2A.Z at yeast promoters requires the preinitiation complex

[The text of this chapter is taken directly from a manuscript published in Elife. 2016 Jul 20;5. pii: e14243. doi: 10.7554/eLife.14243 (Tramantano et al., 2016). I carried out all the experiments in the manuscript, unless otherwise noted in the text or figure legends.]

1. Introduction

The regulation of chromatin structure and its dynamics is integral to the control of gene expression in eukaryotes. The protein core of a canonical nucleosome, modular in nature, consists of a tetramer of histones H3 and H4 [indicated as $(H3\text{-}H4)_2$] and two dimers of histones H2A and H2B (indicated as H2A-H2B) (Arents et al., 1991). Nucleosomal DNA, 147-bp in length, wraps around the octameric histone core in 1.7 left-handed turns making 3 minor groove contacts with each histone pair and additional contacts near the entry-exit sites with H3 (Luger et al., 1997). Repeating units of nucleosomes are organized along the genomic DNA in a non-random fashion with nucleosome-depleted regions (NDRs) overlapping key regulatory elements, such as promoters and replication origins (Eaton et al., 2010; Yuan et al., 2005). Nucleosome-repelling DNA sequences and ATP-dependent remodeling activities contribute to NDR formation (Kaplan et al., 2009; Zhang et al., 2011). Like a molecular sieve, chromatin blocks non-specific protein-DNA interactions and allows localized assembly of DNA binding factors, such as the general transcription factors (GTFs) and RNA polymerase (Pol) II, at the NDRs

(Rhee and Pugh, 2012). Mutants that perturb the native nucleosome organization can lead to transcriptional derepression and initiation from aberrant start sites (Han and Grunstein, 1988; Kaplan, 2003; Whitehouse et al., 2007).

How the transcription machinery engages the nucleosome in and around a promoter and how these nucleosomes are mobilized at different stages of transcription are important questions related to the mechanism of transcriptional control. The GTFs and Pol II assemble on an 80-to-200-basepair NDR to form the 'closed' preinitiation complex (PIC) (Rhee and Pugh, 2012). The nucleosome immediately downstream of the NDR is termed the +1 nucleosome (Albert et al., 2007). In *Saccharomyces cerevisiae*, the +1 nucleosome covers the transcription start site (TSS) of most genes. Therefore, it is expected that at some point during the transcription process the +1 nucleosome must be disassembled. It is currently unclear at what stage of transcription disassembly of the +1 nucleosome occurs. It remains possible that chromatin remodeling enzymes are required to remove the +1 nucleosome before Pol II can engage the TSS. For other promoters where the +1 nucleosome covers the TATA element and for those with an untraditional nucleosome structure called the "fragile nucleosome" within the NDR, histone eviction likely precedes and regulates PIC assembly (Kubik et al., 2015; Rhee and Pugh, 2012). In metazoans, where the TSS is further upstream of the +1 nucleosome than in yeast (Schones et al., 2008), the +1 nucleosome stalls elongation (Weber et al., 2014). In all cases, the disassembly of these promoter-proximal nucleosomes is likely a regulatory barrier for full-length transcript synthesis (Churchman and Weissman, 2011; Weber et al., 2014).

The promoter-proximal nucleosomes at the +1 position and to a lesser extent the -1 position (upstream of the NDR) are enriched for the histone variant H2A.Z (Albert et al., 2007; Raisner et al., 2005). Together with the histone variant H3.3, H2A.Z forms nucleosomes that are

labile in high salt *in vitro* (Jin and Felsenfeld, 2007; Zhang et al., 2005). In yeast, where the major H3 is similar to the H3.3 isoform in metazoans, H2A.Z is preferentially evicted from promoters during gene activation over H2A (Santisteban et al., 2000; Zhang et al., 2005; Venters et al., 2011). Although mutants of *HTZ1* (the gene that encodes H2A.Z in yeast) are viable and exhibit only minor defects in steady-state mRNA levels, H2A.Z is required for rapid transcriptional activation (Dhillon et al., 2006; Halley et al., 2010; Santisteban et al., 2000; Zhang et al., 2005). These findings suggest that H2A.Z nucleosomes are predisposed for disassembly to allow for a rapid transcriptional response. What drives H2A.Z nucleosome disassembly *in vivo* is the focus of this study.

The incorporation of H2A.Z into nucleosomes is catalyzed by the ATP-dependent chromatin remodeling complex SWR1 (Mizuguchi et al., 2004). The ~1 megadalton SWR1 complex comprises the catalytic core protein Swr1, a member of the Swi2/Snf2-related ATPase, plus 13 other polypeptides (Kobor et al., 2004; Krogan et al., 2003; Mizuguchi et al., 2004). SWR1 is targeted to promoters by its intrinsic affinity for the NDR and promoter-specific histone acetylation (Raisner et al., 2005; Ranjan et al., 2013). It catalyzes a histone replacement reaction that involves the coupled removal of a nucleosomal H2A-H2B dimer with the insertion of an H2A.Z-H2B dimer that is delivered to the enzyme by one of several histone chaperones, including Nap1, Chz1, and FACT (Luk et al., 2007, 2010; Mizuguchi et al., 2004). The two H2A-H2B dimers in a homotypic H2A (AA) nucleosome are replaced sequentially, first generating the heterotypic H2A/H2A.Z (AZ) nucleosome as an intermediate (**Figure 2-1A,** *step I-a*) and the homotypic H2A.Z (ZZ) nucleosome as the final product (**Figure 2-1A,** *step I-b*) (Luk et al., 2010). The $(H3\text{-}H4)_2$ tetramer remains associated with the DNA before and after

each step of the replacement reaction as no net loss of nucleosomal species occurs during the histone replacement reaction *in vitro* (Luk et al., 2010).

While it is well established that H2A.Z is enriched at the promoter-proximal nucleosomes, it is underappreciated that substantial amount of H2A is also present at these sites (Luk et al., 2010). Experiments using sequential ChIP and tiling microarray analysis have demonstrated that in a population of G1-arrested cells, nucleosomes in the AA, AZ and ZZ configurations can all be detected at the +1 positions of most promoters (Luk et al., 2010). This observation suggests that the SWR1 reaction that generates ZZ nucleosomes is opposed by a pathway(s) that converts ZZ nucleosomes back to the AA state in a replication-independent manner. Consistent with this dynamic model, rapid, constitutive H3 turnover is observed at most +1 nucleosomes (Dion et al., 2007). Since the $(H3\text{-}H4)_2$ tetramer is at the center of the histone core (Luger et al., 1997), H3 turnover implies complete disassembly of the ZZ nucleosome (**Figure 2-1A**, *step II*). Reassembly likely leads to the formation of the canonical AA nucleosomes as H2A is ~10 times more abundant than H2A.Z and SWR1 does not assemble H2A.Z nucleosomes *de novo* on DNA (Luk et al., 2010; West and Bonner, 1980) (**Figure 2-1A**, *step III*).

The ATP-dependent remodeling complex INO80 has been reported to mediate the reverse replacement reaction [in which a nucleosomal H2A.Z-H2B dimer is replaced by a free H2A-H2B dimer] (**Figure 2-1A**, *steps I-c* and *I-d*) (Papamichos-Chronakis et al., 2011). Analysis of H2A.Z ChIP followed by microarray (ChIP-chip) showed that H2A.Z in *ino80*Δ cells redistributes from promoters to gene body regions as compared to wild-type cells (Papamichos-Chronakis et al., 2011). Deletion mutant of *ARP5*, a gene encoding a critical component of the INO80 complex, exhibited global H2A.Z accumulation especially around the

promoters as demonstrated by the ChIP-exo technique (Yen et al., 2013). However, the ChIP-chip data of a more recent study disagreed, showing that the genome-wide H2A.Z occupancy was similar in *ino80*Δ and wild-type cells (Jeronimo et al., 2015). Therefore, what contributes to the conversion of ZZ nucleosomes to the AA state remains controversial.

This study addresses the hypothesis that the transcription machinery is a major driving force of the disassembly of the +1 H2A.Z nucleosomes. We used the anchor away approach to deplete components of the transcription machinery (Haruki et al., 2008) and a quantitative ChIP-seq approach to probe changes in H2A.Z occupancy genome-wide at single-basepair resolution. We observed reciprocal increase of H2A.Z and decrease of H2A genome-wide after depletion of the PIC. By contrast, nuclear depletion of Ino80 did not cause global H2A.Z accumulation. These findings suggest that the assembly of the Pol II transcription machinery and/or its activity contribute(s) to the constitutive turnover of H2A.Z at yeast promoters.

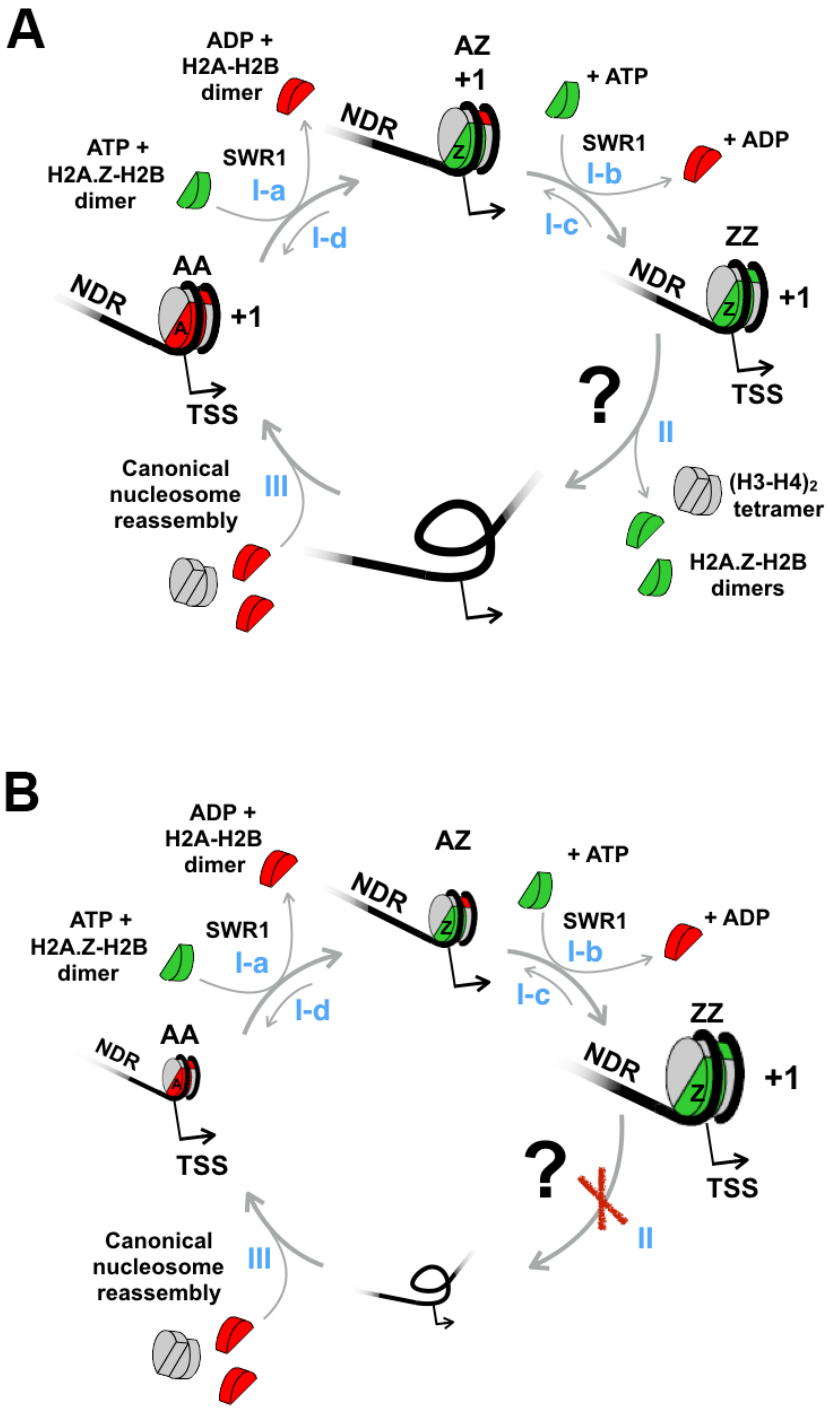

Figure 2-1. A proposed model to account for the constitutive histone turnover at yeast promoters. (**A**) The conversion of a +1 H2A nucleosome to an H2A.Z nucleosome by SWR1 is followed by nucleosome disassembly. Histone chaperones are not shown for simplicity. NDR: nucleosome-depleted region. '+1': +1 nucleosome. TSS: transcription start site. H2A.Z-H2B dimers are in *green*, H2A-H2B dimers in *red*, and $(H3\text{-}H4)_2$ tetramers in *gray*. (Step I-a) SWR1

replaces one nucleosomal H2A-H2B dimer in a homotypic “AA” +1 nucleosome with a dimer of H2A.Z-H2B to generate a heterotypic “AZ” nucleosome. (Step I-b) SWR1 replaces the second H2A-H2B dimer with H2A.Z-H2B dimer generating a homotypic “ZZ” nucleosome. (Steps I-c and I-d) The reported reverse replacement reaction by the INO80 complex (Papamichos-Chronakis et al., 2011). (Step II) The ZZ nucleosome is disassembled by an unknown mechanism indicated by the question mark. (Step III) A canonical AA nucleosome is reassembled. (**B**) Same as (**A**) except step II is blocked.

2. Results

2.1. A quantitative approach for measuring genome-wide levels of H2A.Z

The genomic H2A.Z level at any given promoter in a cell population is in a steady state that is maintained by the deposition mediated by SWR1 and the eviction mediated by putative chromatin remodeling pathway(s) (Luk et al., 2010). To test the contribution of the transcription machinery in H2A.Z eviction genome-wide, conditional yeast mutants were used to block the assembly of the PIC. If eviction of H2A.Z-containing nucleosomes is blocked, H2A.Z levels are expected to increase and H2A levels to decrease, as the SWR1 complex continues to replace nucleosomal H2A-H2B with H2A.Z-H2B dimers (**Figure 2-1B**). To block PIC assembly, TATA-binding protein (TBP) was conditionally depleted from the nucleus using the anchor-away approach with *SPT15*, the gene that encodes TBP (Haruki et al., 2008). When fused to the FKBP12-rapamycin-binding domain (FRB), TBP-FRB can be dragged out of the nucleus in a rapamycin-dependent manner by the FKBP12 tag on the pre-ribosome (Haruki et al., 2008). Previous studies have shown yeast cells expressing *SPT15-FRB* (hereafter referred to as *TBP-FRB*) rapidly depleted TBP from Pol II promoters, blocked Pol II recruitment and shut off transcription within 1 hour of rapamycin treatment (Grimaldi et al., 2014; Haruki et al., 2008; Wong et al., 2014). In our experiments, TBP-FRB relocalized to the cytoplasm with similar kinetics (**Figure 2-2**).

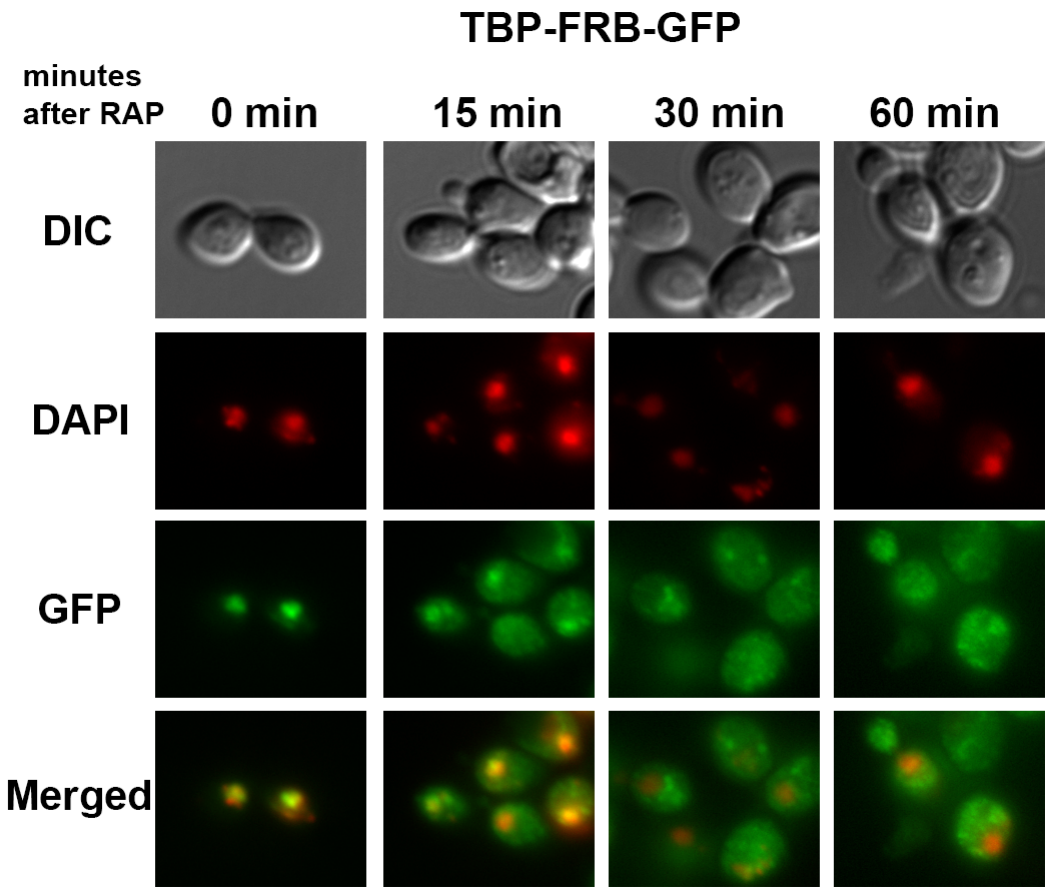

Figure 2-2. Fluorescence microscopy of yeast expressing *TBP-FRB-GFP* with and without rapamycin treatment. At the indicated times after the addition of 1 μg/mL rapamycin (RAP), cells were fixed with 4% formaldehyde for 5 min, washed with PBS and stained with DAPI before imaging using a Zeiss Axio Observer Z1 microscope. DAPI: *red*; GFP: *green*; DIC: differential interference contrast optics.

To measure the relative occupancy of H2A.Z and H2A genome-wide, deep sequencing was combined with quantitative ChIP of H2A.Z (Luk et al., 2010). Specifically, chromatin from fixed haploid yeast cells expressing a 2xFLAG-epitope-tagged H2A.Z was digested with micrococcal nuclease (MNase) to generate mononucleosomes. H2A.Z-containing nucleosomes were separated from the canonical AA nucleosomes by binding to anti-FLAG affinity gel followed by elution using FLAG peptides. Given that H2A.Z is the only H2A variant in budding yeast and the immunoprecipitation (IP) efficiency was consistently over 80% (**Figure 2-3**), the flow-through (FT) of the IP reaction was highly enriched for the homotypic AA nucleosomes (referred to as the H2A nucleosomes hereafter) and the IP fraction was enriched for the heterotypic AZ and homotypic ZZ nucleosomes (referred collectively to as the H2A.Z nucleosomes hereafter) (Luk et al., 2010). The DNA extracted from both the FT and IP fractions, as well as the DNA from the input nucleosomes used for the IP, was mapped by deep sequencing.

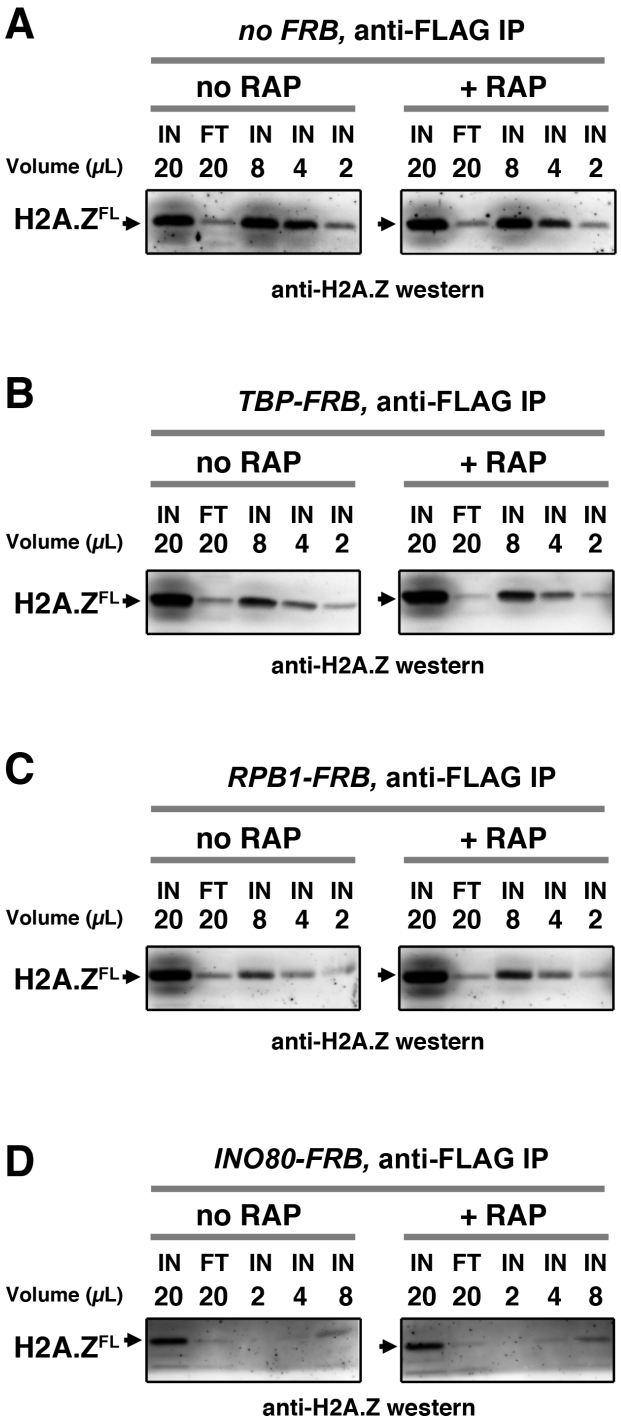

Figure 2-3. Immunoblot analysis to control for anti-FLAG IP efficiency. The nucleosomes used in the IP reactions were prepared from formaldehyde fixed haploid cells expressing the 2xFLAG-epitope tagged Htz1 ($H2A.Z^{FL}$). Nucleosomes were released from crude chromatin by MNase digestion. After centrifugation, the supernatant was filtered through a low-binding PVDF membrane. A sample of the soluble nucleosome was collected as the input (IN) of the IP

reaction. After incubation with anti-FLAG agarose, an equivalent amount of the flow-through fraction (FT) was collected. Both the IN and the FT were heated at 95˚C in SDS-PAGE sample buffer for 30 min to allow decrosslinking before analysis with SDS-PAGE and anti-H2A.Z immunoblotting. Serially diluted samples of the IN fraction were loaded next to the FT lane for comparison. The number above each lane indicates the relative sample volume applied to the gel. Western signal was developed by the ECL Prime reagent (*GE Healthcare*, *Pittsburgh, PA*) and imaged by the ImageQuant FLA4010 imaging system (*GE Healthcare*). Representative western blots for individual IP reactions of both no RAP and + RAP samples are shown for the no *FRB* control in (**A**), *TBP-FRB* in (**B**), and *RPB1-FRB* in (**C**), and *INO80-FRB* in (**D**).

Forty-four reference regions (called no-Z-zones, covering 152,021 bp and 1,161 nucleosomes) with very low H2A.Z but high H2A occupancy were manually chosen and were used to normalize the FT fraction data to the input (**Figure 2-4A**). Depletion of signal in the normalized FT fraction data relative to the input represents the immuno-depleted H2A.Z associated DNA. The amplitude of the H2A.Z data was adjusted using a curve fitting algorithm such that the sum of the normalized profiles of the H2A.Z fraction and FT fraction surrounding the +1 nucleosome region (N = 4,738) equals, to a first approximation, the input profile (Luk et al., 2010) (**Figure 2-4B**). This approach, called quantitative ChIP-seq or qChIP-seq, is similar to ChIP-coupled quantitative PCR (ChIP-qPCR) in that occupancy is reported in relation to the input of each ChIP reaction but is genome-wide. Unlike standard ChIP-seq, which typically involves normalization by equalizing the read counts of ChIP samples and reports ChIP signals in relation to some background or threshold (e.g. mean of genomic ChIP signal) that may vary among samples, the qChIP-seq method allows more quantitative comparison between samples, especially when a global change in H2A.Z occupancy is expected.

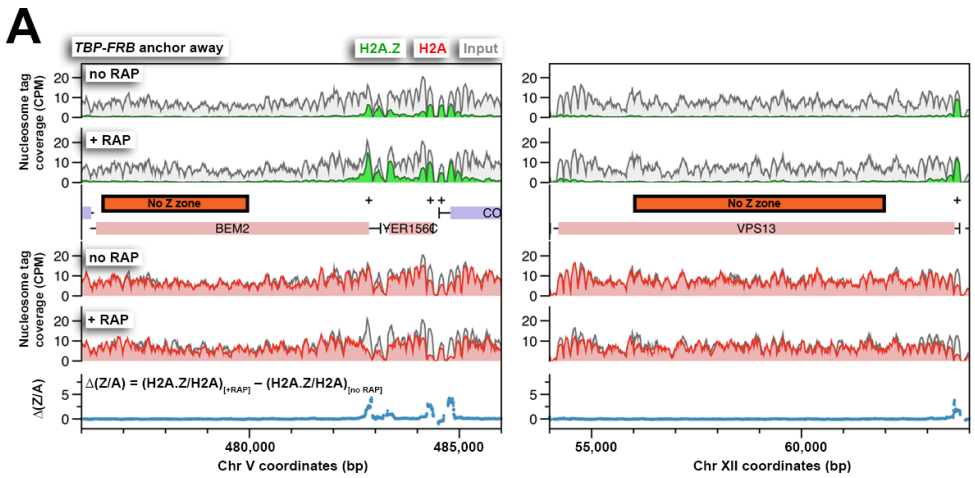
A
TBP-FRB anchor away
H2A.Z
H2A
Input
no RAP
+ RAP
Nucleosome tag coverage (CPM)
No Z zone
BEM2
YER156C
CO
VPS13
Δ(Z/A) = (H2A.Z/H2A)[+RAP] – (H2A.Z/H2A)[no RAP]
480,000
485,000
55,000
60,000
Chr V coordinates (bp)
Chr XII coordinates (bp)

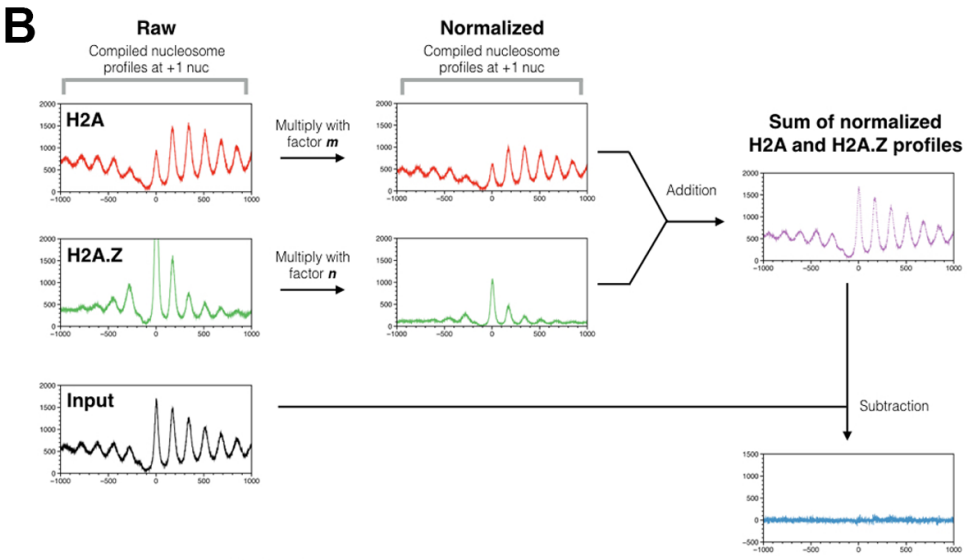
B
Raw
Normalized
Compiled nucleosome profiles at +1 nuc
H2A
H2A.Z
Input
Multiply with factor m
Multiply with factor n
Addition
Sum of normalized H2A and H2A.Z profiles
Subtraction

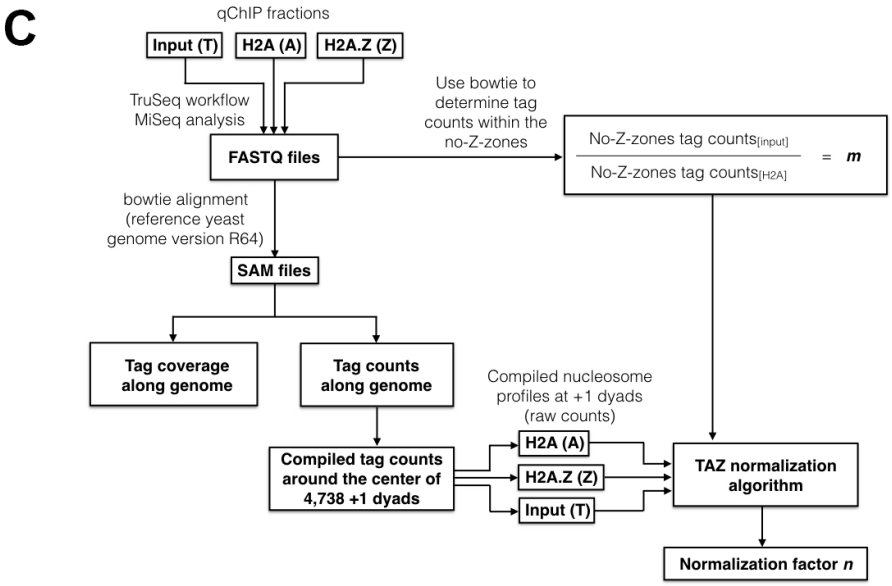
C
qChIP fractions
Input (T)
H2A (A)
H2A.Z (Z)
TruSeq workflow
MiSeq analysis
FASTQ files
Use bowtie to determine tag counts within the no-Z-zones
No-Z-zones tag counts[input] / No-Z-zones tag counts[H2A] = m
bowtie alignment (reference yeast genome version R64)
SAM files
Tag coverage along genome
Tag counts along genome
Compiled tag counts around the center of 4,738 +1 dyads
Compiled nucleosome profiles at +1 dyads (raw counts)
H2A (A)
H2A.Z (Z)
Input (T)
TAZ normalization algorithm
Normalization factor n

Figure 2-4. The strategy used to normalize relative H2A and H2A.Z occupancy. (**A**) Examples of the no-Z-zones used in the normalization of the H2A profile. (**B**) An overview of the 'TAZ' normalization approach used to rescale the H2A.Z and H2A nucleosomal profiles. The compiled tag counts (midpoints) in relation to the distance from the +1 nucleosomal dyads (n = 4,738) were plotted for H2A (A), H2A.Z (Z) and input (T) nucleosomes, which are in *red, green,* and *black*, respectively. To normalize the raw data, the scaling factors, *m* and *n*, were applied to the H2A and H2A.Z profiles respectively. The scaling factor *m* was determined for each IP reaction by dividing the tag count within the no-Z-zones of the input fraction by that of the H2A fraction. The scaling factor *n* was subsequently determined by a curve-fitting algorithm such that the sum of the resulting profiles ($m \times$ H2A + $n \times$ H2A.Z) equals, to a first approximation, the input nucleosomal profile. (**C**) The informatics pipeline of TAZ normalization. The sequencing tags of the H2A, H2A.Z, and input fractions (in FASTQ file format) were mapped to the yeast genome by bowtie (Langmead et al., 2009). Mapped reads were either presented as tag coverage (density covered by paired-end reads) or tag counts (density of mid-points of paired-end reads) along the yeast genome. Bowtie was also used to determine the tag counts within the no-Z-zones in the input and the H2A fractions. The TAZ curve-fitting algorithm is provided in a Python script, which requires four inputs: the scaling factor *m* and the compiled nucleosome profiles of H2A, H2A.Z and input around the +1 dyads. The algorithm generates the scaling factor *n* for normalization of the H2A.Z profile.

2.2. PIC assembly is required for genome-wide H2A.Z eviction at promoters

Using qChIP-seq, the coverage of nucleosomal DNA was determined for the H2A.Z (green), the FT (indicated as H2A in red), and the input (gray) fractions in the *TBP-FRB* haploid strain and the isogenic untagged control strain (*no FRB*). Under permissive conditions (no RAP), H2A.Z was most prevalent at the +1 nucleosomal positions (marked by '+'), less at the -1 positions and progressively less towards the 3' end of genes in agreement with published results (Albert et al., 2007) (**Figures 2-5A** and **2-5B**, *top,* no RAP). This phenomenon is further demonstrated when the H2A.Z and input profiles were compiled at the dyads of 4,738 +1 nucleosomes (**Figures 2-5C** and **2-5D**, *top left*). The FT fraction is a good representation of nucleosomal H2A levels, at least qualitatively, for two reasons. First, although the FT fraction may contain unstable histone-DNA complexes that are devoid of H2A, e.g. tetrasomes, or non-histone complexes (Reja et al., 2015), these structures are highly depleted in these experiments as the chromatin was subjected to extensive MNase digestion (unless indicated otherwise, below). Second, an earlier study that used an anti-H2A antibody to ChIP the FT fraction followed by high-resolution tiling microarray analysis produced an AA nucleosome profile that is highly similar to the FT profiles of our current experiments (Luk et al., 2010) (**Figures 2-5C** and **2-5D**, *bottom left*). Therefore, the qChIP-seq data are consistent with previous conclusions that nucleosomes enriched for H2A dominate in coding regions and that, while depleted at the +1 positions, a substantial amount of H2A nucleosomes remains (**Figures 2-5C** and **2-5D**, *bottom left*) (Luk et al., 2010). The FT profile is referred to as the H2A profile hereafter.

Rapamycin treatment of *TBP-FRB* cells for 1 hour resulted in H2A.Z accumulation at the promoter-proximal nucleosomes of most genes, with a corresponding depletion of H2A signal (compare + RAP and no RAP in **Figures 2-5A** and **2-5C** and in **Figure 2-6A**). Rapamycin

treatment alone did not cause significant change in histone dynamics as the untagged wild-type cells exhibited similar promoter-specific H2A.Z levels before and after rapamycin treatment (**Figures 2-5B** and **2-5D**, **Figure 2-6B**). To confirm that the increase of H2A.Z levels in the *TBP-FRB* strain was not an artifact of normalization, qPCR was employed to measure the immunoprecipitated DNA in the H2A.Z fraction relative to the input at three +1 nucleosome regions and two coding regions. Similar to the sequencing analysis, the qPCR experiments indicated an increase in H2A.Z nucleosomal DNA at +1 nucleosomes after depletion of TBP, with no change observed for DNA located within the open reading frames (ORFs), confirming the robustness of the qChIP-seq approach (**Figure 2-5E**).

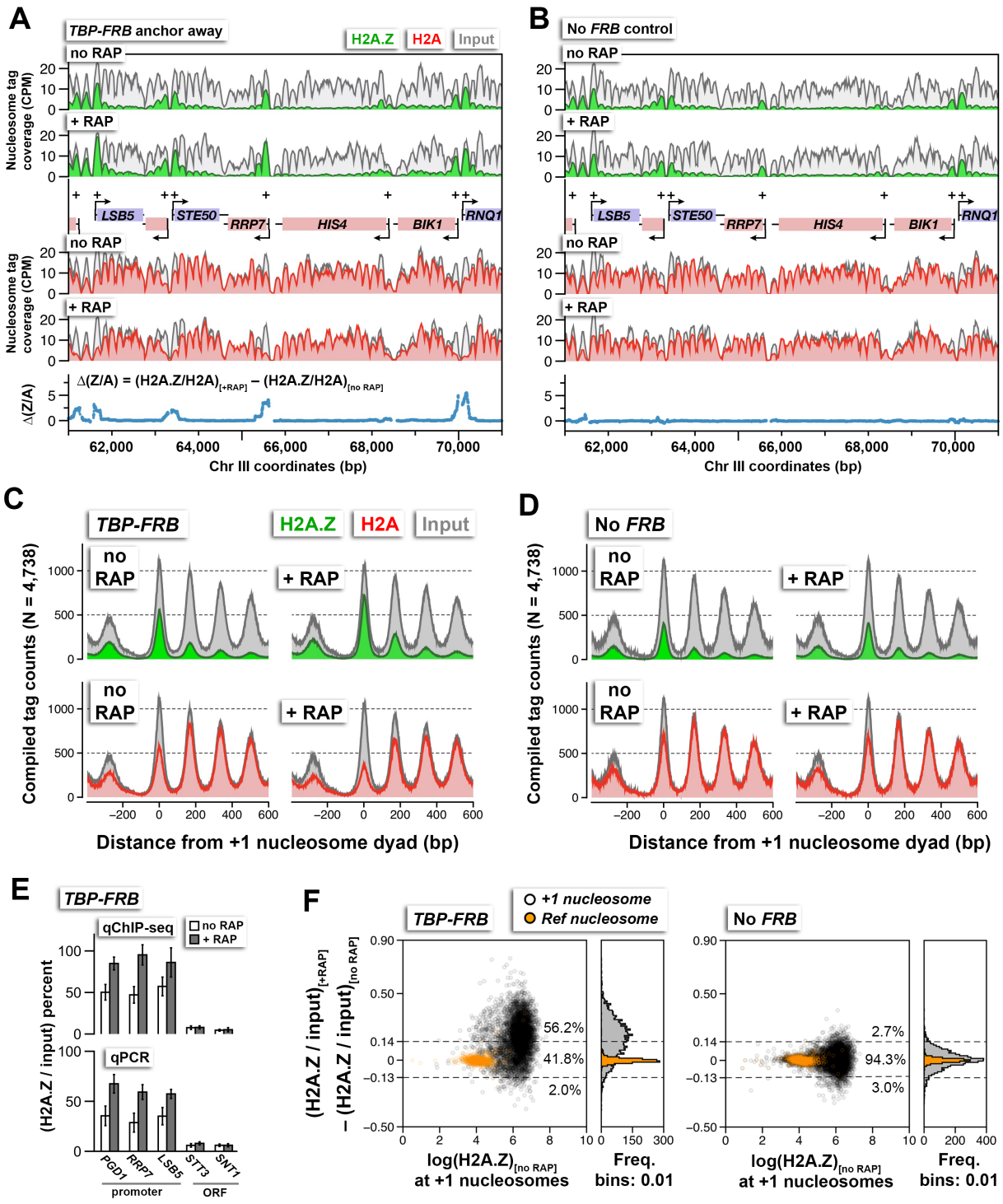

Figure 2-5. H2A.Z nucleosome occupancy determined by qChIP-seq in the TBP-FRB and the untagged control (*no FRB*) strains with and without rapamycin (RAP) treatment. (**A**,**B**) Sequencing tag coverage of H2A.Z (in *green*), FT (indicated as H2A in *red*), and input (in *gray*) at a representative genomic region on chromosome III. Blue traces indicate Δ(Z/A), the difference of the H2A.Z-to-H2A (Z/A) ratio with rapamycin treatment minus that without

treatment. Plus signs and arrowheads mark +1 nucleosomes and transcription start sites, respectively. (**C, D**) Compiled read counts (midpoints) of H2A.Z (*green*), H2A (*red*), and input (*gray*) nucleosomes were centered around the dyad of 4,738 +1 nucleosomes. (**E**) Verification of the qChIP-seq data by qPCR using primer pairs covering the +1 nucleosomes of the indicated promoters and regions within the indicated open reading frames (ORF). (**F**) Scatter plots and histograms showing the change in (H2A.Z/input) of the +1 and reference nucleosomes as a function of endogenous H2A.Z level before rapamycin treatment. The (H2A.Z/input) value was the ratio of H2A.Z tag coverage over input tag coverage within a 120 bp region around the nucleosome dyad. *Open black circles* mark the +1 nucleosomes (Rhee et al., 2014). *Orange dots* mark the reference nucleosomes used for normalization. Dotted lines represent the upper and lower thresholds for significant change in H2A.Z levels, which are defined as two standard deviations from the median of the no *FRB* control. The percentages of data points within and outside the threshold regions are indicated. The qChIP-seq and qPCR data represent averages of 3-5 independent ChIP reactions (technical replicates) of two independent cultures (biological replicates). The error bars in **E** represent standard deviation.

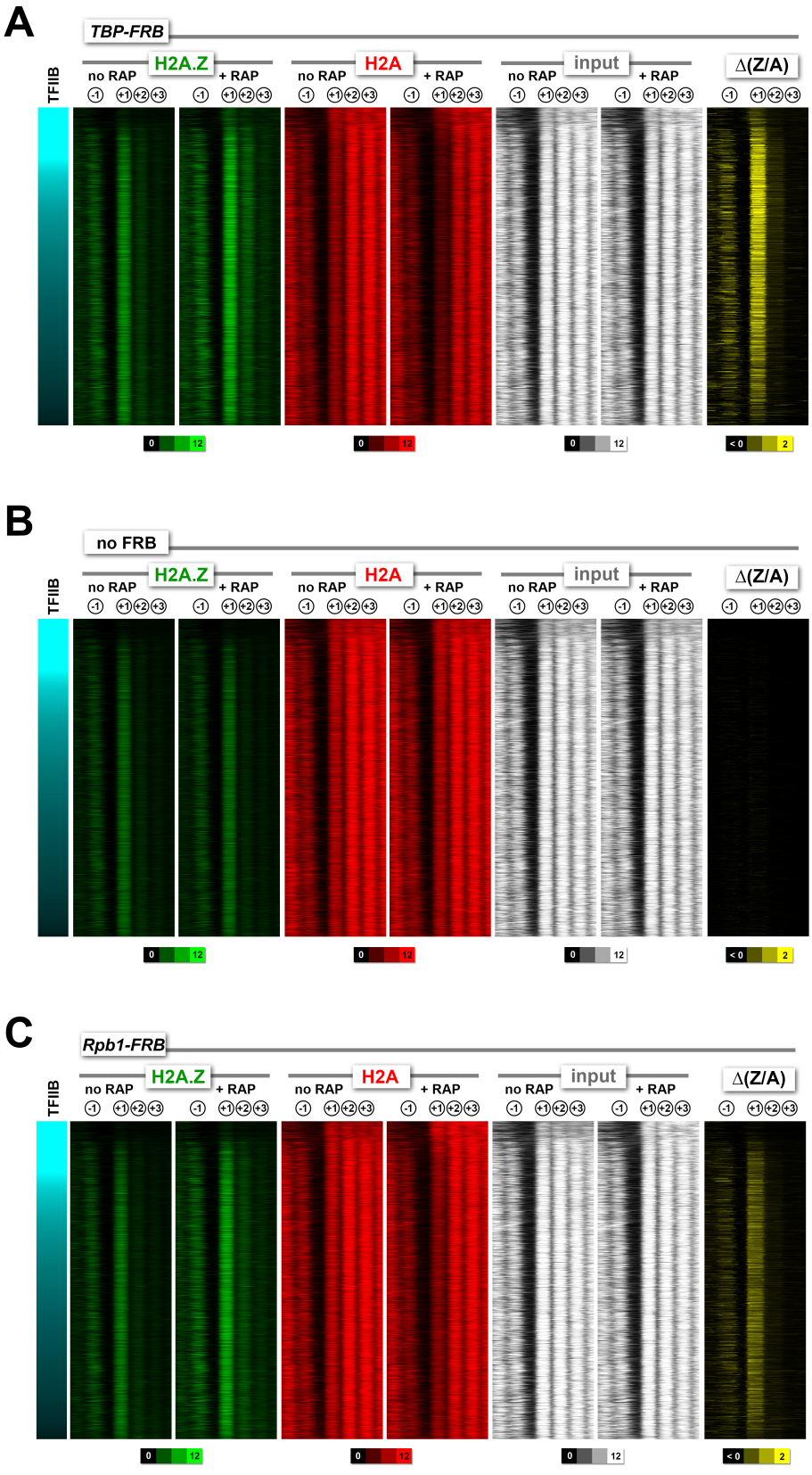
A
TBP-FRB
TFIIB
H2A.Z
H2A
input
Δ(Z/A)
no RAP
+ RAP
-1 +1 +2 +3
0 12
< 0 2
B
no FRB
C
Rpb1-FRB

Figure 2-6. Heatmaps of H2A.Z, H2A and input nucleosomes for the *TBP-FRB*, *no FRB*, and *RPB1-FRB* strains. Nucleosome tag coverage of H2A.Z (in *green*), H2A (in *red*) and input (in *white*) were plotted around the +1 dyads (n = 4,182) for *TBP-FRB* in (**A**), no *FRB* in (**B**) and *RPB1-FRB* in (**C**) before and after rapamycin treatment. Genes were sorted by TFIIB/Sua7 occupancy (Rhee and Pugh, 2012). **Christy Au** performed the qChIP-seq experiment for one of the biological replicates of *RPB1-FRB*.

To evaluate the H2A.Z change at the +1 positions genome-wide, the change in (H2A.Z/input) ratios at 4,738 +1 nucleosomes after TBP depletion {i.e. $(H2A.Z/input)_{[RAP]} - (H2A.Z/input)_{[no\ RAP]}$} was plotted against the endogenous H2A.Z levels represented by the logarithmically transformed H2A.Z tag counts before rapamycin treatment (**Figure 2-5F**). A threshold for significant change in (H2A.Z/input) was defined by two standard deviations above and below the median of the untagged control (**Figure 2-5F**, dotted lines). The change in (H2A.Z/input) values of the reference nucleosomes used in normalization was plotted for comparison (**Figure 2-5F**, *orange dots*). Fifty-six percent of +1 nucleosomes exhibited a significant increase in relative H2A.Z signal upon TBP depletion (**Figure 2-5F**). The (H2A.Z/input) signals of the two biological replicates were highly reproducible (**Figures 2-7A** and **2-7B**). Note the global shift of data points towards the upper right quadrant in the +RAP data as compared to the no RAP sample, indicating a global increase of relative H2A.Z in both biological replicates (compare **Figures 2-7A** and **2-7B**). By contrast, a similar shift of data points towards the upper right quadrant was not observed for the no FRB control (**Figures 2-7C** and **2-7D**).

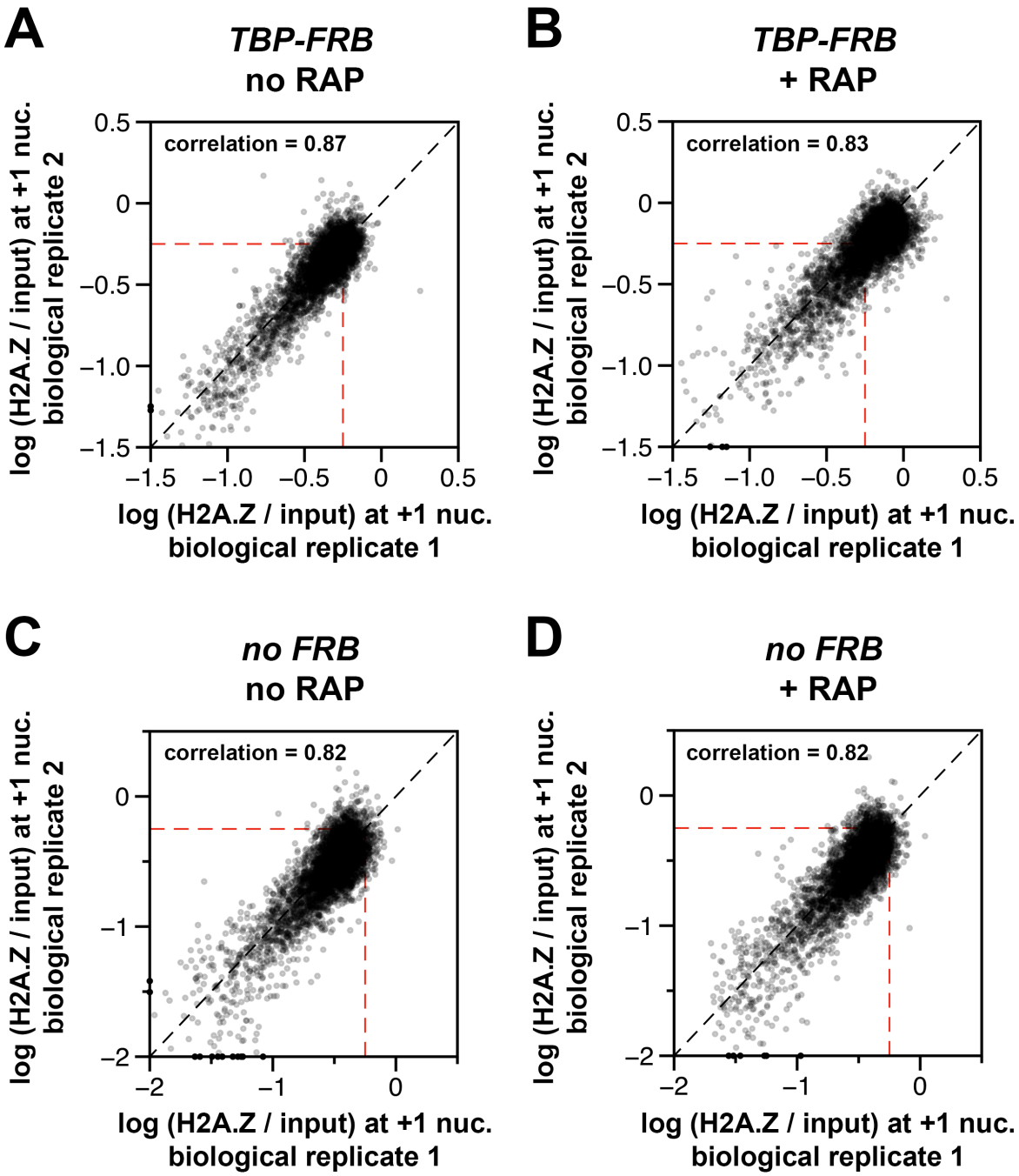

Figure 2-7. Concordance of relative H2A.Z occupancy between biological replicates. The (H2A.Z/input) signals of the biological replicates at the +1 nucleosomal positions ((Rhee et al., 2014), n = 4,738) were plotted against each other for *TBP-FRB,* no RAP in (**A**), *TBP-FRB,* + RAP in (**B**), no *FRB*, no RAP in (**C**), and no *FRB*, + RAP in (**D**). The biological replicates represent independent yeast cultures. *Dotted red lines*: arbitrary reference perimeter set at -0.25 on both axes.

It is noteworthy that under the permissive condition, the *TBP-FRB* strain exhibited a higher endogenous H2A.Z occupancy compared to the untagged strain (compare no RAP in **Figures 2-5C** and **2-5D** and in **Figures 2-7A** and **2-7C**). The difference likely reflects a partial defect of the *TBP-FRB* allele that has predisposed the cells to H2A.Z accumulation. But importantly, the measurement of *change* in the (H2A.Z/input) ratio (**Figure 2-5F**) normalizes any differences in the ground state (no RAP) and highlights the functional consequence of the depletion of TBP or other factors in question (below).

The change in (H2A.Z/H2A) ratios {i.e. $(H2A.Z/H2A)_{[RAP]} - (H2A.Z/H2A)_{[no\ RAP]}$}, which is referred to as Δ(Z/A) hereafter, provides an even more sensitive, nonetheless non-linear, indicator of H2A.Z dynamics because of the antagonistic change in H2A.Z and H2A occupancy. As shown in **Figure 2-8A**, 72% +1 nucleosomes exhibited an increase in Δ(Z/A) signal upon TBP depletion. When the Δ(Z/A) values were plotted along the chromosome coordinates, this parameter clearly identified sites with strong H2A.Z dynamics (**Figures 2-5A** and **2-5B**, *blue traces*). The Δ(Z/A) parameter will later be used to identify novel transcription start sites.

To test if depletion of another component of the PIC could also lead to H2A.Z accumulation, we targeted Rpb1, the largest subunit of Pol II, for nuclear depletion by anchor-away. The *RBP1-FRB* construct has previously been shown to effectively shut off transcription (Haruki et al., 2008). Similar to the results of TBP-FRB removal, nuclear depletion of Rpb1-FRB led to strong H2A.Z accumulation and H2A depletion at most promoters (**Figure 2-9 and Figure 2-6C**).

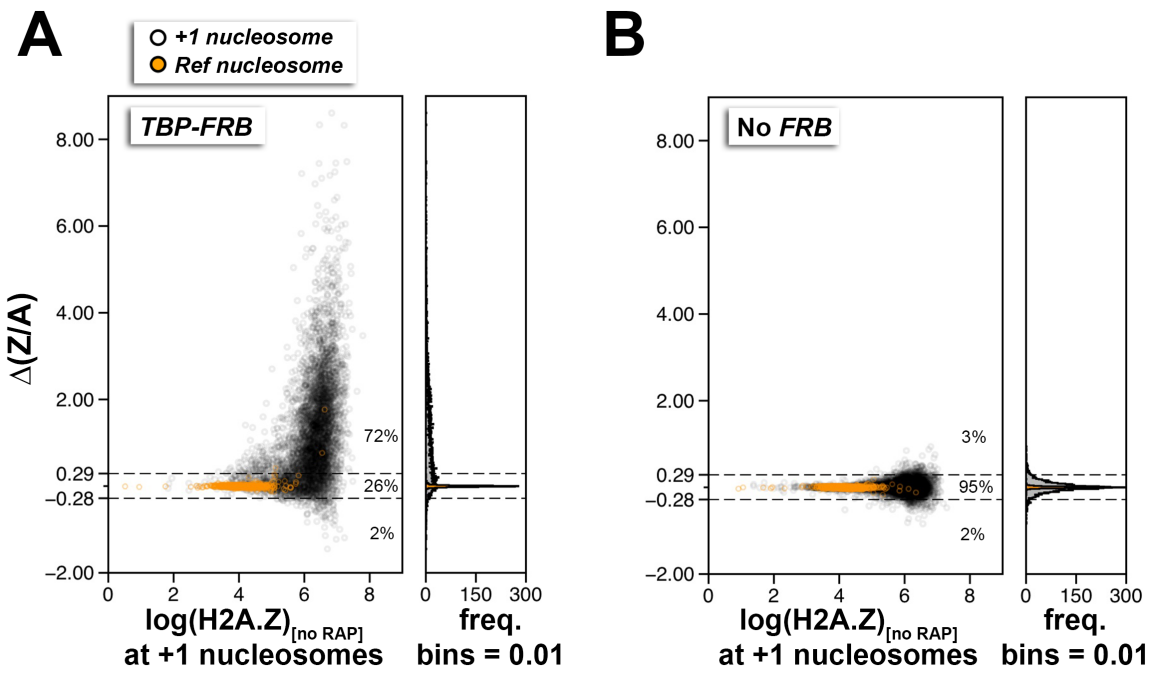

Figure 2-8. Using Δ(Z/A) as a parameter to identify +1 nucleosomes with PIC-dependent H2A.Z eviction. (**A, B**) Scatter plots and histograms showing the Δ(Z/A) values of +1 or reference nucleosomes as a function of endogenous H2A.Z level (before rapamycin treatment) for the *TBP-FRB* and the no FRB control, respectively. *Gray dots* mark the +1 nucleosomes. *Orange dots* mark the reference nucleosomes used for normalization. Dotted lines represent the upper and lower thresholds for significant change in H2A.Z levels, which are defined as two standard deviations from the median of the no *FRB* control. The percentages of data points within and outside the threshold regions are indicated.

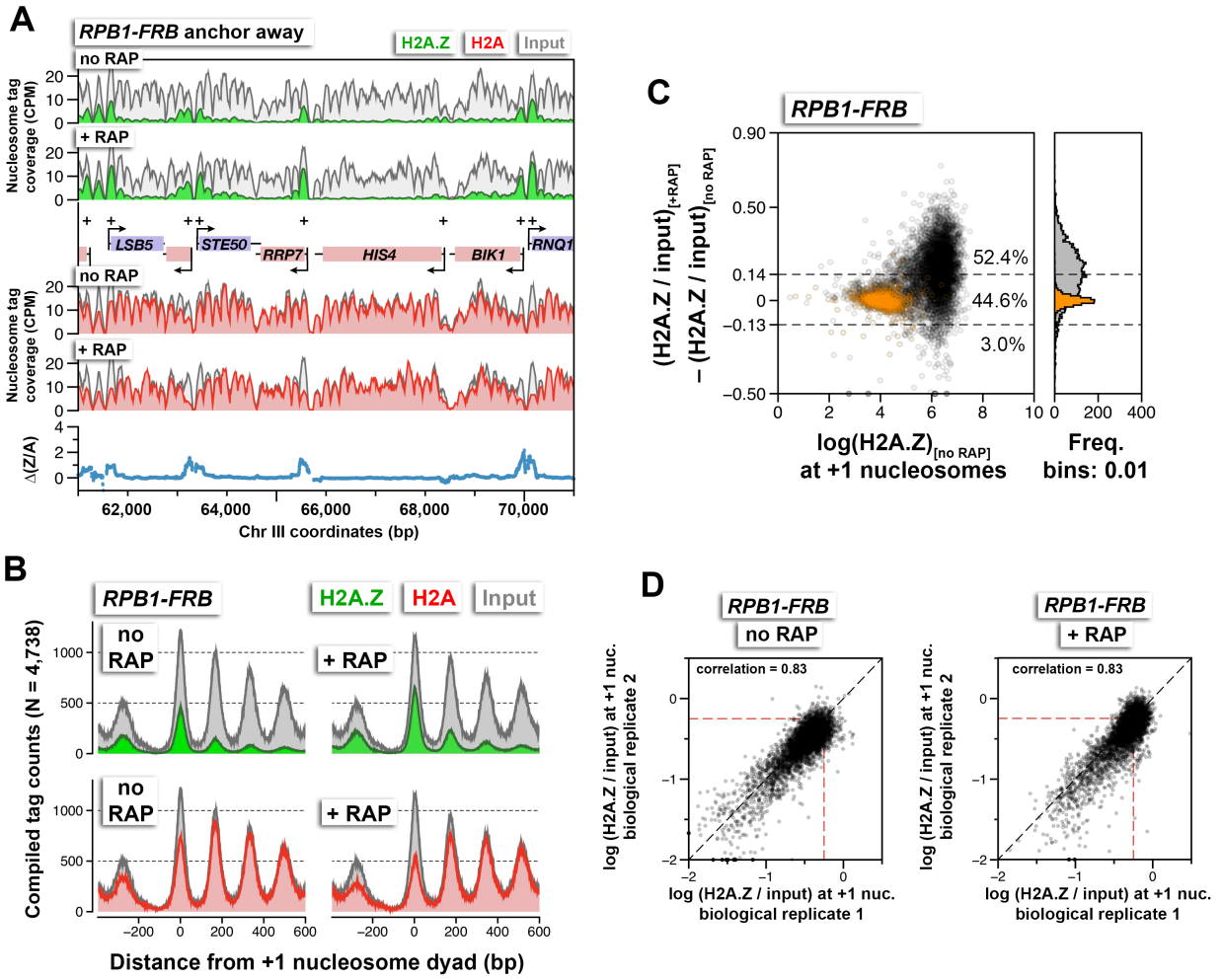

Figure 2-9. Relative H2A.Z occupancy before and after Rpb1 depletion. (**A**) Sequencing tag coverage of H2A.Z (in *green*), FT (indicated as H2A in *red*), and input (in *gray*) at a representative genomic region on chromosome III. Blue traces indicate Δ(Z/A), the difference of the H2A.Z-to-H2A (Z/A) ratio with rapamycin treatment minus that without treatment. Plus signs and arrowheads mark +1 nucleosomes and transcription start sites, respectively. (**B**) Compiled read counts (midpoints) of H2A.Z (in *green*), H2A (in *red*), and input (in *gray*) nucleosomes were centered around the dyad of 4,738 +1 nucleosomes. (**C**) Scatter plots and histograms showing the change in (H2A.Z/input) of the +1 or reference nucleosomes as a function of endogenous H2A.Z level. *Gray circles* mark the +1 nucleosomes. *Orange filled circles* mark the reference nucleosomes. Dotted lines are the upper and lower thresholds for significant change in H2A.Z levels. All data in **A-C** represent averages of two biological replicates. **Christy Au** performed the qChIP-seq experiment for one of the biological replicates of *RPB1-FRB* (**D**) Scatter plots showing the log(H2A.Z/input) data of +1 nucleosomes in the two biological replicates with or without rapamycin treatment.

2.3. H2A.Z accumulation in response to PIC depletion is not due to aberrant accumulation of the SWR1 complex

One explanation for the increase in H2A.Z levels at the +1 promoter upon TBP depletion is that the balance between H2A.Z eviction and deposition of H2A.Z nucleosomes by SWR1 has been disrupted. SWR1 continues to convert H2A nucleosomes to the H2A.Z containing forms but with no eviction to restore these nucleosomes back to the AA state in the absence of the PIC. Consistent with this idea, sites with strong H2A.Z dynamics are more enriched for endogenous SWR1 (**Figure 2-10A**). An alternative explanation for this phenomenon, however, is that TBP depletion does not block H2A.Z eviction but instead leads to recruitment of aberrantly high levels of SWR1 to promoters as the PICs dissociate. This model predicts that SWR1 levels should increase at promoters upon TBP depletion. To distinguish between these two possibilities, ChIP-qPCR was used to monitor the occupancy of the Swr1 subunit in the *TBP-FRB* strain at different times after rapamycin treatment. The promoter regions of *SWR1* itself and *FUN12* were chosen because these sites are known to be enriched for SWR1 (Ranjan et al., 2013; Yoshida et al., 2010) and exhibited strong changes in H2A.Z dynamics upon TBP depletion (**Figure 2-10B**). Rather than accumulating at the promoters of these two genes, SWR1 dissociated shortly after TBP-FRB depletion as demonstrated by the decrease in Swr1 ChIP signal (**Figure 2-10C**, experiment performed by **Christy Au**). This observation supports the idea that the PIC is required to actively evict H2A.Z nucleosomes. In addition, the coincidental accumulation of H2A.Z and depletion of SWR1 suggest that endogenous SWR1 dissociates from promoters after depositing H2A.Z. This is in agreement with the *in vitro* observation that SWR1 has a lower affinity for the homotypic H2A.Z nucleosome product than the homotypic H2A nucleosome substrate (Ranjan et al., 2015).

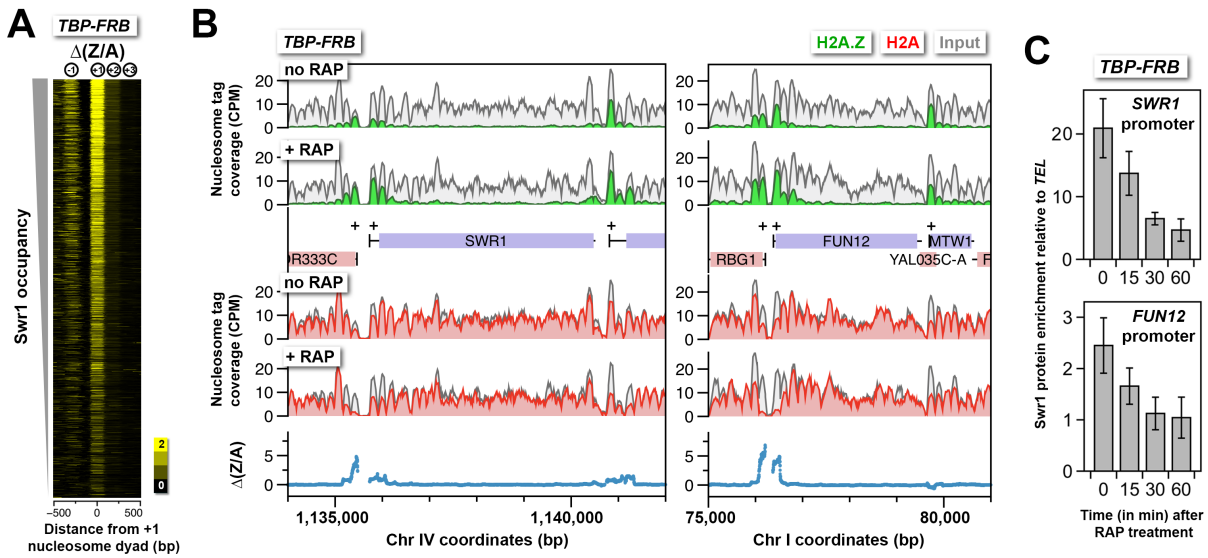

Figure 2-10. H2A.Z accumulation is not due to aberrant accumulation of the SWR1 complex. (**A**) A heat map showing the Δ(Z/A) after nuclear depletion of TBP-FRB. The regions were sorted by endogenous SWR1 occupancy and centered at the +1 dyads (n = 4,738) (Venters and Pugh, 2009). (**B**) Sequencing tag coverage of H2A.Z, H2A and input nucleosomes surrounding the *SWR1* and *FUN12* genes. (**C**) ChIP-qPCR analysis was performed using an antibody directed against Swr1 and primers targeting the promoters of *SWR1* and *FUN12* relative to a control region near *TEL6R* (Ranjan et al., 2013). Swr1 enrichment values represent the mean of four independent ChIP reactions from two biological replicates. Error bars: standard deviation. **Christy Au** performed the ChIP-qPCR experiment and analysis shown in (**C**).

2.4. Constitutive PIC-dependent H2A.Z eviction is associated with promoters of active and infrequently transcribed genes that are generally TFIID enriched

Yeast promoters that are TFIID-enriched or -depleted are apparently regulated by different mechanisms (Rhee and Pugh, 2012). Although both types of promoters require TBP for transcription, TFIID-enriched genes are often TATA-less and associated with a more open NDR, whereas TFIID-depleted promoters generally contain a consensus TATA element and are more covered with nucleosomes and more enriched with the SAGA complex (Basehoar et al., 2004; Rhee and Pugh, 2012). To see if the +1 nucleosomes at these two types of promoters exhibit differential H2A.Z dynamics, the occupancy of H2A, H2A.Z and input nucleosomes, and the corresponding Δ(Z/A) values, before and after rapamycin treatment were sorted by TFIID enrichment and transcript abundance (Lipson et al., 2009; Rhee and Pugh, 2012). As seen in **Figure 2-11A**, the +1 nucleosomes that exhibited stronger H2A.Z accumulation after TBP depletion are generally more enriched for TFIID.

The ribosomal protein (RP) genes are regulated by TFIID and are among the most highly transcribed (Rhee and Pugh, 2012; Warner, 1999). Their promoters are unusual in that the endogenous +1 nucleosomes are generally depleted for H2A.Z but relatively enriched for H2A (**Figure 2-11B,** n = 128). Upon depletion of TBP, relative H2A.Z accumulates dramatically at the +1 position (**Figure 2-11B**, *green*). The data suggest that H2A.Z deposition occurs at the RP gene promoters but that H2A.Z nucleosomes are quickly removed by a mechanism that is dependent on TBP, leading to a low steady-state H2A.Z occupancy. Interestingly, Rpb1 depletion led to almost no change in H2A.Z occupancy at the +1 nucleosomes of RP genes (**Figure 2-12**). Since RP genes promoters are occupied by high level of PIC components

(indicated by the TFIIB marker Sua7), partial PIC may remain bound after Rpb1 depletion. This suggests that H2A.Z removal at the RP genes requires TBP but not Pol II.

To further understand the link between transcriptional activity and H2A.Z dynamics, the +1 H2A.Z occupancy of 4,267 promoters before and after TBP depletion was sorted and grouped by the transcriptional frequency of their downstream genes and compared by box plot analysis (**Figure 2-11C**) (Holstege et al., 1998). Before TBP-depletion, the +1 nucleosomes associated with moderately or infrequently transcribing genes exhibited >40% (median) relative H2A.Z occupancy for genes with <16 mRNA/hr (n = 3,887) and ~30% (median) for those with 16-50 mRNA/hr (n = 219). For the top 3% of most highly transcribing genes (>50 mRNA/hr, n = 161) the steady-state H2A.Z occupancy is ~11% (median) before TBP-depletion. Upon rapamycin treatment, substantial increase of relative H2A.Z occupancy is observed in all groups (**Figure 2-11C**). The increase is more dramatic in the most highly transcribing genes, suggesting that the low steady-state H2A.Z occupancy is due to strong transcriptional activity (**Figure 2-11C**, >50 mRNA/hr). Interestingly, when these highly transcribing genes were sorted based on the enrichment of SAGA or TFIID (Basehoar et al., 2004), H2A.Z accumulated to a smaller extent for the SAGA-enriched genes than for the TFIID-enriched genes (**Figure 2-11C**, right). Therefore, unlike the strong TFIID-enriched promoters where low steady-state +1 H2A.Z level is due to robust PIC-dependent H2A.Z eviction activity, low H2A.Z at the strong SAGA-enriched promoters is due to either strong PIC-independent eviction or weak SWR1-mediated H2A.Z deposition or both.

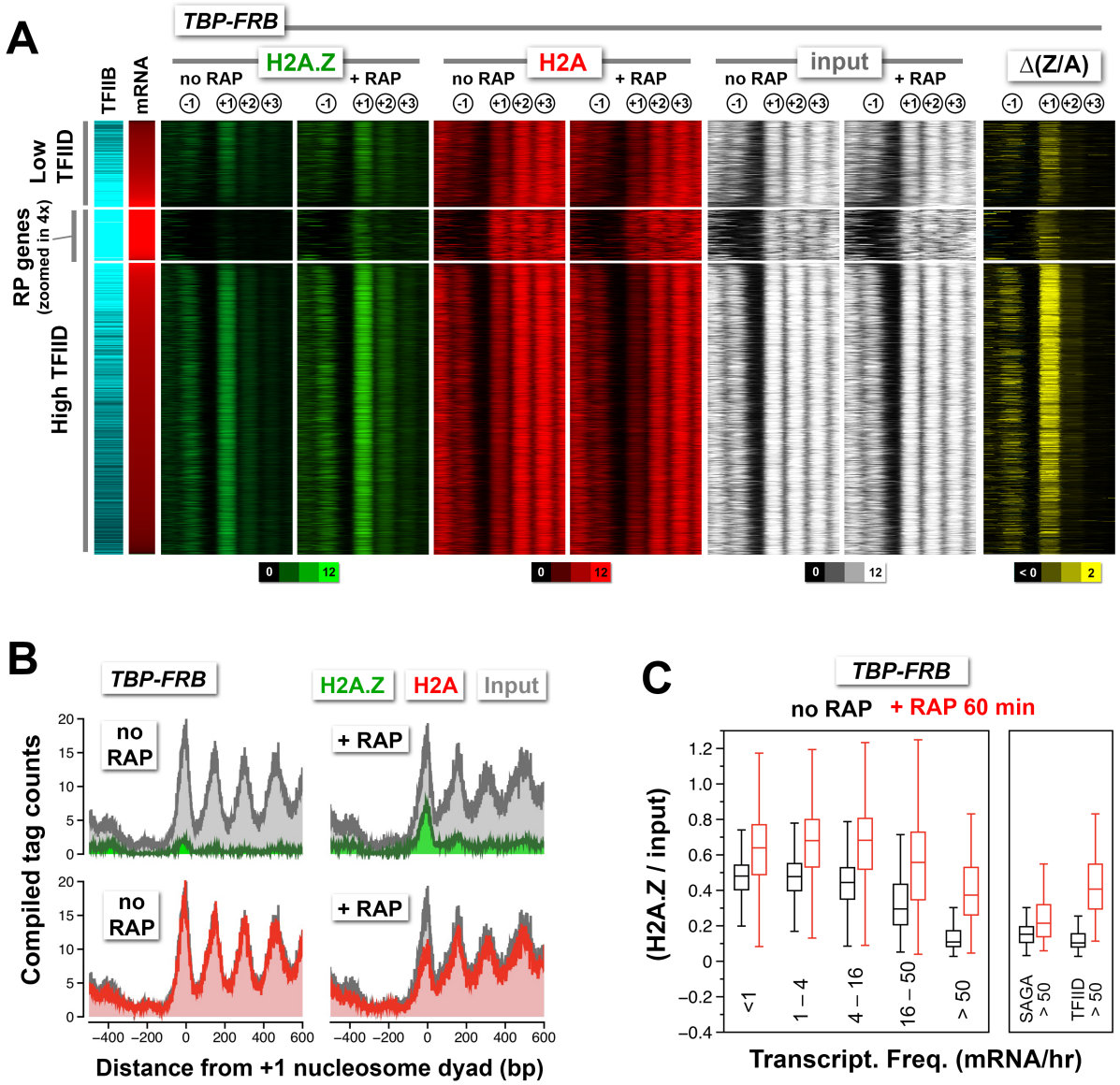

Figure 2-11. Change in nucleosomal H2A.Z and H2A levels near promoters before and after depletion of TBP. (**A**) Heatmaps showing the average normalized tag coverage of H2A.Z (*green*), H2A (*red*) and input (*white*), and the corresponding Δ(Z/A) values (*yellow*) around the +1 dyads of the *TBP-FRB* strain with and without rapamycin treatment. Promoters enriched for the PIC (based on Sua7 occupancy) were grouped into high and low TFIID (based on Taf1 occupancy) and were then sorted by mRNA abundance (n = 3,919) (Lipson et al., 2009; Rhee and Pugh, 2012). The ribosomal protein (RP) genes (n = 128) are "zoomed in 4x" meaning that the line thickness is 4 times of the other genes . (**B**) Compiled nucleosome tag counts of H2A.Z (green), H2A (red), and input (gray) around the +1 dyads of the RP genes. (**C**) The +1 nucleosomes were grouped according to transcriptional frequency (Holstege et al., 1998) and the (H2A.Z/input) values were presented as box plots. *Box*: interquartile range (IQR); *line in box*: median; *whiskers*: range. The most active genes (>50 mRNA/hr) were sub-divided into two groups that are SAGA- or TFIID-enriched. The number of +1 nucleosomes in the transcriptional

frequency groups <1, 1-4, 4-16, 16-50, and >50 mRNA/hr are 937, 1932, 1018, 219 and 161, respectively. There are 22 promoters in the SAGA >50 group and 130 in the TFIID >50 group.

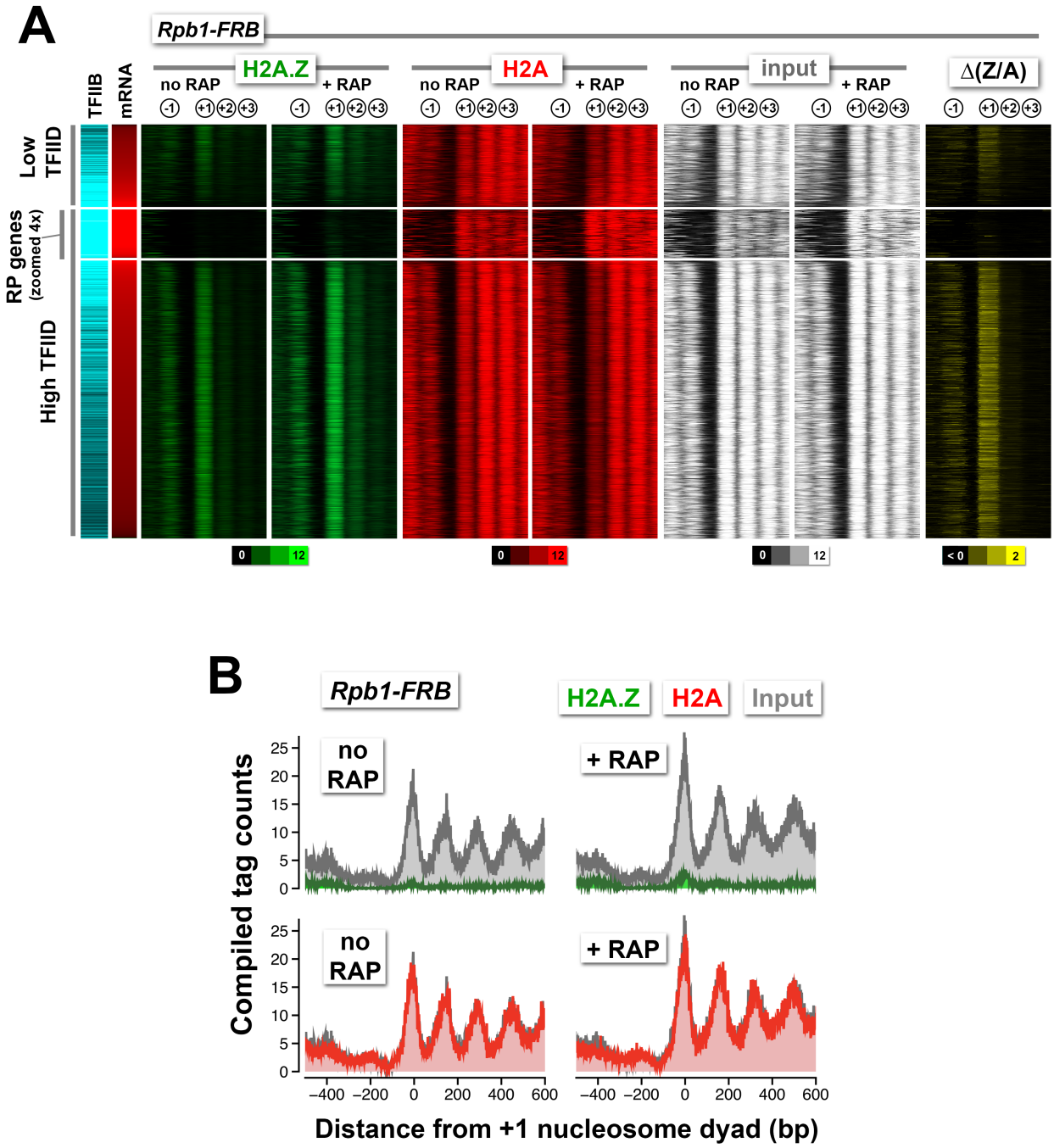

Figure 2-12. Normalized nucleosome tag coverage for H2A.Z, H2A, and input before and after the depletion of Rpb1. (**A**) Heatmaps were plotted and sorted by TFIID/Taf1 as described in **Figure 2-11A.** (**B**) Compiled tag counts of the RP genes. **Christy Au** performed the qChIP-seq experiment for one of the biological replicates of *RPB1-FRB*.

An alternative approach to monitor H2A.Z eviction is to conditionally block H2A.Z deposition and follow the depletion of H2A.Z. Since SWR1-mediated H2A.Z deposition requires Swc5, a subunit of the SWR1 complex (Wu et al., 2005), anchor-away was utilized to deplete Swc5 so as to conditionally block H2A.Z deposition. SWR1 activity of the *SWC5-FRB* strain was strongly inhibited after 30 minutes of rapamycin treatment as demonstrated by the robust loss of H2A.Z occupancy (**Figures 2-13A** and **2-13B** and **Figures 2-14A** and **2-14B**). When the relative H2A.Z levels (H2A.Z/input) of the +1 nucleosomes were sorted and grouped by the transcriptional frequency of the downstream genes, almost background level of H2A.Z was observed in all groups, indicating that robust, constitutive H2A.Z eviction at the +1 position occurs at both active and infrequently transcribed genes (**Figure 2-13C**). To further understand how fast is the eviction of H2A.Z, relative H2A.Z levels were measured at various time points after Swc5 depletion (**Figure 2-15**, experiment performed by **Lu Sun**). At most +1 positions, relative H2A.Z levels dropped below 50% of endogenous levels after 15 minutes of rapamycin treatment, indicating that the occupancy half-life of H2A.Z is less than 15 minutes. Since virtually baseline level of H2A.Z remains after 60 minutes of rapamycin treatment (**Figure 2-15**, *red,* experiment performed by **Lu Sun**), the data also suggest that SWR1 is the sole deposition pathway of H2A.Z at budding yeast promoters.

Next, we tested whether TBP-FRB depletion can slow H2A.Z eviction while the H2A.Z deposition activity of SWR1 is inhibited. Consistent with the idea that the PIC is required for H2A.Z eviction, depleting both TBP and Swc5 in the double mutant resulted in a less dramatic decrease in relative H2A.Z occupancy at most +1 nucleosomes as compared to the single *SWC5-FRB* mutant for the same duration (i.e. 30 minutes) of rapamycin treatment (**Figures 2-13D** and **2-13F** and **Figures 2-14C** and **2-14D**). It is noteworthy that TBP depletion did not completely

prevent the decrease of H2A.Z caused by Swc5 depletion. One explanation is that the kinetics of TBP depletion by anchor away is slower than that of Swc5. Alternatively, a PIC-independent H2A.Z eviction pathway might be operating.

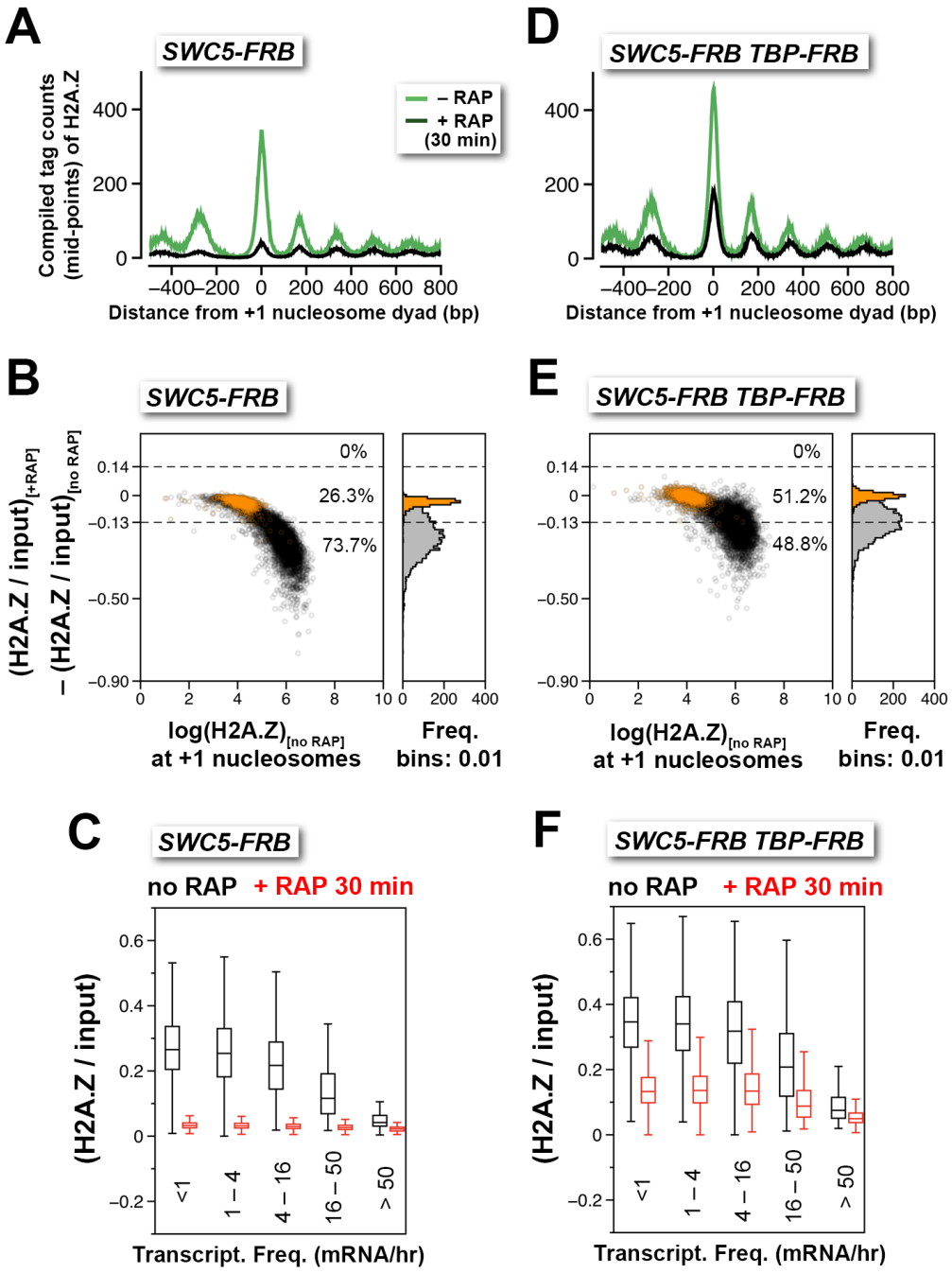

Figure 2-13. Depletion of Swc5 revealed rapid PIC-dependent eviction of H2A.Z at the +1 nucleosome of active and infrequently transcribed genes. (**A**) Compiled tag counts of H2A.Z nucleosomes around the +1 dyads in the *SWC5-FRB* strain before and after 30 min of rapamycin treatment. (**B**) Scatter plot analysis showing the change in relative H2A.Z occupancy against endogenous H2A.Z level in the *SWC5-FRB* strain at the +1 nucleosomes (n = 4,738) after 30 minutes of rapamycin treatment. *Gray*: +1 nucleosomes. *Orange*: reference nucleosomes depleted for H2A.Z. (**C**) Same as **Figure 2C**, except the *SWC5-FRB* strain was used. (**D-F**) Same as **A-C**, except the *SWC5-FRB TBP-FRB* strain was used.

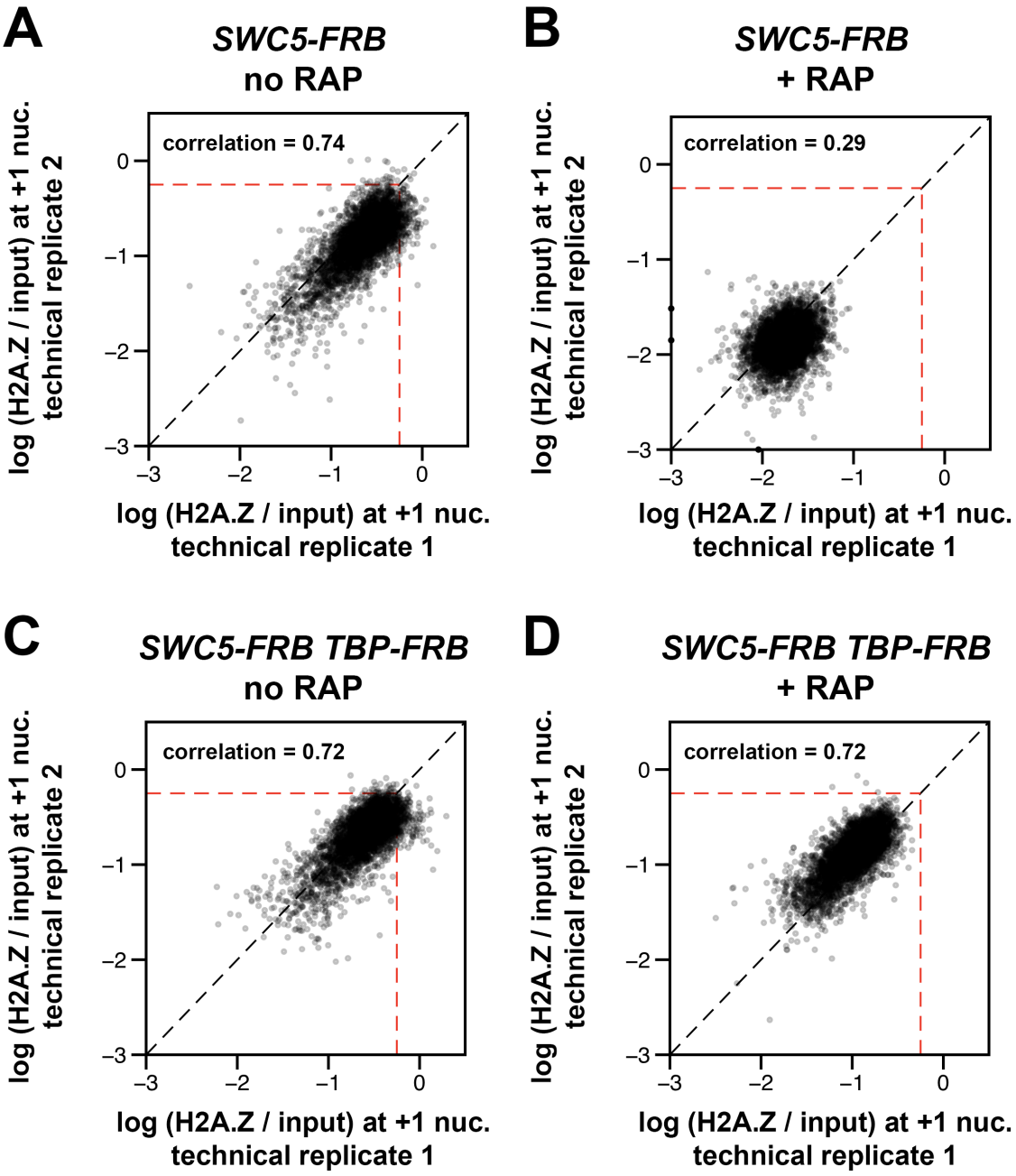

Figure 2-14. Concordance of relative H2A.Z occupancy between technical replicates (independent IP reactions). The +1 nucleosome log(H2A.Z/input) values for the replicates of *SWC5-FRB* and *SWC5-FRB TBP-FRB* were plotted as described in **Figure 2-7**. +RAP: Rapamycin treatment for 30 min. *Dotted red lines*: arbitrary reference perimeter set at -0.25 on both axes.

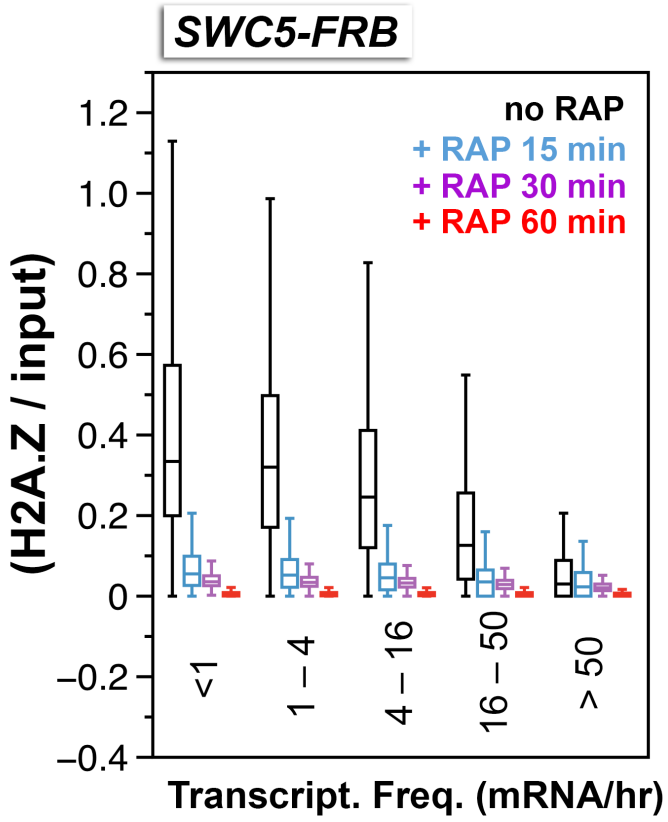

Figure 2-15. Relative H2A.Z occupancy at the +1 nucleosomes of the *SWC5-FRB* strain at different times of rapamycin treatment. Same as **Figure 2-13C** except additional time points after rapamycin treatment were included. The data shown in this figure was provided by **Lu Sun**.

2.5. INO80 cannot account for bulk H2A.Z dynamics

The INO80 complex has been reported to catalyze the reverse H2A.Z replacement reaction in which nucleosomal H2A.Z-H2B dimers are replaced with free H2A-H2B dimers (Papamichos-Chronakis et al., 2011). Therefore, inactivation of the *INO80* gene (which encodes the catalytic core subunit of the INO80 complex) in cells with intact SWR1 activity is expected to accumulate H2A.Z. Endogenous *INO80* was fused to a tandem *FRB-GFP* tag to allow conditional depletion by anchor-away and visualization by fluorescence microscopy. Mutants defective for *INO80* function are hypersensitive to hydroxyurea (Shen et al., 2003). Cells with *INO80-FRB-GFP* (referred to as *INO80-FRB* hereafter) exhibited slow growth in medium containing both hydroxyurea and rapamycin but not hydroxyurea alone, confirming that *INO80* function can be abolished in a rapamycin-dependent manner (**Figure 2-16A**). As expected, in the absence of rapamycin, Ino80 was found in the nucleus (Huh et al., 2003) (**Figures 2-16B** and **2-16C** at 0 min +RAP). After 90 minutes of rapamycin treatment, Ino80 was largely dispersed from the nuclei (**Figure 2-16C**). These cells were then fixed by formaldehyde crosslinking and the H2A.Z and H2A levels were measured by qChIP-seq. No significant global increase of H2A.Z was observed after Ino80 depletion (**Figures 2-17A-C** and **Figure 2-16D**). Instead, nucleosomal arrays became "fuzzier" as demonstrated by the general decrease of nucleosomal peak height and the decrease of valley depth at the linker regions (**Figure 2-17D**, top). By contrast, in the untagged control (*no FRB*), the density and positions of the nucleosomal arrays before and after rapamycin treatment were unchanged (**Figure 2-17D**, middle). Using the difference in nucleosomal density within the linker region between +1 and +2 as a criterion for fuzziness, the chromatin arrays of 983 genes that require Ino80 for positioning were identified by clustering analysis (k = 3). The compiled chromatin arrays of these promoters showed, upon

Ino80 depletion, the -1 and +1 nucleosomes shifted away from the NDR (**Figure 2-17D**, bottom). Importantly, the direction of shift at these nucleosomal positions are consistent with the published results of *ino80*Δ and are reproducible in both biological replicates (Yen et al., 2012) (**Figure 2-16E**). Overall, our data are in agreement with the INO80 remodeler functioning as a histone octamer slider but not an evictor of H2A.Z nucleosomes *in vivo* (Jeronimo et al., 2015; Shen et al., 2003; Yao et al., 2016; Yen et al., 2012).

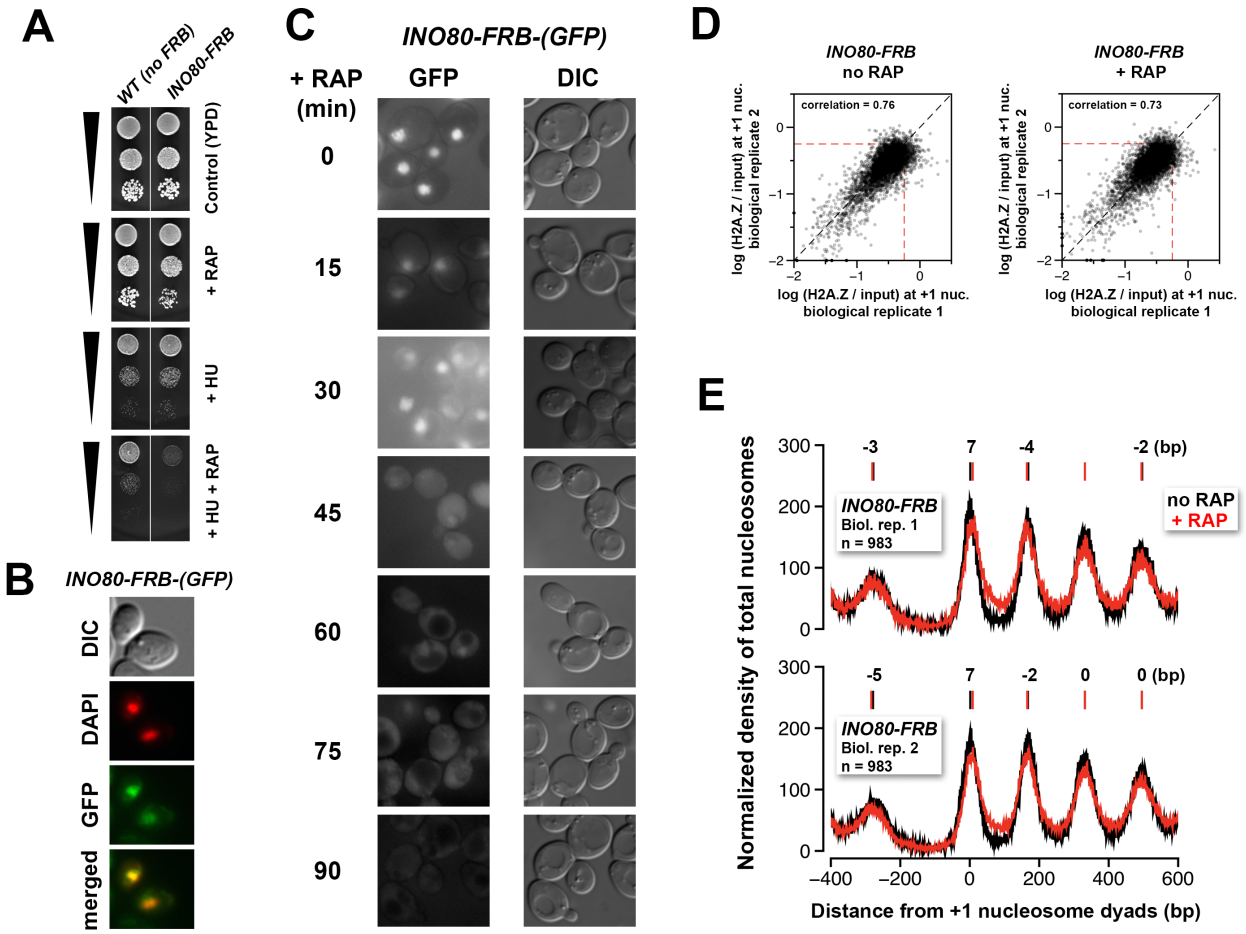

Figure 2-16. Verification of the conditional depletion of Ino80-FRB and concordance of biological replicates. (**A**) Spotting assay of the anchor-away strain bearing the *INO80-FRB* allele, which is fused in-frame with the GFP gene, and the isogenic untagged (no FRB) control in the presence or absence of 100 mM hydroxyurea (HU) and/or 1 µg/mL rapamycin. (**B**) Fluorescence microscopy of fixed yeast cells expressing the *INO80-FRB-(GFP)* construct. The cells were fixed with 4% formaldehyde for 5 min before they were washed with PBS and stained with DAPI (red). (**C**) Fluorescence microscopy of live cells expressing *INO80-FRB-(GFP)* before and after various times of rapamycin treatment. DIC: differential interference contrast optics. (**D**) Scatter plots showing the log(H2A.Z/input) data of +1 nucleosomes in the two biological replicates with or without rapamycin treatment. (**E**) Compiled input nucleosome profiles in *INO80-FRB* before (*black*) and after (*red*) rapamycin treatment of the two biological replicates. The integers above the nucleosomal peaks indicate the shift distance of the peaks after rapamycin treatment. Positive values indicate right-shift and *vice versa*. Peak center positions were determined by curve fitting with a Gaussian model followed local maximum calculation.

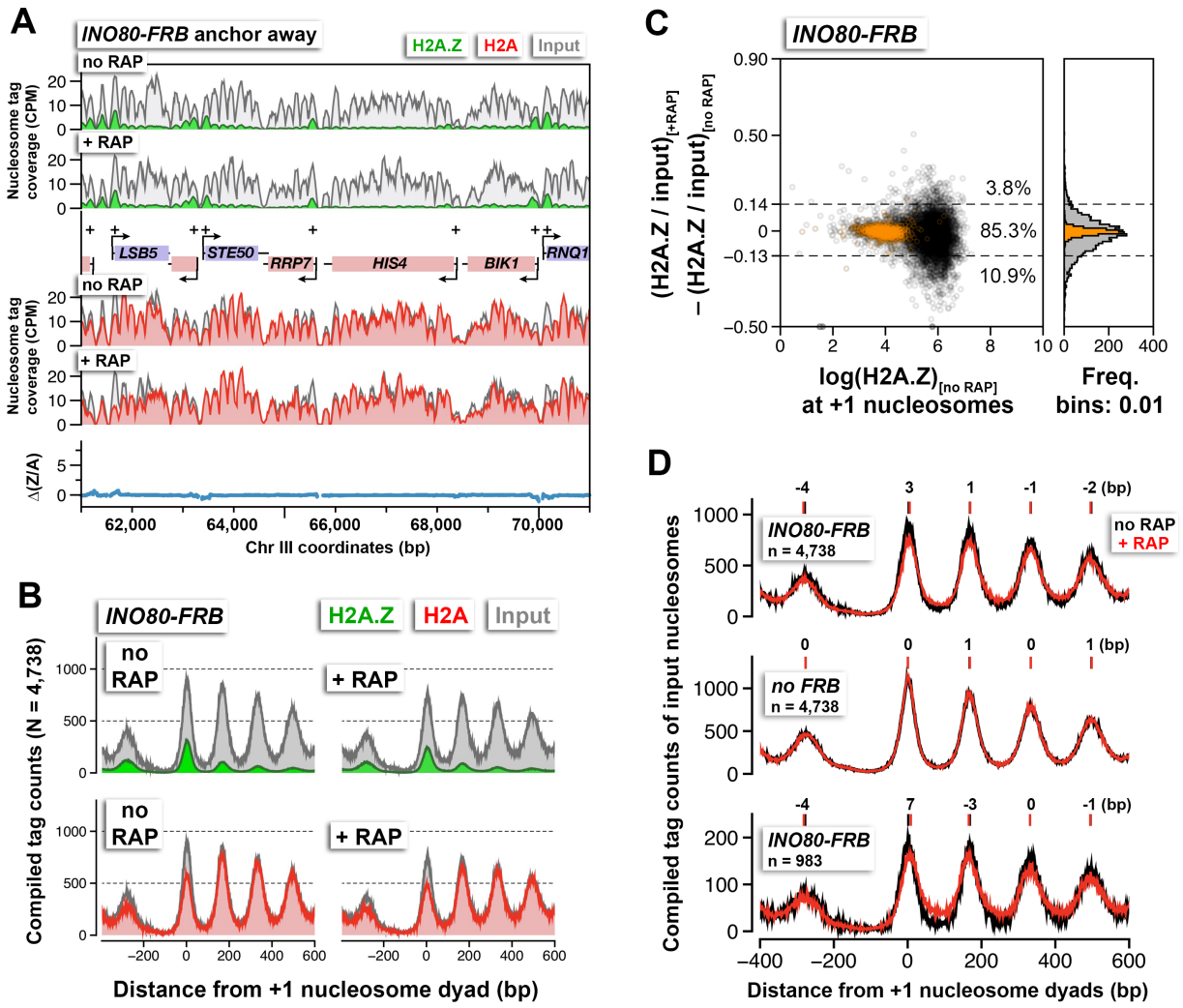

Figure 2-17. Change in relative nucleosomal H2A.Z levels and nucleosomal positions in response to Ino80 depletion. (**A**) Sequencing tag coverage of H2A.Z (*green*), H2A (*red*), and input (*gray*) nucleosomes, as well as the corresponding Δ(Z/A) values were plotted as described in **Figure 2-5A**. (**B**) Compiled read counts around the +1 nucleosome dyads. (**C**) Scatter plot showing the difference in (H2A.Z/input) ratio for individual +1 nucleosomes after Ino80 depletion. The thresholds (dotted lines) were determined as described in **Figure 2-5F**. *Gray*: +1 nucleosomes. *Orange*: reference nucleosomes. (**D**) The compiled input nucleosome profiles before (*black*) and after (*red*) rapamycin treatment in the *INO80-FRB* (*top*) and the untagged control (*no FRB, middle*) strains were re-plotted using the data from **B** and **Figure 2-5D** to highlight any difference in the nucleosomal arrays. *Bottom*: A list of 983 genes with fuzzier nucleosomal organization after Ino80 depletion was compiled and the input nucleosome density was re-plotted. The integers above the nucleosomal peaks indicate shift distance in base pairs. Positive values indicate right-shift after rapamycin treatment and vice versa. Peak center positions were determined by curve fitting with a Gaussian model followed by local maxima calculation. All qChIP-seq data of *Ino80-FRB* represent the mean of two biological replicates.

2.6. NDR formation is upstream of PIC assembly

The nuclear depletion experiments of TBP and Rpb1 also provide insights into the role of the transcription machinery in nucleosomal spacing organization. Both TBP and Rpb1 depletion caused histone octamers to reposition away from the NDR (**Figure 2-18A**). By contrast, no significant positional shift was observed in the nucleosomal arrays of the control cells (**Figure 2-17D**, *no FRB*). Similar results were previously observed by inactivating the transcription machinery with the *rpb1-1* mutation, which contains a temperature sensitive allele of *RPB1* (Weiner et al., 2010). These data are in agreement with the *in vitro* data that showed an elongating Pol II can disassemble the nucleosome in its path, while reassembling the nucleosome at a position slightly more upstream (Clark and Felsenfeld, 1992). But unlike the *rpb1-1* data, which exhibited strong downstream shift in the +1 nucleosomes under the non-permissive condition, the +1 shift upon TBP and Rpb1 depletion was comparatively minor (Weiner et al., 2010) (**Figure 2-18A**). In fact, the nucleosomal positional shift is progressively more dramatic towards the 3' end of the genes in the TBP and Rpb1 depletion experiments (**Figure 2-18A**). Interestingly, the positional shift caused by Rpb1 depletion is greater than that caused by TBP depletion (**Figure 2-18A**). One explanation for the difference is that TBP depletion blocks the Pol II molecules that are initiating but not those that have already engaged in elongation, whereas Rpb1 depletion removes all Pol II from the genome. But in both cases, the size of the NDR remains largely unchanged before and after the depletion of TBP or Rpb1 indicating that the formation of the NDR can be established in the absence of the PIC.

The phenomenon of nucleosome downshift in gene body is exaggerated at the RP genes where Pol II-mediated transcriptional activity is very high (**Figure 2-18B**) (Warner, 1999). But again, the positional shift of the +1 nucleosomes is comparatively insignificant (**Figure 2-18B**).

This observation is important as a recent study showed repression of the RP genes by heat shock can cause their +1 nucleosomes to shift tens of basepairs in the upstream direction, indicating that these +1 nucleosomes are normally pushed downstream when the RP genes are actively transcribed (Reja et al., 2015). Our data showed that PIC is not responsible for the downstream push of the +1 nucleosomes and suggests that a chromatin remodeling enzyme(s) might be responsible for setting up the NDR before PIC assembly.

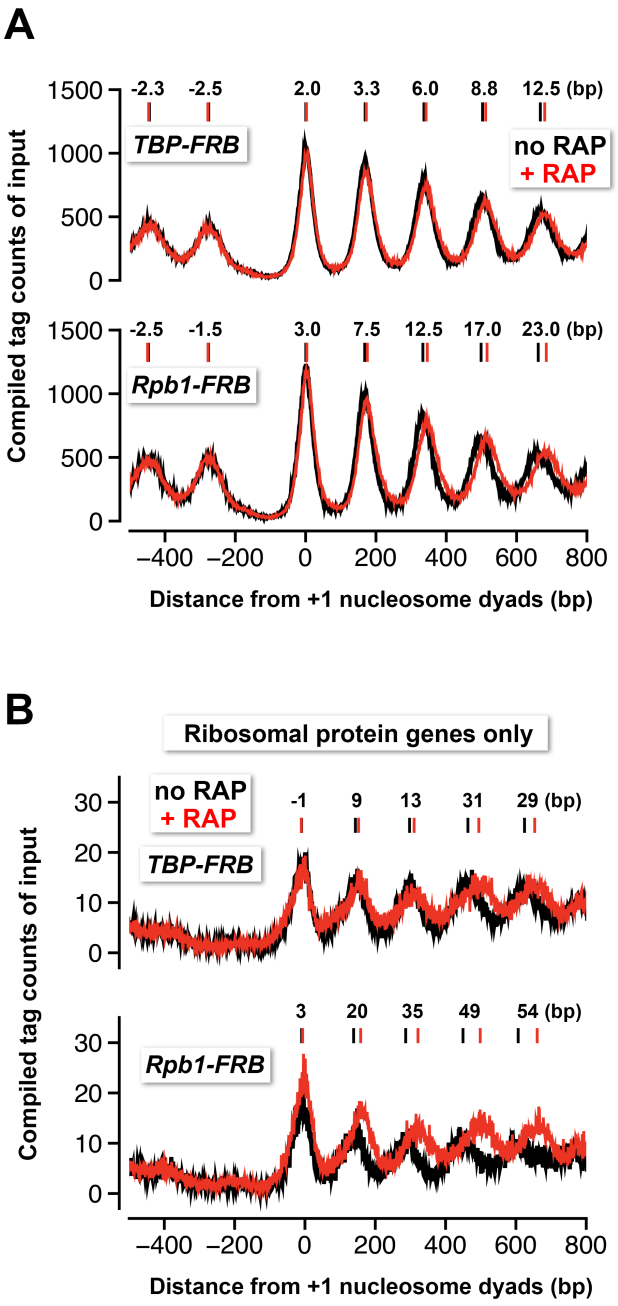

Figure 2-18. Nucleosomes shift away from the NDR in response to TBP and Rpb1 depletion. (**A**) The compiled tag counts of the input nucleosomal fraction (n = 4,738) before (*black*) and after (*red*) nuclear depletion of TBP-FRB (*top*) and Rpb1-FRB (*bottom*) were re-plotted using the data from **Figure 2-5C** and **Figure 2-9B**. The integers above the nucleosomal peaks indicate shift distance after rapamycin treatment. Peak center positions were determined as described in **Figure 2-17D**. (**B**) Same as (**A**) except that the compiled data of the ribosomal protein genes (n = 128) were shown. **Christy Au** performed the qChIP-seq experiment for one of the biological replicates of *RPB1-FRB*.

2.7. Sites of strong H2A.Z dynamics are restricted to the +1 nucleosome of Pol II-transcribed genes, not -1 or fragile nucleosomes

Robust H2A.Z dynamics is generally associated with the +1 nucleosomal position and, to lesser extent, the -1 position [see Δ(Z/A) in **Figure 2-11A**, right]. However, since many yeast genes are oriented divergently, the H2A.Z dynamics observed at the -1 nucleosome of some promoters could be the +1 nucleosome of a divergent promoter. Indeed, when promoters were sorted based on the orientation of the upstream gene, positive Δ(Z/A) values were more often seen in the upstream region of a promoter with a divergent-oriented gene (*Head-Head*) than with a tandem-oriented gene (*Head-Tail*) (Venters and Pugh, 2009) (**Figure 2-19A**). The difference in H2A.Z dynamics at the +1 and -1 positions is exemplified by 44 divergent promoters that are separated by a *bona fide* -1 nucleosome (**Figure 2-20**). At these sites, H2A.Z accumulation was restricted to the +1 positions but not the -1 positions.

In addition to Pol II-transcribed genes, TBP is also required for transcription by Pol I and Pol III (Cormack and Struhl, 1992; Schultz et al., 1992). An earlier study showed that TBP-FRB can be depleted from Pol I and Pol III promoters to ~60% and ~10% of the original levels, respectively, using the same duration of rapamycin treatment (Grimaldi et al., 2014). Contrastingly, at the Pol I-dependent *RDN37* promoter, depletion of TBP-FRB actually caused modest H2A.Z depletion and H2A accumulation (**Figure 2-19B**). The Pol III-dependent tRNA genes have intragenic promoters (Schramm and Hernandez, 2002). These genes are typically flanked by nucleosomes with low H2A.Z content (Albert et al., 2007). After TBP depletion, the flanking nucleosomes showed only a subtle increase in H2A.Z (**Figure 2-19C**). However, there is a substantial encroachment of nucleosome density (presumably H2A-containing) within the tRNA gene-associated NDRs (**Figures 2-19C** and **2-19D**). These results suggest that the

assembly or activity of the Pol III transcription machinery is important for creating the NDRs at these sites.

The NDR region is not completely histone free but is occasionally associated with unstable, histone-containing structures, also known as "fragile nucleosomes", that are hypersensitive to MNase digestion (Kubik et al., 2015; Weiner et al., 2010; Xi et al., 2011). An outstanding question is whether these fragile nucleosomes contain H2A.Z (Pradhan et al., 2015). In some of our qChIP-seq experiments, where the chromatin was under-digested, fragile nucleosomes were observed (**Figure 2-19E**, *cyan arrowhead*). Strikingly, fragile nucleosomes are completely devoid of H2A.Z. The phenomenon is more obvious when sequencing tags around the dyads of 1,953 fragile nucleosomes were compiled (**Figure 2-19F**) (Kubik et al., 2015). When H2A.Z eviction is blocked by TBP depletion, no H2A.Z accumulation was observed at the fragile nucleosome positions (**Figures 2-19E** and **2-19F**). This indicates H2A.Z deposition does not occur at these sites. The lower signal in input of the + RAP sample over the fragile nucleosome was due to slight over-digestion. Overall, our data suggest that H2A.Z deposition and eviction are highly localized at the +1 nucleosomes of Pol II-transcribed genes.

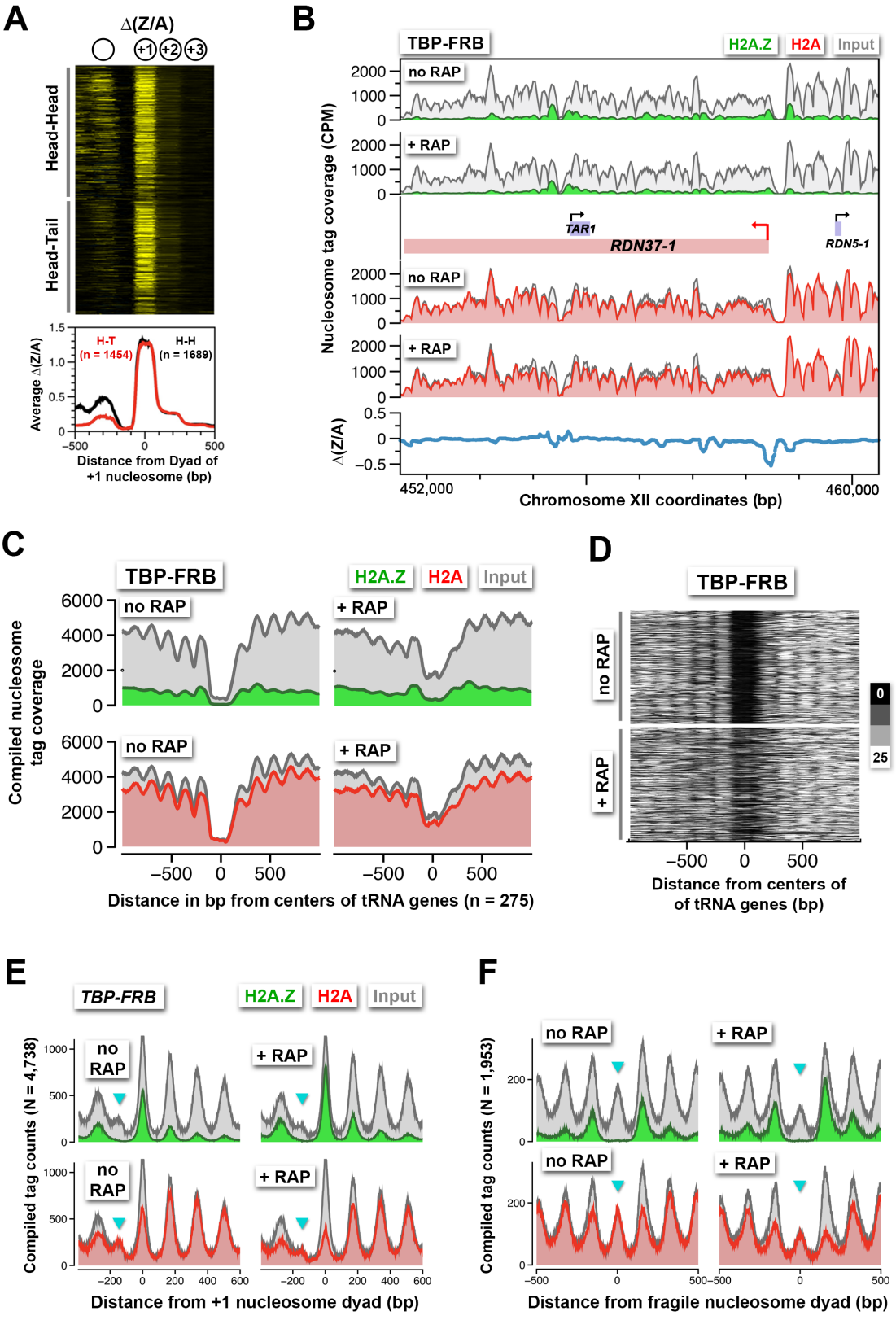
A
Δ(Z/A)
+1
+2
+3
Head-Head
Head-Tail
H-T
(n = 1454)
H-H
(n = 1689)
Average Δ(Z/A)
Distance from Dyad of
+1 nucleosome (bp)
B
TBP-FRB
H2A.Z
H2A
Input
no RAP
+ RAP
Nucleosome tag coverage (CPM)
TAR1
RDN37-1
RDN5-1
Δ(Z/A)
452,000
460,000
Chromosome XII coordinates (bp)
C
TBP-FRB
H2A.Z
H2A
Input
Compiled nucleosome
tag coverage
Distance in bp from centers of tRNA genes (n = 275)
D
TBP-FRB
Distance from centers of
of tRNA genes (bp)
E
TBP-FRB
H2A.Z
H2A
Input
Compiled tag counts (N = 4,738)
Distance from +1 nucleosome dyad (bp)
F
Compiled tag counts (N = 1,953)
Distance from fragile nucleosome dyad (bp)

Figure 2-19. Rapid H2A.Z dynamics is restricted to the +1 nucleosomes of Pol II promoters, not to -1 nucleosomes or fragile nucleosomes. (**A**) A heatmap showing the Δ(Z/A) values of *TBP-FRB* around the +1 dyads of 3,143 promoters sorted by the orientation of the upstream gene. *Head-Head (H-H)*: promoters with an upstream gene oriented divergently. *Head-to-tail (H-T):* oriented in tandem. (**B**) Normalized H2A.Z, H2A, and input nucleosome tag coverage around the repetitive *RDN1* locus. A *red arrow* marks the TSS of the Pol I-controlled *RDN37-1* promoter. (**C**) Compiled tag coverage of 275 tRNA genes with and without rapamycin treatment. (**D**) Heat maps of input nucleosomes around the center of tRNA genes. (**E**) Nucleosome profiles of under-digested chromatin from the *TBP-FRB* strain centered at the dyad of the +1 nucleosomes. *Cyan* triangles mark the peak of fragile nucleosomes. (**F**) Same as (**E**) except the profiles were aligned at the dyad of fragile nucleosomes (Kubik et al., 2015).

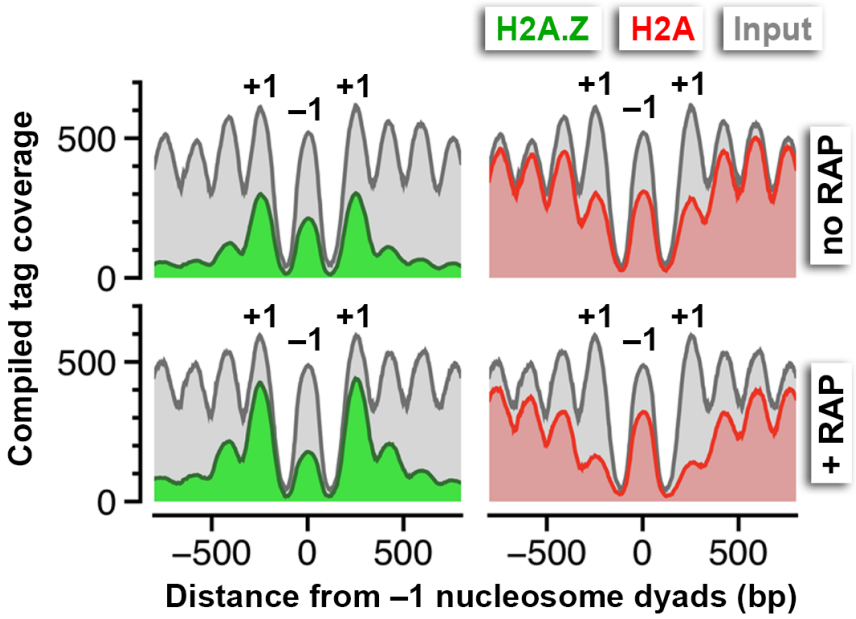

Figure 2-20. Compiled nucleosome tag coverage of 44 divergent promoters in *TBP-FRB* with a bona fide -1 nucleosome flanked by +1 nucleosomes. Tag coverage instead of tag mid-point was plotted to smooth the data.

2.8. H2A.Z accumulation in the absence of TBP can be used to determine internal and cryptic transcription start sites

The finding that H2A.Z dynamics revealed by the *TBP-FRB* mutant is linked to Pol II transcription start sites, raises the possibility that the Δ(Z/A) parameter can be used to identify cryptic, alternative, or previously unassigned transcription start sites. Indeed, the Δ(Z/A) parameter correctly marked the start sites of many previously annotated cryptic unstable transcripts (CUTs) (**Figure 2-21A**, *red arrows*, *CUT531* and *CUT445*) and noncoding RNAs (**Figure 2-21A**, *cyan arrows*, *SUT013* and *ICR1*) (Bumgarner et al., 2012; van Werven et al., 2012; Xu et al., 2009). To identify novel start sites, the Δ(Z/A) profiles around the dyads of all 61,568 annotated nucleosomes of the yeast genome (Kubik et al., 2015; Venters et al., 2011) were sorted by *k*-means clustering (**Figure 2-22A**). Since the +1 nucleosome is expected to have a maximum of Δ(Z/A) signal centered around the dyad as opposed to a +2 or -1 nucleosome, which should have an off-centered Δ(Z/A) maximum contributed by the +1 neighbor, nucleosomes with symmetrically distributed Δ(Z/A) signal were selected (**Figure 2-22A**). The process was reiterated again with the remaining nucleosomes (n = 56,193) to identify +1 nucleosomes with weaker Δ(Z/A) signals (**Figure 2-22A**). This approach identified 4,576 potential +1 nucleosomes, of which 3,684 were known +1 nucleosomes (n = 6,427) of protein-coding and noncoding genes (Jiang and Pugh, 2009b; Kubik et al., 2015; Rhee et al., 2014) (**Figure 2-22A**). The remaining 892 were not previously identified as +1 and therefore could represent novel +1 nucleosomes (**Figure 2-22B**). CUTs are normally degraded by the RNA surveillance machinery but accumulate in the exosome subunit mutant *rrp6*Δ (Xu et al., 2009). Many of the new +1 nucleosomes are associated with subtle, unannotated CUTs revealed by the *rrp6*Δ strain (**Figure 2-21B**, *grey bars*). Therefore global comparison of H2A depletion and

H2A.Z accumulation in the absence of the PIC provides a new parameter for transcription start site determination.

The Δ(Z/A) parameter also identifies alternative and novel start sites masked by other transcripts (**Figure 2-21C**). The transcriptional start site of *GDH2,* which encodes the NAD-linked glutamate dehydrogenase, has previously been mapped to a position on chromosome IV around 74,109 bp (**Figure 2-21C**, *left*, *green arrow*) (Miller and Magasanik, 1991; Xu et al., 2009). The identification of a new +1 nucleosome within the coding region of *GDH2* implies that there is a second start site ~1 kb downstream of the first (**Figure 2-21C**, *left*, *blue arrow*). Concordantly, microarray mRNA profiling data of wild-type cells (**Figure 2-21C**, *black dots*) showed an elevated mRNA level after the second start site indicating that a population of transcripts was indeed initiated from the internal start site (Xu et al., 2009). In the case of *HSE1*, the novel start site identified by H2A.Z accumulation is likely the *bona fide* start site masked by an upstream SUT (stable unannotated transcript) (**Figure 2-21C**, *right*, *blue arrow*). Further high resolution RNA-seq analysis of nascent Pol II transcripts showed that the originally annotated *HSE1* transcribed region (Xu et al., 2009) consists of two transcripts organized in tandem (**Figure 2-22C**). Therefore, the originally annotated TSS of *HSE1* belongs to the upstream SUT that terminates immediately before the newly identified TSS of *HSE1* (*blue arrow*), although read-through transcripts emanating from the upstream TSS cannot be excluded (**Figure 2-22C**).

In another example, H2A.Z-enriched nucleosomes that flank an NDR within the Ty3 retrotransposon accumulated H2A.Z (and lost H2A) after TBP-FRB depletion, implying the presence of a pair of divergent promoters (**Figure 2-21D**). Indeed, our nascent RNA data, as well as standard RNA-seq analysis of mRNA, confirmed the presence of transcripts initiated

from these sites (**Figure 2-21D** and **Figure 2-22D**, nascent RNA data courtesy of **Daniel Labuz** and RNA-seq data courtesy of **Zhimin Liu** and **Mindy Chou**). Cryptic antisense transcription has been reported for the Ty1 retrotransposon and the antisense *TY1* CUT is important for gene silencing and suppression of Ty1 mobility (Berretta et al., 2008). Therefore, the antisense Ty3 CUT identified here may play a similar role (**Figure 2-21D**, *gray bar*).

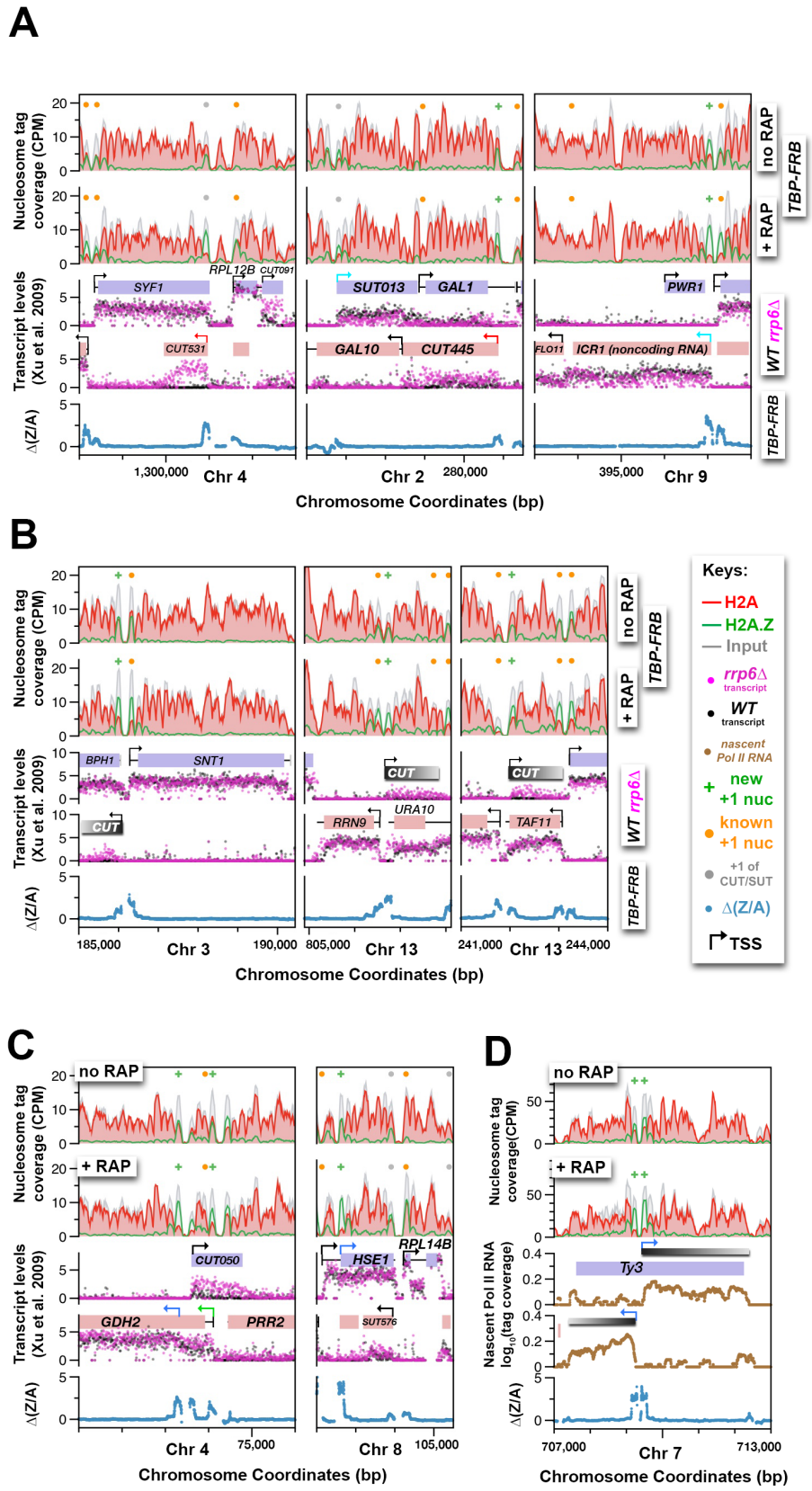
A
Nucleosome tag coverage (CPM)
no RAP
+ RAP
TBP-FRB
Transcript levels (Xu et al. 2009)
WT rrp6Δ
Δ(Z/A)
SYF1
RPL12B
CUT091
CUT531
SUT013
GAL1
GAL10
CUT445
PWR1
FLO11
ICR1 (noncoding RNA)
1,300,000
Chr 4
Chr 2
280,000
395,000
Chr 9
Chromosome Coordinates (bp)
B
BPH1
SNT1
CUT
URA10
RRN9
TAF11
185,000
Chr 3
190,000
805,000
Chr 13
241,000
244,000
Keys:
H2A
H2A.Z
Input
rrp6Δ transcript
WT transcript
nascent Pol II RNA
new +1 nuc
known +1 nuc
+1 of CUT/SUT
Δ(Z/A)
TSS
C
CUT050
GDH2
PRR2
RPL14B
HSE1
SUT576
75,000
105,000
D
Ty3
Nascent Pol II RNA log10(tag coverage)
707,000
713,000
Chr 7

Figure 2-21. Using H2A.Z dynamics before and after TBP depletion to identify cryptic and alternative transcription start sites. (**A**) Genomic regions highlighting representative CUTs and noncoding RNA, e.g. *CUT531, SUT013, CUT445, and ICR1*. Transcript data of wild-type (*black*) and *rrp6*Δ (*purple*) strains are from ref. (Xu et al., 2009). (**B**) H2A.Z dynamics around subtle cryptic transcription start sites. *Gray bars*: unannotated CUTs. (**C**) Previously unannotated alternative start sites marked by strong H2A.Z dynamics (*blue arrows*). (**D**) The cryptic divergent promoters within the coding region of a Ty3 element. *Brown traces:* Nascent Pol II RNA tag coverage. *Orange dots*: previously annotated +1 nucleosomes (Jiang and Pugh, 2009b; Kubik et al., 2015). *Gray dots:* +1 nucleosomes of CUTs and SUTs. *Green* '+' *signs*: new +1 nucleosomes. Nascent Pol II RNA tag coverage courtesy of **Daniel Labuz**.

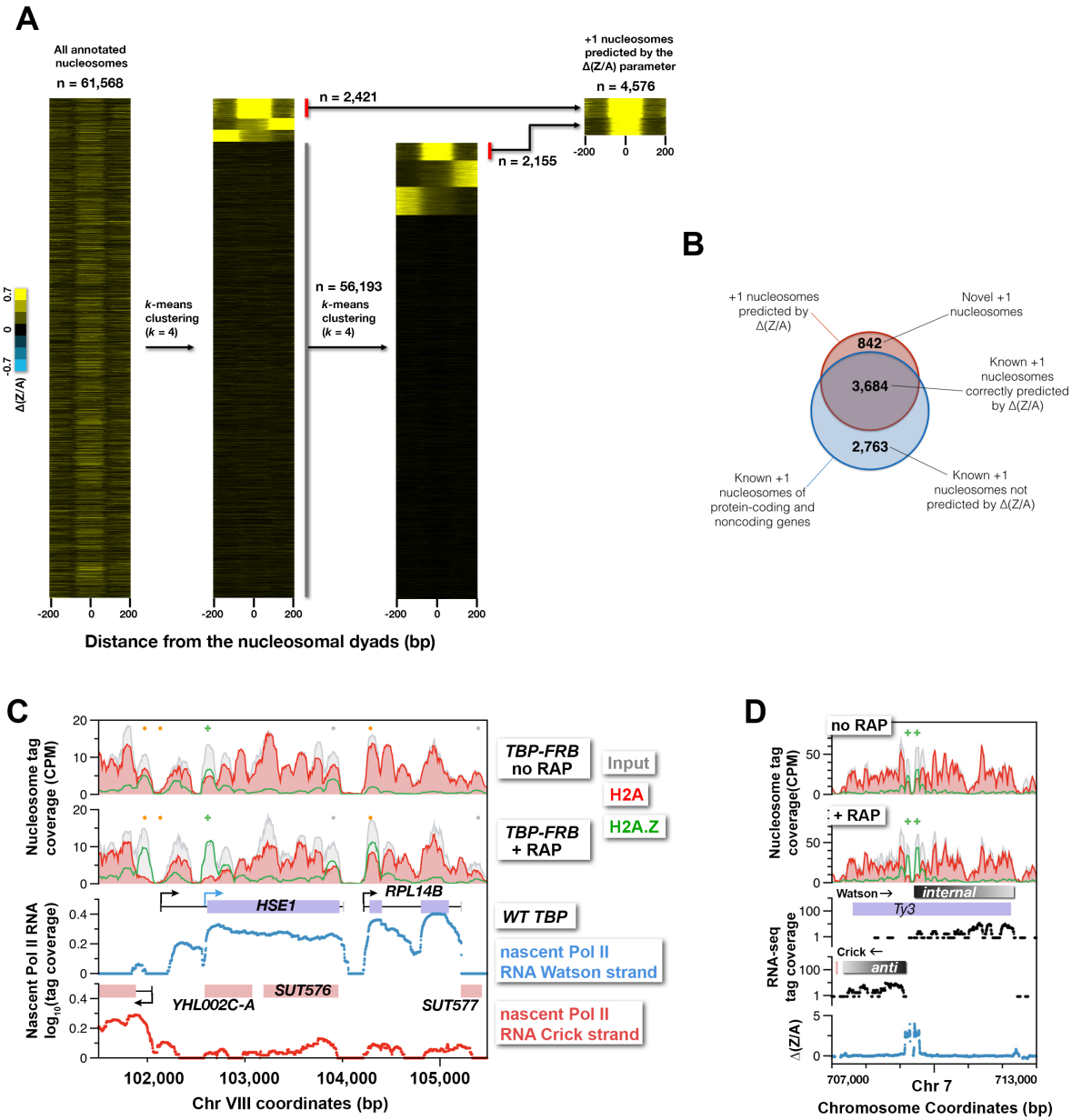

Figure 2-22. Clustering analysis of the Δ(Z/A) profiles associated with TBP-FRB depletion of all nucleosomes on the yeast genome. (**A**) The Δ(Z/A) profiles around the dyads of all 61,568 annotated nucleosomes (Jiang and Pugh, 2009b; Kubik et al., 2015) were sorted by *k*-means clustering (*k* = 4). A group of nucleosomes with robust, symmetrically distributed Δ(Z/A) signals were selected. The procedure was reiterated once with a group of nucleosomes (n = 56,193) with weaker Δ(Z/A) signals. **(B)** Venn diagram showing the overlap of +1 nucleosomes identified by the clustering analysis and known +1 nucleosomes of protein coding and noncoding genes (Jiang and Pugh, 2009b; Kubik et al., 2015). (**C**) Pol II nascent RNA-seq data highlighting the genomic region around the *HSE1* gene. Nascent Pol II RNA tag coverage courtesy of **Daniel Labuz**. (**D**) RNA-seq analysis of mRNA of a wild-type (BY4741) strain. RNA-seq data courtesy of **Mindy Chou** and **Zhimin Liu**.

3. Discussion

3.1. Constitutive histone dynamics at +1 nucleosomes

The promoter-proximal NDR serves not only as a platform for the assembly of the transcription machinery, but also as a hub for the recruitment of an array of chromatin remodeling factors (Rhee and Pugh, 2012; Venters et al., 2011). For any given promoter, these proteins apparently do not co-exist but transiently bind and dissociate in a regulated fashion to set up a chromatin environment in and around the NDR that promotes an accurate transcriptional response. The challenge is to understand how these factors are recruited and dislodged, how they regulate the dynamics of chromatin structure, and in what order these steps occur. This work demonstrates that rapid, constitutive turnover of H2A.Z occurs genome-wide, even at infrequently transcribed genes. At the nucleosomes covering or immediately downstream of the start sites of Pol II transcripts, the relative enrichment of H2A.Z is a steady state maintained by two major opposing forces imposed by the SWR1 complex and the transcription machinery. SWR1 converts H2A nucleosomes to the H2A.Z-containing forms (**Figure 2-23**, *step I*) and the transcription machinery then actively disassembles them.

Given that the SWR1 complex is recruited to the promoter in part through its affinity for long, exposed linker DNA (Ranjan et al., 2013; Rhee and Pugh, 2012), preventing PIC assembly by TBP or Pol II removal could, in theory, allow more SWR1 to bind the NDR leading to H2A.Z accumulation. As for the infrequently transcribed genes, one could argue that the NDRs of these promoters might be occupied with partial PICs that may become accessible to SWR1 binding when TBP or Pol II is removed. Our data argue against this hypothesis in that Swr1 occupancy

decreased, rather than increased, in response to TBP depletion. Therefore, it is the SWR1 complex already residing at the NDR before TBP depletion that is responsible for the increased H2A.Z deposition. However, since the Swr1 occupancy data are based on two promoters (with reliable Swr1 ChIP signal), the possibility that aberrant SWR1 recruitment is not occurring elsewhere in the genome cannot be excluded.

The observation that Swr1 occupancy decreased upon TBP depletion is interesting as it most likely reflects the lower affinity of SWR1 for H2A.Z nucleosomes relative to H2A nucleosomes (Ranjan et al., 2013). As such, after SWR1 has generated the H2A.Z nucleosome product, the enzyme dissociates from the NDR. Alternatively but not exclusively, since optimal SWR1 recruitment requires H3 and H4 tail acetylation, inhibition of transcription could decrease histone acetylation, and thus indirectly impair SWR1 recruitment (Liu et al., 2005; Raisner et al., 2005; Ranjan et al., 2013).

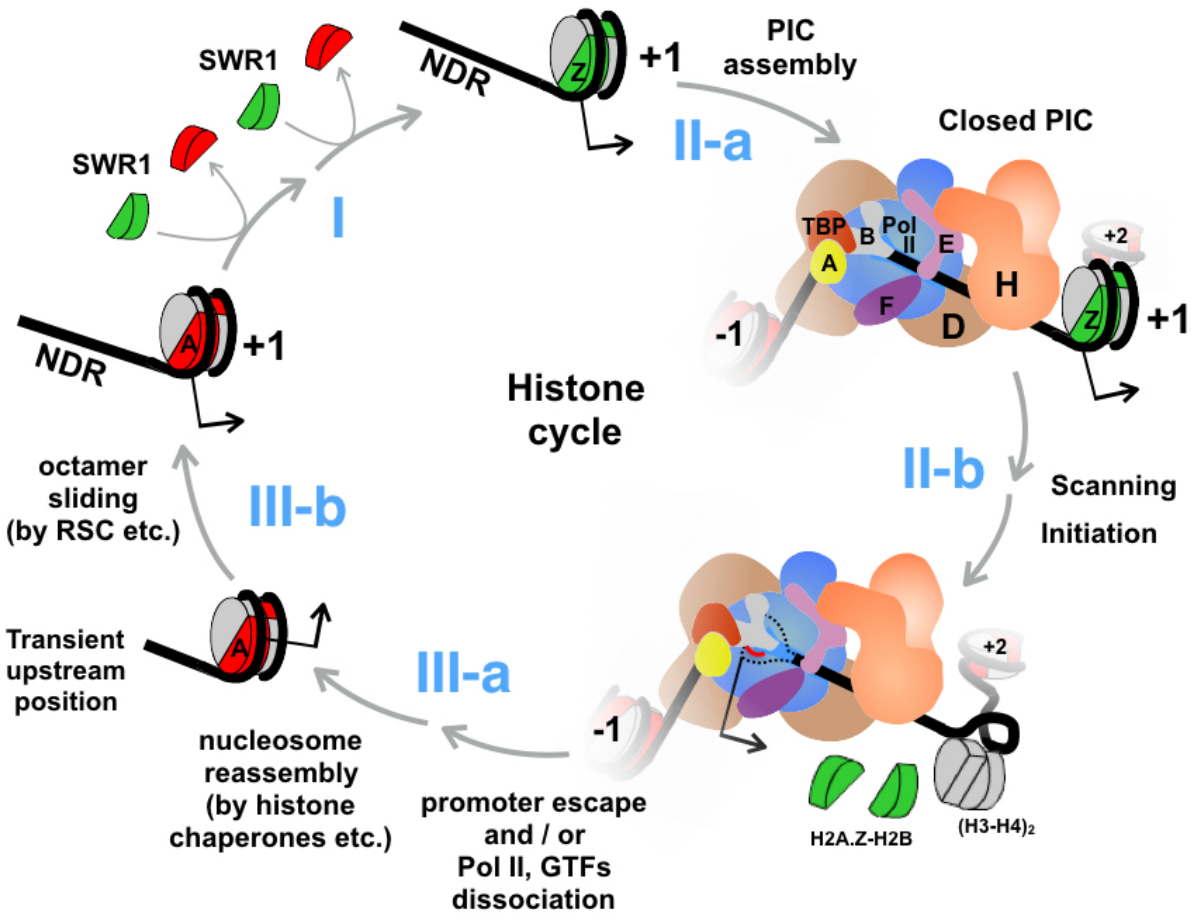

Figure 2-23. An updated histone cycle model. Step I: The SWR1 complex is recruited to the NDR and replaces the two nucleosomal H2A-H2B dimers with H2A.Z-H2B dimers. The H2A.Z-H2B dimers are always bound by histone chaperones *in vivo* but is omitted here for simplicity (Luk et al., 2007). Step II-a: Assembly of the PIC at NDR adjacent to the +1 H2A.Z nucleosome. General transcription factors are identified with single letters for simplicity. The model of PIC was adapted from ref. (Sainsbury et al., 2015) Step II-b: The PIC engages the H2A.Z nucleosome. Dotted black lines depict the unstructured ssDNA, which is not drawn to scale. Red line depicts the nascent RNA. Black arrow indicates the transcription start site (TSS). $(H3\text{-}H4)_2$ tetramers are in *gray*, H2A.Z-H2B dimers in *green*, and H2A-H2B dimers in *red*. Step III-a: After Pol II and GTFs left the promoter, a canonical H2A nucleosome reassembles over the TSS but at an imprecise position that is likely too upstream of the TSS. Step III-b: Chromatin remodelers, such as RSC, slide the octamer downstream to the stereotypic +1 position completing the histone cycle.

3.2. How does the transcription machinery engage the +1 H2A.Z nucleosome?

Perturbation of PIC assembly causes promoter-specific H2A.Z, but not H2A, to accumulate, suggesting that the constitutive disassembly occurs preferentially with H2A.Z-containing nucleosomes (**Figure 2-23**, *steps II-a* and *II-b*). Currently, it is not known whether the heterotypic AZ or the homotypic ZZ form is the preferred nucleosomal state for disassembly as our experiments did not distinguish between these forms. One explanation for the preference of H2A.Z eviction is that the PIC preferentially assembles on promoters that have a +1 H2A.Z nucleosome. Consistent with this idea, optimal TBP recruitment during oleate induction requires H2A.Z and the C-terminal domain of H2A.Z has been reported to bind RNA Pol II (Adam et al., 2001; Wan et al., 2009). Another nonexclusive possibility is that H2A.Z-containing nucleosomes are preferentially recognized by the PIC for disassembly. As such, when the PIC is fully engaged with the +1 H2A.Z nucleosome, some component(s) of the PIC actively disassembles the nucleosome, thereby allowing rapid, robust transcriptional activation. In support of this idea, rapid induction of *GAL1-10*, *PHO5* and the heat-responsive genes requires H2A.Z and is accompanied by preferential eviction of H2A.Z over H2A (Santisteban et al., 2000; Venters et al., 2011; Zhang et al., 2005). But regardless of the basis of how the preference for H2A.Z removal is achieved, our data suggest that the eviction of H2A.Z is, at least in part, coupled to some steps during transcription, rather than an independent process upstream of PIC assembly (**Figure 2-23**, *step II-b*).

A recent report that utilized ChIP and qPCR to monitor histone H3 occupancy showed that inactivation of transcription by the temperature sensitive alleles *rpb1-1* and *tbp ts-1*, led to promoter-proximal H3 accumulation, suggesting that the PIC is required to maintain an open chromatin state at the +1 position that is depleted of all histones (Ansari et al., 2014). In the

current study, the input nucleosomal levels at the +1 positions were largely unchanged for most genes upon TBP (or Rpb1) depletion. This discrepancy may be an artifact caused by a normalization step in our study that equalizes the input tag counts of all samples. Therefore, if inhibition of transcription had indeed caused a global increase in nucleosomal levels, the input nucleosome of the TBP depleted sample would be undercounted. But because the qChIP-seq approach reports H2A.Z IP efficiency, even if the input nucleosome occupancy were indeed higher in the TBP depleted sample, the absolute increase of H2A.Z would in fact be greater in response to TBP depletion, further supporting our conclusion. Furthermore, the TBP depleted sample does not appear to be severely undercounted, as the least transcribed genes (bottom 3%) exhibited similar input nucleosome densities after normalization (**Figure 2-24**). Interestingly, another group has previously used MNase-seq to probe the change of chromatin organization in the *rpb1-1* mutant and showed that the +1 nucleosomes did not accumulate when transcription was blocked (Weiner et al., 2010). We speculate that PIC-dependent disassembly of the +1 H2A.Z nucleosomes involves some metastable sub-nucleosomal intermediates (Ramachandran et al., 2015; Rhee et al., 2014). Since the DNA associated with the sub-nucleosomal species is likely hypersensitive to MNase digestion, it would be underrepresented in our input fraction. By contrast, standard H3 ChIP is likely less biased against the sub-nucleosomal species and therefore revealed H3 accumulation when transcription was blocked (Ansari et al., 2014).

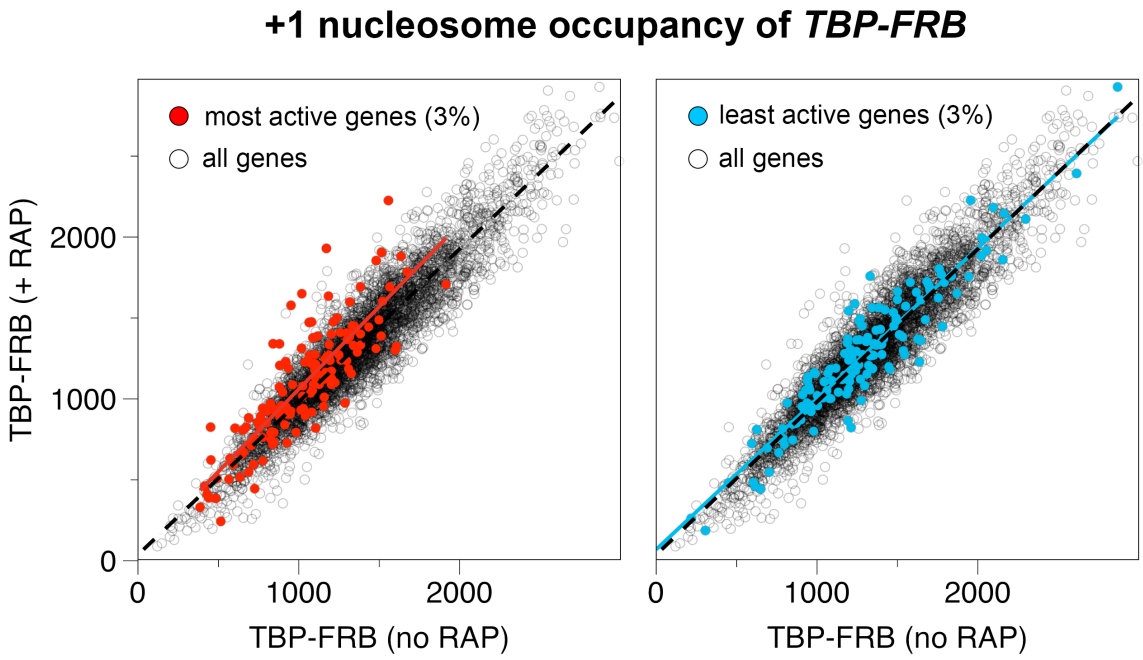

Figure 2-24. Input nucleosome occupancy at the +1 positions before and after TBP depletion. *Left panel:* The occupancy of +1 nucleosomes represents the read coverage within a 120 bp region around the +1 dyad (n = 4,738). The +1 occupancy associated with the top 3% most actively transcribing genes are in red (Lipson et al., 2009). The *red line* and *dotted black line* represent the linear regression for the highlighted genes and all the genes, respectively. *Right panel.* Same as left except that the +1 nucleosomes associated with the bottom 3% least active genes are highlighted. *Blue line* is the corresponding linear regression.

Earlier electron microscopy and genome-wide mapping studies place the PIC immediately upstream of the TSS on the DNA, suggesting that the +1 H2A.Z nucleosome and the PIC (in the closed conformation) can coexist in many promoters (Murakami et al., 2013; Rhee and Pugh, 2012). It is currently unknown which step of the transcription process causes H2A.Z eviction. However, we speculate that promoter scanning mediated by TFIIH is the driving force (**Figure 2-23**, *step II-b*). A recent single-molecule study showed that yeast PIC repeatedly scans the promoter over an extended region (85 base pairs on average), leading to cycles of transcription bubble formation and collapse before committing to promoter escape (Fazal et al., 2015). Formation of such extended transcription bubbles in the NDR will overwind the DNA downstream, leading to a propensity to form positive supercoils in the +1 nucleosomal region. Given that DNA wraps the histone octamer in a left-handed turn (i.e. negative writhe) and that the promoter-distal end of the nucleosome is restricted to rotate freely, positive supercoiling will likely destabilize the +1 nucleosome. Repeated cycles of futile scanning without promoter escape may also occur at infrequently transcribing genes explaining the constitutive H2A.Z dynamics at those promoters. Although we favor a model in which H2A.Z eviction is a direct consequence of the initiation process, we cannot exclude the possibility that a subsequent step of transcription, such as promoter escape or elongation, is the driving force as TBP depletion blocks all steps of transcription. We also cannot exclude TBP or the integrity of the PIC may be required to recruit another factor that functions to disassemble H2A.Z nucleosomes.

Since robust PIC-dependent H2A.Z eviction occurs even at promoters that infrequently fire, this provides an opportunity to use H2A.Z dynamics as a parameter to locate initiation sites that were previously missed by the conventional transcript mapping approach (Xu et al., 2009).

Sites with strong H2A.Z dynamics were able to identify not only initiation sites of protein coding genes, SUTs and CUTs, but also sites that are masked by upstream transcripts. Although this approach cannot pinpoint the location of a TSS at base pair resolution, the sites are generally restricted within the identified +1 nucleosome near the edge adjacent to the NDR. Importantly, since PIC-dependent H2A.Z eviction is linked to an NDR, the direction of the predicted transcripts can be inferred based on the location of the NDR and is almost always pointing away from the NDR. Another limitation of this approach is that it may not identify the TSSs of promoters that are associated with low endogenous H2A.Z deposition activity and/or have low PIC-dependent H2A.Z eviction activity as in case of the SAGA-dominating promoters.

3.3. The *in vivo* contribution of the INO80 remodeler on H2A.Z eviction

Whether the INO80 complex plays a role in evicting H2A.Z at promoters has been controversial. Evidence supporting this idea comes from *in vitro* experiments showing that the INO80 complex can mediate a reaction that replaces the nucleosomal H2A.Z-H2B dimer with H2A-H2B, which supposedly opposes the reaction catalyzed by SWR1 (Papamichos-Chronakis et al., 2011), as well as *in vivo* experiments showing a global increase of H2A.Z occupancy in *ino80*Δ or *arp5*Δ (both components of the INO80 complex) strains (Papamichos-Chronakis et al., 2006; Yen et al., 2013). However, a more recent study showed *ino80*Δ mutants exhibited normal H2A.Z occupancy at promoters (Jeronimo et al., 2015). Our experiments agree with the latter study arguing that INO80 does not contribute to global eviction of H2A.Z, as no accumulation of H2A.Z was observed when Ino80 was depleted. One explanation for the discrepancy between these various experiments is that *ino80*Δ and *arp5*Δ are both associated with genome instability,

resulting in aneuploidy that complicates the interpretation of genomic data (Chambers et al., 2012 and Ashby Morrison personal communication). To circumvent this problem, we assayed H2A.Z occupancy within two hours of conditionally depleting Ino80 from the nucleus, thereby minimizing aneuploidy. Furthermore, the previous studies used ChIP-chip and ChIP-exo to measure H2A.Z occupancy (Jeronimo et al., 2015; Papamichos-Chronakis et al., 2011; Yen et al., 2013). However, these approaches may not be ideal for comparing H2A.Z occupancy in different strains. Standard microarray normalization involves scaling with data averages that could mask any global occupancy change (Quackenbush, 2002). ChIP-exo measures the distribution of crosslinking points between the immunoprecipitated protein and DNA that could be influenced by variation of crosslinking efficiency in mutants with chromatin dynamics defects (Yen et al., 2013). The qChIP-seq approach conducted here takes into account the input, flow-through, and IP fractions of each IP reaction and uses the immuno-depleted signal in the flow-through to scale the IP signal. Therefore, occupancy data reflects IP efficiency relative to input at individual nucleosomal sites and is not influenced by global occupancy change. It is also less sensitive to variation in crosslinking efficiency as formaldehyde crosslinking serves only to preserve the histone-DNA interaction during the pull down. Our data showed that Ino80 depletion did not cause H2A.Z accumulation, arguing against the INO80 remodeler being the main evictor of H2A.Z in the constitutive turnover process. This observation however is not inconsistent with INO80 being recruited to remodel specific promoters in response to induction as seen in the *PHO5* and *GAL* genes (Barbaric et al., 2007; Rosonina et al., 2014).

Although INO80 is not involved in the constitutive eviction of H2A.Z at the +1 positions, our data suggest that INO80 does contribute to the positioning of nucleosomes near the promoters. While the sliding defect associated with Ino80 depletion is reproducible and

consistent with previous studies (Yao et al., 2016; Yen et al., 2012), the defect is small compared to that associated with mutants in genes encoding other chromatin remodelers, such as *RSC, CHD1*, *ISW1*, and *ISW2* (Gkikopoulos et al., 2011; Hartley and Madhani, 2009; Ocampo et al., 2016; Whitehouse et al., 2007). Therefore, the role of INO80 in nucleosome positioning could be indirect or redundant with another remodeling factor.

3.4. An updated model of histone dynamics at yeast promoters

We propose an updated "histone cycle" model to unify the molecular events that lead to the promoter-specific H2A.Z dynamics (**Figure 2-23**). First, ATP-dependent remodelers, such as RSC, are recruited to the promoter region by sequence specific DNA-binding factors to establish the NDR (Badis et al., 2008; Hartley and Madhani, 2009) (**Figure 2-23,** *step III-b*). SWR1 is recruited to the NDR by its affinity for extended stretches of naked DNA and, to lesser extent, promoter-specific histone acetylation (Hartley and Madhani, 2009; Ranjan et al., 2013). SWR1 then converts the canonical AA nucleosome to the AZ and ZZ chromatin states sequentially (Luk et al., 2010) (**Figure 2-23**, *step I*). For promoters that contain a fragile nucleosome within the NDR region (omitted in **Figure 2-23** for simplicity), this structure is somehow refractory to the SWR1-mediated histone replacement reaction. SWR1 dissociates from the promoters after depositing H2A.Z at the +1 position due to its lower affinity for the H2A.Z nucleosomal product (Ranjan et al., 2013). The PIC assembles at the NDR adjacent to the newly formed +1 H2A.Z nucleosome (Rhee and Pugh, 2012). At some point when the PIC engages the TSS, the H2A.Z nucleosome disassembles. This may involves sub-nucleosomal intermediates before all histones are completely evicted from the DNA. Following promoter

escape or unproductive dissociation of the PIC, a nucleosome with the major histones, H2A, H2B, H3, and H4, reassembles completing the histone cycle (**Figure 2-23**, *step III-a*).

The promoter-specific histone dynamics described by the histone cycle appears to be a general phenomenon in yeast. We show that the Pol II transcription machinery has a major contribution to the eviction step of H2A.Z in the histone cycle. Together, chromatin remodelers and the transcription machinery choreograph the movement of histones within the promoter leading to a dynamic chromatin architecture conducive for transcription. How these enzymes are coordinated to set the histone cycle in motion will be the next important question.

4. Materials and methods

4.1. Yeast strains and culture conditions

The genotypes of the yeast strains used in this study are listed in **Table 2-1**. The anchor-away strains HHY221, HHY170 and HHY209 were obtained from *Euroscarf* (Haruki et al., 2008). The H2A.Z FLAG tagged strains yEL152 (no FRB tag control), yEL154 (*SPT15-FRB-GFP*), yEL170 *(RPB1-FRB),* and yEL189 *(INO80-FRB-GFP)* were constructed by integrating a *2xFLAG-URA3* fragment at the 3' end of the *HTZ1* gene in the precursor strains HHY221, yEL098, yEL090, and yEL123, respectively. yEL098 is a tetrad segregant of the diploid HHY221 x HHY209 strain and yEL090 is a segregant of the diploid HHY221 x HHY170. The *2xFLAG-URA3* fragment was obtained by PCR amplification of the *pRS416-HTZ1-2xFLAG* plasmid as described in ref. (Mizuguchi et al., 2004). Successful integration was confirmed by colony PCR and sequencing.

The *SWC5-FRB* (yEL219) and *SWC5-FRB TBP-FRB* (yEL220) strains were generated by integrating the *FRB-HIS3MX6* fragment at the 3' end of the *SWC5* coding region in yEL152 and yEL154, respectively, using the one-step gene replacement procedure (Longtine et al., 1998). The *FRB-HIS3MX6* fragment was amplified by PCR using the plasmid *pFA6a-FRB-HIS3MX6* (P30579, *Euroscarf*) as template (Haruki et al., 2008). Similarly, the *INO80-FRB-GFP* precursor strain (yEL123) was generated by transforming HHY221 (yEL044) with a *FRB-GFP-HIS3MX6* PCR product targeting the 3' end of *INO80.* The *FRB-GFP-HIS3MX6* fragment was amplified from the plasmid *pFA6a-FRB-GFP-HIS3MX6* (P30581, *Euroscarf*) (Haruki et al., 2008).

For microscopy, yeast cells were grown in YPD at 30˚C to an OD_{600} of 1 before rapamycin was added to a final concentration of 1 μg/mL. Cells before and after the addition of rapamycin were removed at the indicate times and were fixed with 4% formaldehyde for 5 min followed by washing with 1x PBS and staining with 1 μg/mL DAPI. For the microscopy analysis of the *INO80-FRB-GFP* cells in **Figure 2-16**, live cells were used in order to shorten the lag time between imaging and fixation before the qChIP-seq analysis.

The yeast cells used in quantitative ChIP were cultured at 30˚C in 2 L of yeast extract-peptone-dextrose (YPD) to an optical density 600 (OD_{600}) of 0.8 before 1 μg/mL rapamycin was added and incubated for the indicated duration. The rapamycin-treated culture, as well as the untreated control, were fixed with 3% paraformaldehyde for 7.5 minutes and quenched by 0.12 M glycine as previously described (Luk et al., 2010). Cell pellets equivalent to 400 mL culture were aliquoted and washed with 1x PBS before flash frozen and stored at –80˚C.

Table 2-2. Table of yeast strains used in Chapter Two

Strain	Genotype	Source/reference	Method
W303	*ade2-1 trp1-1 can1-100 leu2-3,112 his3-11,15 ura3 GAL psi*$^{+}$	Standard Strain	
HHY221 (yEL044)	*W303 MATa TOR1-1 fpr1Δ::loxP-LEU2-loxP rpl13a::RPL13A-2×FKBP12-loxP*	(Haruki et al., 2008)	
HHY170 (yEL066)	*W303 MATα TOR1-1 fpr1Δ::natMX4 rpl13a::RPL13A-2xFKBP12-TRP1 rpb1::RPB1-FRB::kanMX6*	(Haruki et al., 2008)	
HHY209 (yEL073)	*W303 MATα TOR1-1 fpr1Δ::natMX4 rpl13a::RPL13A-2xFKBP12-TRP1 spt15::SPT15-FRB-GFP::kanMX6*	(Haruki et al., 2008)	
yEL098	*W303 MATa TOR1-1 fpr1Δ::loxP-LEU2-loxP rpl13a::RPL13A-2×FKBP12-loxP spt15::SPT15-FRB-GFP-kanMX6*	This study	Tetrad segregant of HHY221 and HHY209
yEL090	*W303 MATa TOR1-1 fpr1Δ::natMX4 rpl13a::RPL13A-2xFKBP12-TRP1 rpb1::RPB1-FRB::kanMX6*	This study	Tetrad segregant of HHY221 and HHY170
yEL123	*HHY221 INO80-FRB-GFP::HISMX6*	This study	PCR-based integration using pFA6a-*FRB-GFP-HIS3MX6* (EUROSCARF: P30581)
yEL152	*HHY221 htz1::HTZ1-2xFLAG-URA3*	This study	PCR-based integration using pRS416-HTZ1-2xFLAG (pEL353) as template
yEL154	*yEL098 htz1::HTZ1-2xFLAG-URA3*	This study	PCR-based integration using pRS416-HTZ1-2xFLAG (pEL353) as template
yEL170	*yEL090 htz1::HTZ1-2xFLAG-URA3*	This study	PCR-based integration using pRS416-HTZ1-2xFLAG (pEL353) as template
yEL189	*yEL123 htz1::HTZ1-2xFLAG-URA3*	This study	PCR-based integration using pRS416-HTZ1-2xFLAG (pEL353) as template
yEL219	*yEL152 SWC5-FRB::HISMX6*	This study	PCR-based integration using pFA6a-*FRB-HIS3MX6* (EUROSCARF: P30579)
yEL220	*yEL154 SWC5-FRB::HISMX6*	This study	PCR-based integration using pFA6a-*FRB-HIS3MX6* (EUROSCARF: P30579)
yEL297	*W303 MATa TOR1-1 fpr1Δ::P RPL13A-2XFKBP12::P KIN28-FRB RBP3-3xFLAG-p-kanMX-p*	This study	PCR-based integration using p3xFLAG p-kanMX-p (pEL362) as template (Mizuguchi G. et al. 2004)

4.2. qChIP-seq

Cells equivalent to 400-mL culture volume were spheroplasted and lysed with a 7-mL dounce homogenizer (piston B, Wheaton) as previously described (Luk et al., 2010). After centrifuging the lysate (~1000 µL) at 13,000 x g for 10 min at 4˚C, the chromatin-enriched pellet was washed 3 times with buffer A [50mM HEPES (pH 7.5), 80mM NaCl, 0.25% Triton X-100, 2x protease inhibitor cocktail (*Roche*, cOmplete EDTA-free)]. The pellet was resuspended in 1/2 x lysate volume of buffer A plus 1 mM of $CaCl_2$. The suspension was pre-incubated to 37˚C for 2 min before digestion with 1.5-1.8 U/µL MNase (Worthington) at 37˚C for 10-20 min. The concentration of MNase and duration of digestion were empirically determined for each sample to achieve ~90% mono-nucleosomal form. After stopping the digestion reaction by the addition of 10 mM EGTA, the sample was centrifuged at 20,400 x g for 15 min at 4˚C. The supernatant, which contained the soluble nucleosomes, was cleared by passage through a low-binding PVDF filter (Ultrafree GV, Millipore).

Before the soluble nucleosomes were subjected to quantitative ChIP, a 50 µL aliquot was saved. The DNA extracted from this sample represents the input nucleosome fraction. The remaining sample (~500 µL) was diluted 10-fold in buffer B [25mM HEPES-KOH pH 7.6, 80 mM KCl, 1 mM EDTA, 1x protease inhibitors (PI, which consists of 1.7 mg/mL PMSF, 3.3 mg/mL benzamidine hydrochloride, 0.1 mg/mL pepstatin A, 0.1 mg/mL leupeptin, 0.1 mg/mL chymostatin)] followed by incubation with 1/20x volume (~250 µL resin volume) of anti-FLAG M2 affinity gel (A2220, *Sigma Aldrich*) at 4˚C for 4 hr. The flow-through of the IP reaction would represent the H2A nucleosome fraction. The bead-bound H2A.Z nucleosomes were washed three times with buffer C [25 mM HEPES-KOH pH 7.6, 0.3 M KCl, 1 mM EDTA, 0.01% NP-40, 1x PI] and eluted with 2x resin volume (~500 µL) of buffer D (25mM HEPES-

KOH pH 7.6, 0.3M KCl, 1 mM EDTA, 0.1% NP-40, 0.1% DOC, 1x PI, 0.5 μg/μL 3xFLAG peptides) at 4˚C overnight. The eluate was cleared by passage through a GV 0.22 μm filter (Ultrafree-MC, *Millipore*). The FLAG eluate would represent the H2A.Z nucleosome fraction.

To extract the nucleosomal DNA, the sample was adjusted to 400 μL with molecular grade water followed by the addition of 32 μL 5M NaCl, 8 μL 0.5M EDTA, 20 μL 10% SDS, 2.5 μL 20 μg/μL glycogen (*Life Technologies*), and 8 μL of 20 mg/mL proteinase K (*Life Technologies*). The mixture was incubated at 55˚C for one hour to facilitate protein digestion and 65˚C for > 15 hours to reverse the crosslinks. The DNA was purified by standard phenol-chloroform extraction followed by ethanol-NaOAc precipitation. The pellet was resuspended in 100 μL of 5 μg/mL RNase (*Roche*) in 1x TE pH 8.0 and incubated at 37˚C for > 1 hour. The resulting nucleosomal DNA was purified using the QIAquick spin column (*Qiagen*) and quantified by the Qubit HS assay (*Life Technologies*).

To prepare the DNA libraries for sequencing, 30 ng of nucleosomal DNA was treated with 5 U of alkaline phosphatase (CIP, *NEB*) for 1 hr at 37˚C followed by the addition of 20 μg glycogen (*Life Technologies*). The mixture was then purified by standard phenol-chloroform extraction and ethanol-NaOAc precipitation. The DNA was resuspended in 12 μL of the TruSeq Resuspension Buffer (*Illumina*) and quantified by the Qubit HS assay. Ten nanograms of CIP-treated DNA was applied to the TruSeq ChIP workflow (*Illumina*) with the following modifications. After the end-repair step, instead of using the AMPure beads for purification, the sample was purified by standard phenol-chloroform extraction and ethanol-NaOAc precipitation. The adapter-ligated DNA was amplified on a PCR machine by 15 thermal cycles. The PCR product was quantified by the Qubit assay (*Life technologies*) and the quality was verified by agarose electrophoresis and SYBR green staining. Densitometry was performed on a Typhoon

FLA9500 scanner station installed with the ImageQuant TL software (*GE Healthcare*). Paired-end sequencing (33 cycles) was performed on a MiSeq sequencer (*Illuimna*).

4.3. Bioinformatics

Sequencing reads were aligned to the *S. cerevisiae* genome (SGD version R64-1-1) using Bowtie 1.1.2 (Langmead et al., 2009). Aligned data of the H2A.Z, H2A and input nucleosome fractions were processed without smoothing using a combination of custom Python scripts and BEDTools programs (Quinlan, 2014). They were plotted along the genome either as tag coverage (density covered by paired-end reads) or tag counts (density of mid-points of paired-end reads). The amplitude of the H2A.Z (Z), H2A (A), and input (T or total) nucleosome profiles was scaled using an approach called 'TAZ normalization' (**Figure 2-4**). First, the tag counts within 44 reference regions (called the no-Z-zones), which are enriched for H2A but depleted for H2A.Z (**Figure 2-4A**), were determined by Bowtie. The normalization factor *m*, representing the ratio of no-Z-zones tag count of the input fraction over that of the H2A fraction, was used to scale the H2A nucleosome profile (**Figure 2-4B**). To normalize the H2A.Z nucleosome profile for each IP reaction (technical replicate), the tag counts around 4,738 promoters were compiled around the +1 dyads for the H2A, H2A.Z and input fractions. The normalization factor *n*, was determined by a curve fitting algorithm such that the sum of the compiled profiles of H2A and H2A.Z ($m \times$ H2A + $n \times$ H2A.Z) equals, to a first approximation, the compiled profile of the input (**Figure 2-4B**). Finally, the input profiles for each IP reaction were converted to counts per million (CPM) by the normalization factors *c*. The products of $c \times$

m and $c \times n$ represent the final normalization factors for the H2A and H2A.Z nucleosome profiles, respectively.

All qChIP-seq experiments with the exception of the experiment in **Figure 2-13** represent the average of two biological replicates (i.e from independent cultures). In **Figure 2-13**, the qChIP-seq data of *SWC5-FRB* and *SWC5-FRB TBP-FRB* strains represent the averages of two independent IP reactions (technical replicates) of the same biological sample. The biological replicate for *SWC5-FRB* is shown in **Figure 2-14**, which included additional time points after rapamycin treatment. Data averaging was performed on the normalized tag coverage or tag counts after the TAZ normalization step; therefore, sequencing reads were not pooled.

4.4. Immunoblotting and ChIP-qPCR analyses

Antibodies against the yeast Swr1 and H2A.Z were gifts of Carl Wu. The anti-FLAG (F1804) and the anti-H2A (39235) antibodies were purchased from *Sigma Aldrich* and *Active Motif,* respectively. For H2A and H2A.Z western, both antibodies were used at a dilution of 1:2,000. ChIP-qPCR analysis was performed as previously described with the following modifications (Aparicio et al., 2005). ChIP reactions were performed using 1.25 mg dynabeads conjugated to Protein A or G. Five microliter of anti-Swr1 was used in each ChIP reaction. qPCR was performed on a LightCycler 96 Real-Time PCR system (*Roche*). The primers used in qPCR are listed in **Table 2-2**.

Table 2-2. Primers for ChIP-qPCR analysis in Chapter Two

Location	Orientation	Chr	Start	End	Sequence	References
PGD1 promoter	Forward	chrVII	449836	449856	AGAATTTCATCG CGTGCTTC	This work
PGD1 promoter	Reverse	chrVII	449972	449992	CAAAACGGACAC AACAGCAG	This work
RRP7 promoter	Forward	chrIII	65476	65496	TTCCTGGCTTTTG GGTAGTG	This work
RRP7 promoter	Reverse	chrIII	65611	65631	AAGAGGCATTTA GGGCGAAC	This work
LSB5 promoter	Forward	chrIII	61501	61523	TGAAACTGTTTT GACCTTGACG	This work
LSB5 promoter	Reverse	chrIII	61688	61710	GAAAGATCGTCT CGGTGATAGC	This work
STT3 ORF	Forward	chrVII	453890	453912	TCAGGGAAGCGT ACTATTGGTT	This work
STT3 ORF	Reverse	chrVII	454058	454080	TCGTAAGATTTC TCTTCAGGGG	This work
SNT1 ORF	Forward	chrIII	186784	186785	ATTCGTCAACAA GAAAAATTGG	This work
SNT1 ORF	Reverse	chrIII	186845	186868	TACTTTCCGGAG TTGAACTAGTG	This work
SWR1 promoter	Forward	chrIV	1135754	1135779	CGTGCAAAAAGG ATAGATTTTGAG C	Ranjan et al. 2013
SWR1 promoter	Reverse	chrIV	1135958	1135981	CACCACCAGCCT TTTTGTCTTTC	This work
FUN12 promoter	Forward	chrI	76396	76416	AGGGCAATCAGG AACATCAG	This work
FUN12 promoter	Reverse	chrI	76515	76544	TGCGCTGCTTTC TGGATTTGGAGT TGGCG	Ranjan et al. 2013
TEL6R	Forward	chrVI	269500	269524	GCGTAACAAAGC CATAATGCCTCC	Ranjan et al. 2013
TEL6R	Reverse	chrVI	269614	269638	CTCGTTAGGATC ACGTTCGAATCC	Ranjan et al. 2013
RPS14B promoter	Forward	chrX	73674	73694	AGTCGCAAGAAC TTGCCTTC	Wong et al. 2014
RPS14B promoter	Reverse	chrX	73728	73748	CTCTCTTGCGAT GAAGATGC	Wong et al. 2014
RPS28 promoter	Forward	chrVII	310804	310824	CTCGCAGTTTTT CGCTTGTT	Wong et al. 2014
RPS28 promoter	Reverse	chrVII	310878	310898	GAGAAAGCAAA CGCCATCTT	Wong et al. 2014

4.5. Pol II nascent transcript sequencing

Native elongating transcript sequencing (NET-seq) was performed essentially according to (Churchman and Weissman, 2012) but with the following modifications. Briefly, yeast cells expressing *RPB3-3xFLAG* (yEL297) were cultured in 6 L YPD to a final OD of 2. Washed cells were pulverized in Buffer E (20 mM HEPES-KOH pH 7.6, 20% Glycerol, 50 mM KOAc, 1 mM EDTA, 1x PI) for 15 min using the Freezer Mill (*SPEX*). The resulting whole cell extract was incubated with 40 Units/mL of DNase I (DPRF, *Worthington*), 25 Units/mL of SUPERase RNase Inhibitor (*Ambion*) and 10 mM $MnCl_2$ at 4˚C for 30 min before centrifugation at 48,000 x g for 30 min. Immunopurification was performed using 12 mL (1-L culture equivalent) of cleared lysate and 400 µL (bed-volume) of anti-FLAG agarose (*Sigma-Aldrich*) on a rotator at 4˚C for 2.5 hrs. After washing with Buffer F (20 mM HEPES-KOH pH 7.6, 10% Glycerol, 110 mM KoAc, 0.1% NP-40, 1x PI), elution was performed with 400 µL of 0.5 µg/µL 3xFLAG peptide in Buffer G (20 mM HEPES-KOH pH 7.6, 10% Glycerol, 110 mM KOAc, 0.1% NP-40, 1mM DTT, 1x PI) on a rotator at 4ºC for 2 hrs. RNA co-eluted with the Rpb3-3xFLAG Pol II complex was purified on a miRNeasy column (*Qiagen*) according to manufacturer protocol. Ribosomal RNA was removed for further enrichment of Pol II nascent RNA by the Yeast Ribo-Zero kit (*Illumina*). cDNA library was prepared using the TruSeq stranded mRNA library prep kit (*Illumina*). Sequencing reads were aligned to the yeast genome with Bowtie as described above. A combination of custom Python scripts and BEDTools programs (Quinlan, 2014) were used to generate tag coverage for **Figure 2-21D** and **Figure 2-22C**. The NET-seq data represents the average of two biological replicates.

Chapter Three: Unpublished results

1. H2A.Z nucleosomes are more labile than canonical H2A nucleosomes but do not spontaneously disassemble *in vivo*

Whether the stability of the H2A.Z nucleosome is contributing to the preferential eviction of H2A.Z from promoter-proximal nucleosomes *in vivo* is still not clear. Several studies have shown that H2A.Z nucleosomes are unstable in high salt (Abbott et al., 2001; Jin and Felsenfeld, 2007; Zhang et al., 2005) suggesting that the intrinsic instability of H2A.Z nucleosomes may be the cause of histone dynamics at promoters. However, the salt concentrations used in these studies varied significantly, perhaps because nucleosomes from different sources were used (i.e. metazoans versus yeast or recombinant versus native). To systematically assess the contribution H2A.Z has on nucleosome stability, I used an *in vitro* salt wash assay to probe if H2A.Z nucleosomes disassemble at a lower salt concentration than their canonical H2A counterparts (**Figure 3-1A**). Nucleosomes were incubated with varying concentrations of NaCl in the presence of excess bacteriophage lambda DNA to capture any dissociated histones. The mixtures were then desalted by gel filtration before analysis by native gel electrophoresis. Nucleosomal DNA and free DNA levels were quantified by staining with SYBR Green I. H2A and H2A.Z protein levels were determined by immunoblotting analysis (**Figure 3-1B**).

The H2A and H2A.Z containing nucleosomes were reconstituted using recombinant yeast histone octamers and DNA containing the Widom 601 positioning sequence, as previously

described (Lowary and Widom, 1998; Luk et al., 2010). Consistent with the literature, recombinant H2A.Z nucleosomes disassembled in buffers with lower ionic strength (~700 mM) than recombinant H2A nucleosomes (~900 mM) (**Figures 3-1B**, *left* and *middle* and **3-1C**, *brown* and *blue lines*). In addition, I purified native nucleosomes from yeast cells to test if the histone modifications present *in vivo* would affect their salt sensitivity. Native nucleosomes were obtained by digesting yeast chromatin with MNase followed by sucrose gradient purification. The native nucleosomes dissociated at a lower salt concentration than their recombinant counterparts (~550 mM for native H2A.Z and ~750 mM for native H2A) indicating the *in vivo* histone modifications do have an effect on the salt sensitivity of nucleosomes (**Figure 3-1B**, *right* and **3-1C**, *green* and *red lines*). However, the salt concentration required to disrupt the native H2A.Z nucleosomes is significantly higher than the physiological ionic strength (~150 mM), making it unclear if salt sensitivity *in vitro* is relevant to nucleosome disassembly *in vivo*.

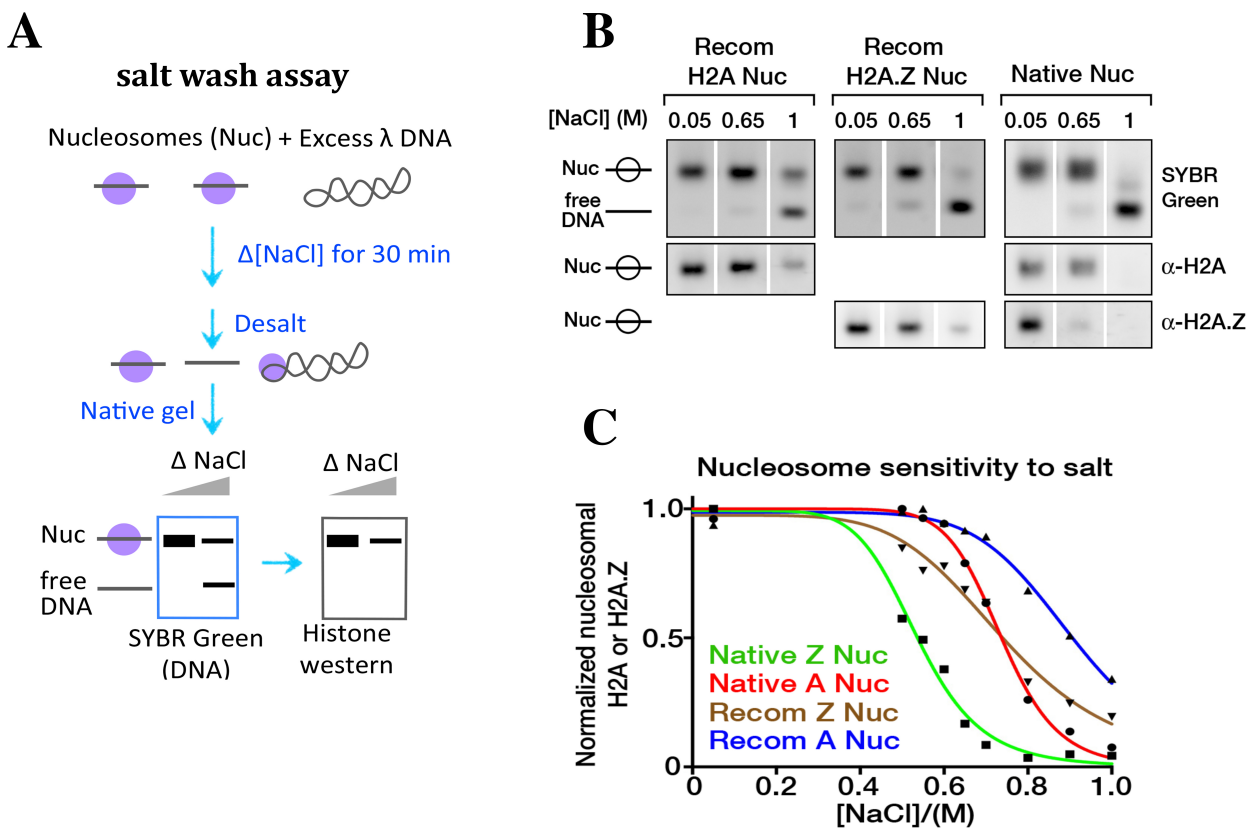

Figure 3-1. H2A.Z containing nucleosomes are more susceptible to salt induced dissociation than H2A nucleosomes. (**A**) Recombinant and native H2A and H2A.Z nucleosomes were incubated with differing concentrations of salt (NaCl) for 30 minutes in the presence of excess lambda DNA. Any histones that dissociate from the nucleosomes will be re-bound by the lambda DNA. The native nucleosomes contain histone modifications and consist of a mixture of H2A and H2A.Z nucleosomes (~10:1 H2A.Z:H2A). After treatment with salt, the samples were desalted on a G50 column and analyzed by native agarose gel electrophoresis and western blotting. (**B**) Native agarose gels stained with SYBR Green I (*top panels*) were analyzed by immunoblotting (*bottom panels*) for recombinant H2A nucleosomes (*left*), recombinant H2A.Z nucleosomes (*middle*), and native nucleosomes (*right*). The location of the nucleosomal (nuc) band and free DNA band are indicated on the left. The concentration of salt used for each lane is shown at the top. Recombinant H2A nucleosomes were immunoblotted with α-H2A antibody, H2A.Z nucleosomes with α-H2A.Z antibody and native nucleosomes with both. (**C**) Quantification of intact H2A and H2A.Z nucleosomes in **B**. Normalized nucleosomal signals represent the percent band intensity of the α-H2A or α-H2A.Z western relative to the 0.05 M NaCl lane normalized to total DNA. nuc: nucleosomes, Recom: recombinant.

To test if intrinsic instability is the predominant mechanism responsible for H2A.Z nucleosome disassembly *in vivo* I inhibited all active cellular processes by using sodium azide (NaN_3) to shutdown ATP production (**Figure 3-2A**). The cells were treated with paraformaldehyde to crosslink the chromatin, which was then isolated and nucleosomes solubilized by MNase treatment. The crosslinks were reversed and the nucleosomal fractions were examined for the presence of H2A.Z. If H2A.Z nucleosomes are inherently unstable then they should dissociate from chromatin spontaneously once ATP-dependent processes are inhibited. Since the SWR1 complex requires ATP, I do not expect any new H2A.Z deposition. After adding 0.1% NaN_3 to cells I saw no change in chromatin bound H2A.Z (**Figure 3-2B**, *left*). This suggests that H2A.Z nucleosomes do not spontaneously disassemble *in vivo*.

To confirm that our assay is sensitive enough to detect H2A.Z depletion, I inactivated H2A.Z deposition using the anchor away technique to conditionally deplete the SWR1 subunit Swc5 from the nucleus (Haruki et al., 2008). Anchor away takes advantage of the flux of ribosomal proteins transiting the nucleus to sequester target proteins to the cytosol (**Figure 3-2C).** Previous work has demonstrated that Swc5 is essential to the H2A.Z deposition activity of SWR1 (**Figure 2-15** and unpublished data of Lu Sun). Depleting Swc5 from the nucleus using anchor away (*SWC5-FRB*) phenocopies the formamide sensitivity of an *htz1*Δ suggesting that rapamycin treatment successfully depletes Swc5 and blocks H2A.Z deposition (**Figure 3-2D**). Interestingly, the *SWC5-FRB* allele is more sensitive to formamide in the presence of rapamycin than the *swc5*Δ mutant, perhaps because its depletion removes additional SWR1 components from the nucleus. Swc5 nuclear depletion resulted in a ~50% decrease of nucleosomal H2A.Z after one hour demonstrating that our assay can detect nucleosomal H2A.Z depletion (**Figure 3-2B**, *right*). Since asynchronous cells were used, at most 15% of the

reduction of H2A.Z can be attributed to dilution of chromatin bound H2A.Z by DNA replication (cell density increased by 30% after addition of RAP) and therefore a minimum of 35% was due to replication-independent remodeling activities.

These data suggest that passive eviction or intrinsic instability is not a major pathway for H2A.Z nucleosome eviction *in vivo*. Rather, energy-dependent activities, such as ATP-dependent remodeling, transcription, and histone modifications, are likely playing key roles.

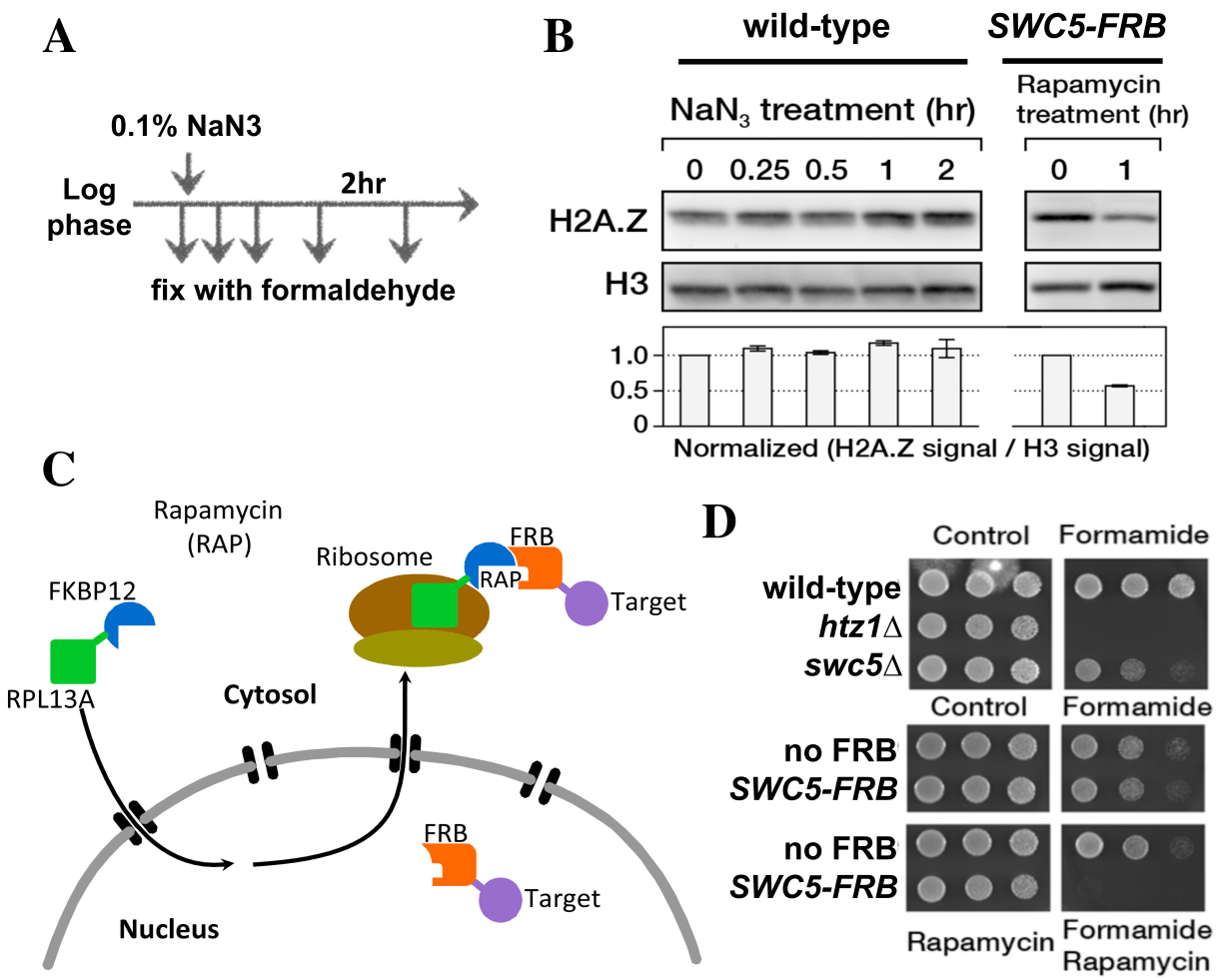

Figure 3-2. Intrinsic instability is not a major mechanism of H2A.Z nucleosome disassembly *in vivo*. (**A, B**) Log phase yeast cells were incubated with 0.1% NaN_3 for various times or with 1.0 µg/mL rapamycin. They were fixed with 3% paraformaldehyde before the chromatin was isolated from the cells. Nucleosomes were solubilized by digestion with micrococcal nuclease (MNase). After reversing the crosslinks, the nucleosomal fractions were analyzed by SDS-PAGE and immunoblotting shown in (**B**). Quantification of (**B**) represents ratios of H2A.Z over H3 signals normalized to time zero. Error bars refer to the range of two experiments. (**C**) Depiction of the anchor away approach. The FKBP12 (rapamycin binding protein) and FRB (a domain of the human mTOR) tags were fused to the 60S ribosomal subunit RPL13A (anchor) and Swc5 subunit (target), respectively. In the presence of rapamycin (RAP) a tight ternary complex will form between Rpl13A-FKBP12, RAP, and Swc5-FRB thereby sequestering Swc5-FRB to the cytosol (Haruki et al., 2008). (**D**) Spotting assay in the presence or absence of 2% formamide and/or 1.0 µg/mL rapamycin.

2. Conditional depletion of the Kin28 subunit of TFIIH results in moderate accumulation of H2A.Z at promoters-proximal nucleosomes

When +1 nucleosomes were ranked and grouped by transcript abundance of their downstream genes (Holstege et al., 1998), a significant rapamycin-dependent increase in Δ(H2A.Z/input) were observed for all five of the transcriptional frequency groups in the *TBP-FRB* cells but not the untagged (*no FRB*) control (**Figure 2-11C** and **Figure 3-3B**, compare *solid black dots* and *white dots*). The amount of H2A.Z accumulation is progressively more prominent when gene expression levels are high (**Figure 2-11C** and **Figure 3-3B**, *solid black dots*). Therefore, basal, constitutive H2A.Z eviction is associated with both active and infrequently transcribed genes but additional H2A.Z eviction is linked to more transcription activity.

TBP loss prevents PIC assembly, and hence transcription initiation and elongation at all genes (Grünberg and Hahn, 2013). To further define the specific step at which H2A.Z eviction occurs, an attempt to impede promoter escape was made by depleting Kin28, the catalytic subunit of the TFIIH kinase module (Hahn and Young, 2011). Pol II dissociates from the GTFs during promoter escape before engaging in productive elongation (Hahn and Young, 2011). This step is facilitated by the kinase module of TFIIH, which phosphorylates serine 5 (Ser 5) on the heptapeptide repeats of the carboxyl-terminal domain (CTD) of Rpb1, the largest subunit Pol II (Feaver et al., 1994). A recent study showed Kin28 depletion by anchor away causes Pol II occupancy to redistribute from the coding region to promoters and stay associated with the mediator complex, indicative of a defect in promoter escape (Wong et al. 2014). Hypothetically, if promoter escape is the driving force of H2A.Z eviction, Kin28 depletion should phenocopy TBP depletion in that the H2A.Z eviction defect should be stronger for active genes where events of promoter escape are more frequent. It should be noted, however, that PIC assembly is also

partially impaired upon Kin28 depletion (Wong et al. 2014); therefore, some defect in H2A.Z eviction is still expected if steps before promoter escape, e.g. promoter scanning by TFIIH or PIC assembly, provide the driving force.

Kin28-FRB was successfully depleted from tested promoters after one hour of rapamycin treatment, observed by ChIP-qPCR (**Figure 3-3C,** unpublished data of Christy Au). Genome wide levels of H2A.Z were measured before and after Kin28 depletion by qChIP-seq. A global H2A.Z eviction defect at +1 nucleosomes was observed (**Figures 3-3D** and **3-3E**), although it is less dramatic than that observed in *TBP-FRB* cells (compare **Figures 3-3D** and **3-3E** with **Figures 2-5C** and **2-5F**, respectively). Importantly, when +1 nucleosomes were sorted and grouped according to transcript abundance, the eviction defect as measured by Δ(H2A.Z/input) did not increase with transcription abundance, in contrast to the *TBP-FRB* depletion strain (compare **Figure 2-11C** with **Figure 3-3A** and **Figure 3-3B**, compare *gray dots* with *solid black dots*). This result appears to argue against promoter escape being the major driving force for H2A.Z eviction. Interestingly, Kin28 and TBP depletion have a comparable H2A.Z eviction defect at infrequently transcribed genes (**Figure 3-3B**, compare *gray dots* with *solid black dots* at <1 mRNA/hr). Given that the amount of PIC components at infrequently transcribed genes is limiting, the partial loss of PICs upon Kin28 depletion could result in a strong negative effect on PIC-dependent H2A.Z eviction. By contrast, active genes may still have some TBP binding to the promoter causing PIC assembly, explaining why these genes did not have a strong increase in relative H2A.Z.

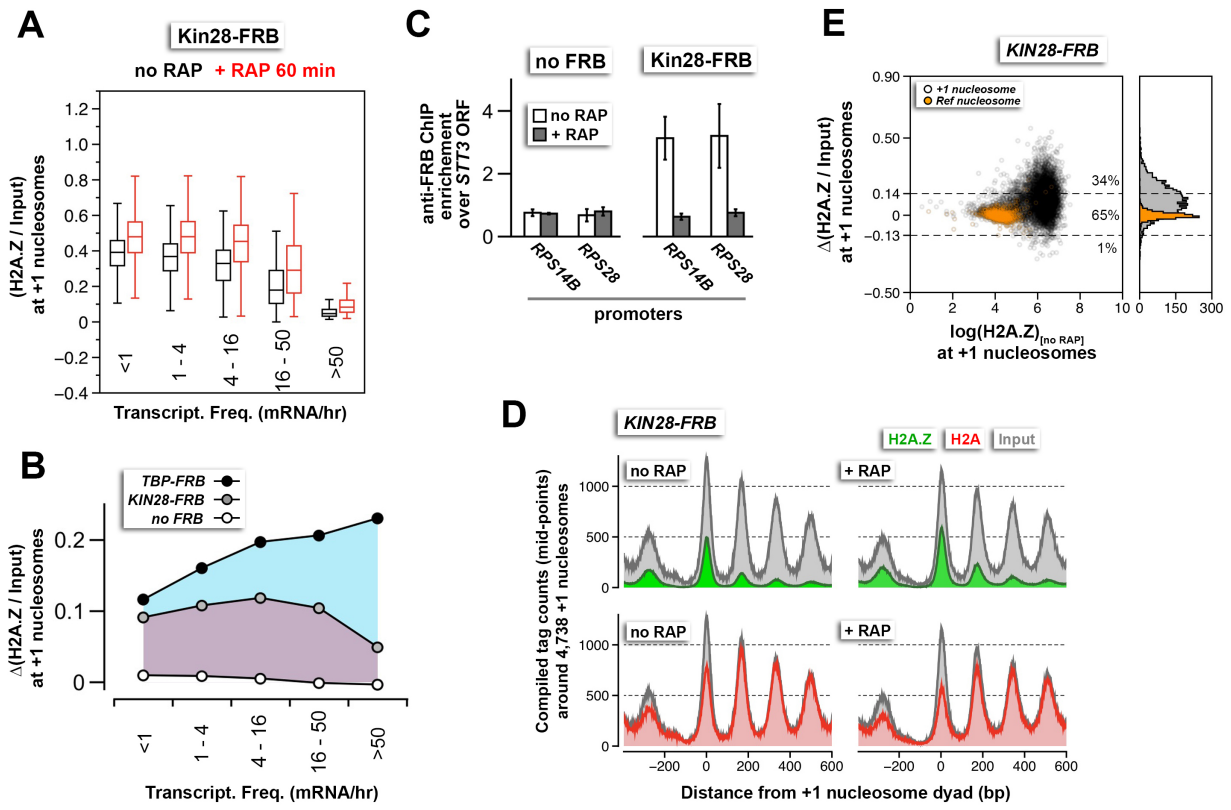

Figure 3-3. Change in relative nucleosomal H2A.Z levels in response to Kin28 depletion. (**A**) The +1 nucleosomes were grouped according to transcriptional frequency (Holstege et al., 1998) and the (H2A.Z/input) values were presented as box plots as described in **Figure 2-11C**. *Box*: interquartile range (IQR); *line in box*: median; *whiskers*: range. (**B**) The change in (H2A.Z/input) upon rapamycin treatment [Δ(H2A.Z/input)] in *KIN28-FRB* (*gray dots*), *TBP-FRB* (*solid black dots*), and the untagged (*no FRB*) control (*white dots*) for each of the five transcriptional frequency groups in (**A**) and **Figure 2-11C** were re-plotted in **B**. (**C**) α-FRB ChIP-qPCR analysis of the untagged (*no FRB)* control and *KIN28-FRB* strains at time 0 (*white bars*) and 1 hr (*gray bars*) after rapamycin treatment (unpublished data of Christy Au). The primers used to probe *RPS14B* and *RPL28* were identical to those in (Wong et al., 2014). (**D**) Compiled read counts (midpoints) of H2A.Z (*green*), H2A (*red*) and input (*gray*) nucleosomes were centered around the dyad of 4,738 +1 nucleosomes (Rhee et al., 2014) before (no RAP) and after Kin28 depletion (+ RAP). (**E**) Scatter plots and histograms showing the change in (H2A.Z/input) of the +1 and reference nucleosomes as a function of endogenous H2A.Z level before rapamycin treatment. The Δ(H2A.Z/input) value was determined as described in **Figure 2-5F**. *Open black circles* in **E** mark the +1 nucleosomes (Rhee et al., 2014). *Orange dots* mark the reference nucleosomes used for normalization as described in **Figure 2-4**. The thresholds (dotted lines) were determined as described in **Figure 2-5F**. The percentages of data points within and outside the threshold regions are indicated. The qChIP-seq and qPCR data represent averages of three independent ChIP reactions (technical replicates) of 2-3 independent cultures (biological replicates). The error bars in **C** represent standard deviation.

3. Deletion mutants of *ARP5* and *ARP8*, which encode critical subunits of INO80 complex, does not result in global accumulation of H2A.Z

The INO80 complex is an ATP-dependent remodeler and part of the same family of remodelers as SWR1. Craig Peterson's group has reported that INO80 can remove a nucleosomal H2A.Z-H2B dimer and insert an H2A-H2B dimer via a histone replacement mechanism *in vitro* (Papamichos-Chronakis et al., 2011). If this is true *in vivo*, I expect inactivation of INO80 activity will lead to the coordinated accumulation of H2A.Z and depletion of H2A at promoters, similar to *TBP-FRB*. However, when Ino80 is depleted using anchor away no significant global change in relative H2A.Z levels at promoters or within the coding region of the gene is observed, as measured by qChIP-seq (**Figures 2-17A-C**). Therefore, I concluded that INO80 does not have a significant role in regulating H2A.Z dynamics at the majority of yeast genes.

To further support this conclusion I decided to measure nucleosomal H2A.Z and H2A in *arp8Δ* and *arp5Δ* mutants using qChIP-seq. Both *ARP8* and *ARP5* encode critical subunits of the INO80 complex (van Attikum et al., 2007; Saravanan et al., 2012; Yao et al., 2016). In fact, deletion mutant of *ARP5* has previously been shown to accumulate H2A.Z, specifically at promoter regions (Yen et al., 2013). Therefore, chromatin from wild type (WT) cells and cells mutant for *ARP5* or *ARP8* were purified and subjected to qChIP-seq to determine the relative levels of H2A and H2A.Z genome-wide. In agreement with conditional depletion of Ino80 (**Figure 2-17**), no significant accumulation of H2A.Z was observed at the +1 nucleosomal position or within the coding region in *arp5*Δ and *arp8*Δ mutant cells (compare WT to *arp5*Δ or *arp8*Δ in **Figures 3-4A** and **3-4B**, *top*). In fact, there was a small but noticeable decrease in H2A.Z levels at the +1 position in both mutants.

Since examining the compiled tag counts, which reflect the averaged nucleosomal signals of all genes, could obscure any changes that might be occurring in a small subset of genes, I then evaluated the change in H2A.Z occupancy at individual +1 positions genome-wide (**Figure 3-4C** and **3-4D**); method described in detail in **Section 2.2** and **Figure 2-5F**. Briefly, the change in (H2A.Z/input) ratios in the mutants relative to the WT {i.e. $(\text{H2A.Z/input})_{[arp5\Delta \text{ or } arp8\Delta]} - (\text{H2A.Z/Input})_{[WT]}$} was plotted against the endogenous H2A.Z levels of the WT. As stated in **Chapter Two**, the threshold for significant change in (H2A.Z/input) is signified by two standard deviations above and below the median of the untagged (*no FRB*) anchor away control strain. However, it should be noted that the anchor away strains come from a different strain background (W303) than the WT, *arp5*Δ and *arp8*Δ mutant strains (BY4741) that were used in this experiment. Therefore, using the *no* FRB anchor away control strain to determine the threshold for significant change for the *arp5*Δ and *arp8*Δ mutants might not be entirely accurate. In the future, a biological replicate of the WT should be performed and new thresholds calculated as two standard deviations above and below the median of the WT. However, when using the thresholds defined in **Chapter Two**, only 7.2% and 2.7% of +1 nucleosomes demonstrated a significant increase in relative H2A.Z levels in the *arp5*Δ and *arp8*Δ mutant cells, respectively (**Figures 3-4C** and **3-4D**)**.** These results are in agreement with the Ino80 depletion experiment, in which 3.8% of +1 nucleosomes demonstrated a significant increase in relative H2A.Z signal (**Figure 2-17C**). By comparison, 56.0% of +1 nucleosomes exhibited a significant increase upon TBP depletion (**Figure 2-5F**) and 52.4% upon Rpb1 depletion (**Figure 2-9C**). It is interesting to note that 24.8% and 32.0% of +1 nucleosomes exhibited a significant decrease in relative H2A.Z signal in *arp5*Δ and *arp8*Δ mutant cells, respectively (**Figures 3-4C** and **3-4D**). However, what is responsible for this decrease in relative H2A.Z levels is not clear.

Previous studies, as well as my own data, have demonstrated a role for INO80 in histone octamer sliding (Shen et al., 2003; Yao et al., 2016; Yen et al., 2012; **Figure 2-17D**). In agreement with this function, the nucleosomal arrays are "fuzzier" in *arp5*Δ and *arp8*Δ mutants, indicated by a decrease in nucleosomal peak height, broadening of the peak and an increase in signal within the linker regions (compare input *(gray)* nucleosomes in **Figures 3-3A** and **3-3B**, *top*). The chromatin arrays of 983 genes, previously determined to require Ino80 for positioning (**Figure 2-17D**), were compiled and input nucleosomes plotted in **Figure 3-3E**. Similar to Ino80 depletion, the promoter-proximal -1 and +1 nucleosomes shifted away from the NDR in *arp5*Δ and *arp8*Δ mutants (**Figure 3-3E**). In addition, nucleosomes within the coding region shifted toward the NDR in *arp5*Δ and *arp8*Δ mutants, which were not previously observed upon depletion of Ino80 (compare **Figure 3-3E** and **Figure 2-17D**, *bottom*). As shown in **Figure 2-18A** the positional shift of gene body nucleosomes toward the NDR is indicative of a defect in Pol II activity. Therefore, one possible explanation for this discrepancy would be if the transcriptional frequency of the 983 genes examined were decreased in *arp5*Δ and *arp8*Δ mutants but unaffected in *INO80-FRB* after 90 min of rapamycin treatment.

Overall, I conclude that INO80 complex does not have a dominant role in the constitutive turnover of H2A.Z nucleosomes at the promoter genome-wide. Instead, our data suggest that INO80 contributes to the positioning of the promoter-proximal nucleosomes by sliding histone octamers away from the NDR and this positioning may have a positive effect on gene expression at some genes. However, our data does not rule out the possibility that INO80 may be responsible for evicting H2A.Z at a small subset of unique promoters upon induction.

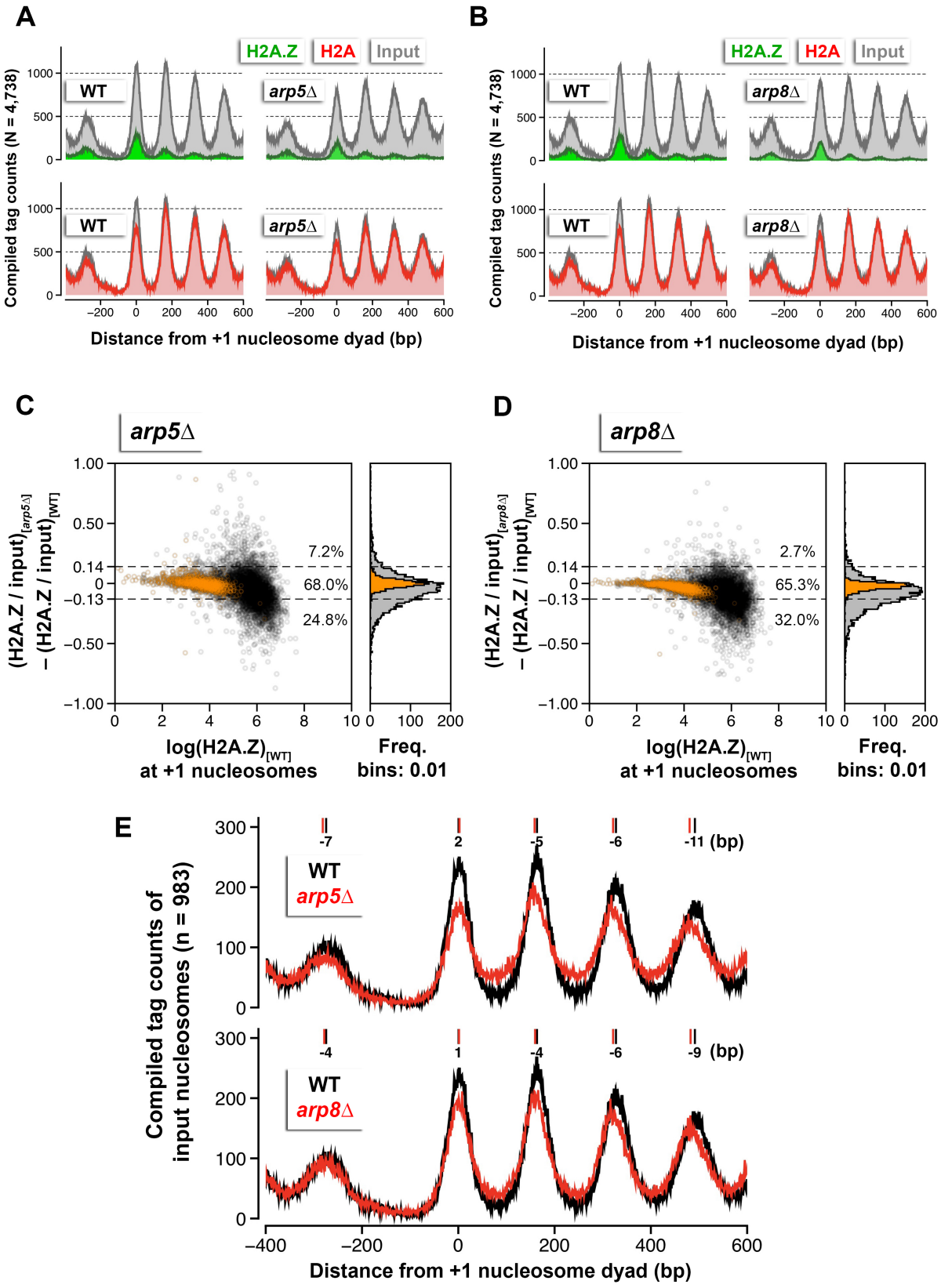
A
H2A.Z
H2A
Input
WT
arp5Δ
Compiled tag counts (N = 4,738)
Distance from +1 nucleosome dyad (bp)
B
WT
arp8Δ
C
arp5Δ
(H2A.Z / input)[arp5Δ] – (H2A.Z / input)[WT]
7.2%
68.0%
24.8%
log(H2A.Z)[WT] at +1 nucleosomes
Freq. bins: 0.01
D
arp8Δ
2.7%
65.3%
32.0%
E
Compiled tag counts of input nucleosomes (n = 983)
WT
arp5Δ
-7
2
-5
-6
-11 (bp)
WT
arp8Δ
-4
1
-4
-6
-9 (bp)
Distance from +1 nucleosome dyad (bp)

Figure 3-4. Relative H2A.Z levels in *arp5*Δ and *arp8*Δ mutants. (**A**) Compiled read counts (midpoints) of H2A.Z (*green*), H2A (*red*), and input (*gray*) nucleosomes were centered around +1 nucleosome dyads (Rhee et al., 2014) in wild type (WT) and *arp5*Δ mutants. (**B**) Same as **A** except for *arp8*Δ mutants. (**C**, **D**) Scatter plots and histograms showing the change in (H2A.Z/input) of +1 and reference nucleosomes relative to WT for *arp5*Δ (**C**) and *arp8*Δ (**D**), as a function of endogenous H2A.Z level in WT cells. *Open black circles* in **C** and **D** mark the +1 nucleosomes (Rhee et al., 2014). *Orange dots* mark the reference nucleosomes used for normalization as described in **Figure 2-4**. The thresholds (dotted lines) were determined as described in **Figure 2-5F**. The percentages of data points within and outside the threshold regions are indicated. (**E**) The compiled tag counts of the input nucleosomal fraction in WT cells (*black*) and *arp5*Δ (top, *red*) or *arp8*Δ (bottom, *red*) was plotted for the 983 Ino80-dependent genes determined in **Figure 2-17D** using data from **Figures 3-5A** and **3-5B**. The integers above the nucleosomal peaks indicate shift distance in base pairs. Positive values indicate right-shift in mutant relative to WT and vice versa. Peak center positions were determined as described in **Figure 2-17D**.

4. Robust H2A.Z dynamics is linked to TFIID, which binds free histones *in vitro*

The +1 nucleosomes that exhibit strong H2A.Z dynamics revealed by TBP-FRB depletion are associated with promoters that are generally more enriched for TFIID than SAGA complex (**Figures 2-11A** and **2-11C**). To assess if other component(s) of the transcription machinery are linked to H2A.Z turnover, +1 nucleosomes were ranked and binned according to change in H2A.Z (ΔZ) or change in H2A (ΔA) levels after TBP-FRB depletion and plotted against the standardized occupancy of GTFs and Pol II (Rhee and Pugh, 2012) (**Figure 3-5A**). While other components of the PIC exhibit slight positive correlations with H2A.Z accumulation the trends are much less dramatic when compared to TFIID (**Figure 3-5A**). In addition, a strong inverse correlation is observed when the ranking of ΔA is plotted against TFIID occupancy (**Figure 3-5A**). This suggests that TFIID may also play a role in the reformation of H2A nucleosomes after H2A.Z disassembly.

TFIID includes TBP and is one the first factors recruited to the promoter during transcription initiation making it a likely candidate for recognition of the +1 H2A.Z nucleosome. TFIID consists of 14 TBP-associating factors (Tafs), nine of which bear the histone fold domain (HFD) (Papai et al., 2011). *In vitro*, the Taf-associated HFD proteins can form heterodimeric complexes resembling histone dimers and they have been shown to bind core histones *in vitro* (Hoffmann et al., 1996). Therefore, I hypothesized that the TFIID complex may be able to bind histones. This idea was tested using immunoprecipitates of yeast extracts containing FLAG-tagged Taf1 or Taf2, the largest subunits of TFIID, which were incubated with recombinant $(H3\text{-}H4)_2$ tetramers, H2A-H2B dimers or H2A.Z-H2B dimers and then washed with a buffer containing 0.3 M KOAc, 10% glycerol and 0.01% NP-40 (**Figure 3-5B**). The bound histones were then eluted with FLAG peptides and analyzed by immunoblotting using antibodies to either

histone H3 or H2B. TFIID binds to $(H3\text{-}H4)_2$ tetramers and to H2A.Z-H2B and H2A-H2B dimers with no apparent preference (**Figure 3-5B**). This result suggests that TFIID may function as a histone chaperone to assist nucleosome disassembly.

To determine whether TFIID can preferentially bind or disassemble H2A.Z nucleosomes *in vitro*, **Christy Au** and I affinity purified TFIID from yeast extracts, which was further enriched by mono S chromatography (Sanders et al., 2002) (**Figure 3-5C**). The following experiments were initiated by me and continued by **Christy Au**. Nucleosomes containing H2A or H2A.Z were reconstituted on a 204-bp DNA with the 147-bp Widom "601" positioning sequence near one end and a 50-bp linker on the other (Lowary and Widom, 1998). The TATA element was omitted from the DNA to remove the complication of TFIID binding directly to the DNA through TBP and to mimic the +1 nucleosome of a TATA-less promoter. The resulting nucleosomes were end-labeled with the fluorescent dyes Cy3 or Cy5 to mark the H2A-containing (AA) or H2A.Z-containing (ZZ) nucleosomes, respectively, and were further purified by sucrose gradient sedimentation. Equimolar amounts of the differentially labeled AA and ZZ nucleosomes (0.1 pmol each) were incubated with TFIID (0.125 pmol) in a competition assay (Ranjan et al., 2013) (**Figure 3-5D**, experiment done by **Christy Au**). The addition of TFIID caused a supershift of both AA and ZZ nucleosomes at similar ratios indicating that TFIID binds both nucleosomal species with no apparent preference (**Figure 3-5D**, experiment done by **Christy Au**). To see if TFIID can disrupt the nucleosomes after binding, the bound nucleosomes were released from TFIID by the addition of competitor DNA. Intact nucleosomes were released without any free DNA indicating that the binding was reversible and that TFIID did not disrupt the nucleosomes after binding (**Figure 3-5E**, experiment done by **Christy Au**). Therefore, TFIID alone is not sufficient to dissociate H2A.Z nucleosomes.

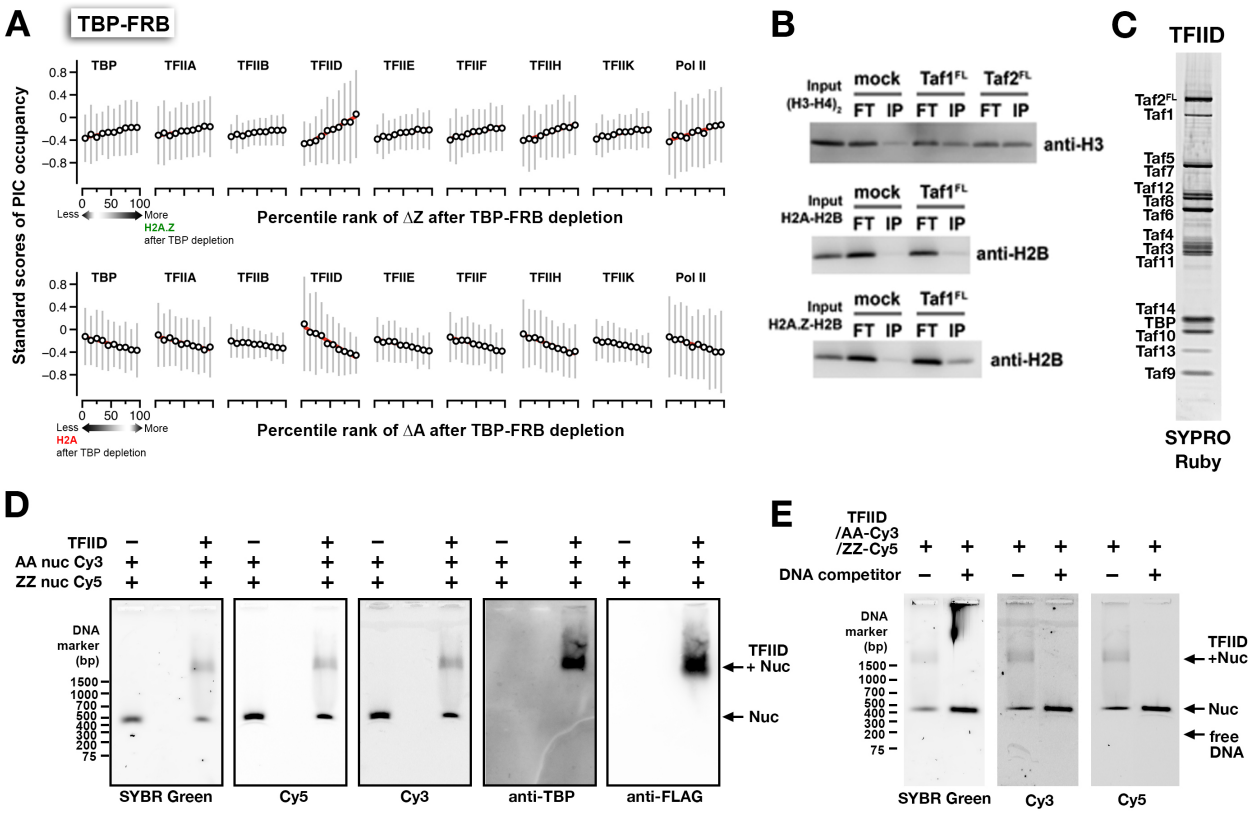

Figure 3-5. TFIID does not preferentially bind H2A.Z nucleosomes or H2A.Z-H2B dimers. (**A**) Correlation of the change in H2A.Z (ΔZ) or H2A (ΔA) levels with the occupancy of PIC components after TBP-FRB depletion (Rhee and Pugh, 2012). The genes in *TBP-FRB* cells were ranked and binned into ten percentiles according to the amplitude of ΔZ or ΔA around the +1 positions. Positive values along the x-axis reflect an increase in nucleosomal occupancy and vice-versa. Standard score of PIC occupancy corresponds to the averaged score within each bin. The red line in each plot represents a linear curve fitting function. (**B**) TFIID binding assay for free histones. TFIID was immunoprecipitated from whole cell extracts prepared from yeast expressing the FLAG tagged *TAF1* or *TAF2*, as well as an untagged control strain. The beads were incubated with recombinant $(H3\text{-}H4)_2$ tetramers, H2A-H2B dimers or H2A.Z-H2B dimers and bound proteins eluted with FLAG peptides. Equivalent amounts of FLAG eluates (IP) and FT fractions, as well as 17% of input histones, were analyzed by SDS-PAGE and immunoblotting with α-H3 and α-H2B antibodies. (**C**) TFIID complex was affinity purified from yeast extracts with α-FLAG beads and further enriched by mono S chromatography (data contributed by **Christy Au**). Purified TFIID analyzed by SDS-PAGE and stained with SYPRO Ruby (*Invitrogen*). (**D**) Gel shift assay with purified TFIID complex from **C** incubated with recombinant H2A.Z/H2A.Z nucleosomes (ZZ) and H2A/H2A (AA) nucleosomes end-labeled with the fluorescent dyes Cy5 or Cy3, respectively (data contributed by **Christy Au**). ZZ nucleosomes will fluoresce in Cy5 scan and AA nucleosomes in Cy3 scan. Immunoblotting with α-FLAG and α-TBP antibodies was performed to confirm the presence of TFIID at the shifted nucleosomal bands. (**E**) TFIID bound nucleosomes from **D** were incubated with competitor DNA to sequester TFIID and check if nucleosome structure was disrupted after binding (data contributed by **Christy Au**).

Chapter Four: Discussion

In budding yeast, the coordinated recruitment of chromatin remodeling factors, such as RSC and SWI/SNF, to the promoter region establishes a chromatin structure that is relatively depleted of histones at most genes, thereby guiding the transcription machinery to assemble upstream of the +1 nucleosome (Badis et al., 2008; Brown et al., 2011; Bryant et al., 2008; Ganguli et al., 2014; Hartley and Madhani, 2009; Lee et al., 2007; Parnell et al., 2008; Rhee and Pugh, 2012). Furthermore, formation of the promoter NDR recruits the chromatin remodeler SWR1 which, in turn, catalyzes a histone exchange reaction, converting homotypic H2A nucleosomes to homotypic H2A.Z nucleosomes at the +1 position (Luk et al., 2010; Ranjan et al., 2013). Previous studies have demonstrated that rapid H3 turnover is occurring at the +1 position of most genes, suggesting that +1 nucleosomes are undergoing repeated cycles of complete nucleosome disassembly followed by reassembly (Dion et al., 2007; Rufiange et al., 2007). My thesis work demonstrated that component(s) of the Pol II transcription machinery are required for catalyzing the preferential eviction of H2A.Z from the +1 nucleosomal position at both active and infrequently transcribed genes. I proposed the 'histone cycle' model to explain the events contributing to the constitutive turnover of H2A.Z at promoter-proximal nucleosomes genome-wide (**Figure 2-23**).

In this section I will discuss outstanding questions regarding the histone cycle model as well as propose some future experiments to further dissect the mechanism of the PIC-dependent H2A.Z eviction process. In our experiments, constitutive turnover of H2A.Z was blocked with

conditional depletion mutants of the transcription machinery (*TBP-FRB* and *RPB1-FRB*). Since TBP is required to nucleate PIC assembly and Rpb1 is one of the core subunits of Pol II, removal of these proteins will likely cause disassembly of the entire PIC. This means that all steps after PIC assembly, i.e. promoter melting, promoter escape, and productive elongation are blocked. Therefore, the H2A.Z eviction defect associated with PIC depletion could be due to any of these steps. In addition, I could not identify which component(s) of the transcription machinery provide the driving force that actively disassembles +1 H2A.Z nucleosomes. In fact, it remains possible that the transcription machinery is indirectly evicting H2A.Z nucleosomes through the recruitment of an unknown chromatin remodeler, which becomes absent from promoters after PIC depletion. Future experiments should be dedicated to determining the mechanistic steps at which H2A.Z nucleosomes are remodeled when genes are preparing for transcription. Specifically, during what step(s) of transcription are the H2A.Z nucleosomes being disassembled, what component(s) of the PIC are driving this disassembly, and how are H2A.Z nucleosomes preferentially evicted over H2A nucleosomes.

1. Are the molecular events of promoter melting and/or promoter escape responsible for driving disassembly of H2A.Z nucleosomes at the promoter?

During transcription initiation, the 10-polypeptide TFIIH complex plays important roles in promoter melting and promoter escape, specifically the DNA-dependent translocase subunit, Ssl2, and the cyclin-dependent protein kinase subunit, Kin28 (Gibbons et al., 2012). After PIC assembly, promoter melting is mediated by the Ssl2 translocase subunit of TFIIH, which unwinds or 'melts' ~10-15 bp of DNA downstream of TBP (Kim et al., 2000) (**Figure 1-2**). The

single stranded DNA template is then inserted into the activation cleft of Pol II to form the 'open complex' and initiate the polymerization reaction (Murakami et al., 2013; Wang et al., 1992). When the nascent RNA chain grows >10 nucleotides, a conformational change in the 'open complex' occurs, allowing the release of an elongating Pol II, while the GTFs remain behind at the promoter or dissociate, in a process called promoter escape (Hahn, 2004; Holstege et al., 1997; Yudkovsky et al., 2000) (**Figure 1-2**). During the transition from promoter escape to productive elongation the TFIIH kinase subunit, Kin28, phosphorylates the heptapeptide (YSPTSPS) repeat on the CTD of Pol II (Egly and Coin, 2011; Hsin and Manley, 2012). According to the cryo-EM structure of yeast PIC, TFIIH is positioned in close proximity to the +1 nucleosome (Murakami et al., 2013). Therefore, I speculate that the activities of TFIIH during promoter melting and/or promoter escape are playing a major role in driving the preferential disassembly of H2A.Z nucleosomes at the +1 position. If promoter melting is the driving force, I expect inactivation of Ssl2 will lead to H2A.Z accumulation, whereas Kin28 inactivation will not. If promoter escape or elongation is the driving force, then Kin28 inactivation will accumulate H2A.Z.

1.1. Inactivating Kin28 subunit of TFIIH to evaluate if promoter escape or elongation provides the driving force of H2A.Z eviction

In an effort to test if the kinase activities of TFIIH during promoter escape and elongation are important for H2A.Z eviction I previously used an anchor-away mutant of the TFIIH kinase subunit, Kin28 (*KIN28-FRB*), detailed in **Section 3.3**. The Struhl lab has shown that Kin28 depletion, caused by rapamycin treatment in the *KIN28-FRB* mutant, led to redistribution of Pol

II from the gene body to the promoter, indicative of a defect in promoter escape (Wong et al., 2014). Using a similar growth condition, I depleted Kin28 and observed an accumulation of H2A.Z at the +1 position that was less dramatic than what was observed for TBP depletion (**Figure 3-3**). Although these data are consistent with promoter escape being able to drive H2A.Z eviction; the depletion of Kin28 by anchor away also leads to a strong decrease in TBP occupancy at promoters (Wong et al., 2014, my unpublished data). This result suggests the PIC could also be depleted when Kin28 was removed. Therefore, it is unclear whether the defect in H2A.Z eviction at promoters is due to the loss of Kin28 or the loss of the entire PIC. Given this potential caveat I cannot conclude whether H2A.Z eviction is occurring before or after promoter escape.

In an attempt to circumvent the PIC assembly defect caused by Kin28 depletion, future experiments should, instead utilize an ATP-analog sensitive mutant of TFIIH (*kin28-as*) to block promoter escape. This *kin28-as* allele encodes a Kin28 protein that bears a space-creating mutation within the ATP binding pocket of the kinase that allows for specific binding of a bulky ATP analog (Lopez et al., 2014). In the *kin28-as* mutant, the kinase activity of the Kin28 protein can be inactivated by adding the chemical inhibitor 1-NA-PP1 (Liu et al., 2004). Previous studies have demonstrated that treatment of *kin28-as* cells with 1-NA-PP1 for one hour resulted in an increase of Pol II occupancy at the 5' end of the gene and a decrease in the coding region, consistent with a defect in promoter escape (Kanin et al., 2007; Wong et al., 2014). Importantly, the inactivation of Kin28 with 1-NA-PP1 should have no effect on the Ssl2 translocase subunit of TFIIH and subsequent promoter melting. Using qChIP-seq the relative levels of H2A.Z and H2A can be measured genome-wide, as described above, before and after the inactivation of Kin28 by 1-NA-PP1. If promoter escape or elongation is driving H2A.Z eviction then H2A.Z

levels will increase and H2A levels will decrease after inactivation of Kin28, similar to TBP depletion. However, if some step prior to promoter escape, such as assembly of the PIC or promoter melting, is the driving force for H2A.Z eviction then H2A.Z levels should not change.

1.2. Are H2A.Z nucleosomes more susceptible to disassembly from TFIIH mediated DNA unwinding?

During promoter melting and open complex formation, the upstream DNA is held in a fixed position by TBP as the TFIIH translocase subunit, Ssl2, pulls the downstream DNA into the active center of Pol II (Fishburn et al., 2015) (**Figure 4-1**). This activity drives the unwinding of the DNA duplex near the TATA region, resulting in the formation of a single stranded DNA structure called the 'transcription bubble' (Kim et al., 2000). Recently, the Kornberg lab demonstrated that the yeast PIC repeatedly scans the promoter for the TSS over a ~85 bp region, which leads to cycles of transcription bubble formation and collapse before committing to promoter escape (Fazal et al., 2015). Since the DNA region between TBP and the +1 nucleosome is topologically constrained (meaning that the two DNA ends are not free to rotate) the formation of the transcription bubble overwinds the downstream DNA, leading to a topological strain on the +1 nucleosome (**Figure 4-1**). Given that overwound DNA is topologically equivalent to positive supercoils and that the nucleosomal DNA wraps around the octamer core in a negative supercoil, I propose that Ssl2 mediated transcription bubble formation within the NDR destabilizes the +1 nucleosome and that nucleosomes containing H2A.Z, which are more labile, are preferentially disassembled compared to those containing H2A. In addition,

the turnover of H2A.Z at infrequently transcribed genes can be explained by transcription bubble formation and collapse without commitment to promoter escape and elongation.

To test if topological stress can remove H2A.Z nucleosomes preferentially, I propose an *in vitro* approach. Circular chromatin arrays can be used to mimic the topologically constrained promoter architecture (Dyer et al., 2004). These chromatin arrays will be generated by standard chromatin assembly protocols using H2A.Z- or H2A-containing histone octamers and a negatively supercoiled DNA plasmid, in the presence of the histone chaperone Nap1. In addition, native NDR and nucleosomal positioning sequences can be inserted into the plasmid to better mimic the promoter architecture. As an alternative to this approach, native chromatin circles can be affinity purified from yeast using the 8xLacO-bearing TALO8 minichromosome system (Unnikrishnan et al., 2010). After obtaining the chromatin arrays, positive supercoils can be introduced (described below) into the circular chromatin array to simulate Ssl2 mediated DNA unwinding. The idea is to test if the formation of positive supercoils can be a driving force for nucleosome disassembly and whether H2A.Z nucleosomes are more prone to disassembly by positive supercoils than H2A nucleosomes. In the sections below I propose two methods to cause DNA unwinding:

1.2.1. Using ethidium bromide intercalation to produce DNA unwinding

Ethidium bromide (EtBr) is a nucleic acid intercalating agent and incorporation between bases causes the DNA to unwind (Balcerski and Pysh, 1976; Hayashi and Harada, 2007). This has been shown on a circular *E. coli* chromosome where addition of EtBr can remove negative supercoils in a concentration dependent manner (Weitao et al., 2000). EtBr has also been

successfully used to dissociate mononucleosomes and the degree of dissociation was time dependent (McMurray and van Holde, 1986). To test if the formation of positive supercoils can be a driving force for nucleosome disassembly circular H2A- or H2A.Z-containing arrays will be treated with or without EtBr, or will be nicked with an endonuclease (e.g. Nb.BbvCI, *New England Biolabs*) to release topological constrain before treatment with EtBr. The arrays will then be digested with MNase and analyzed by qPCR using primers corresponding to sequences within the nucleosome. I expect the EtBr treated samples to give less qPCR signal at the indicated nucleosomal region compared to the nicked or untreated control if histone eviction has occurred. In addition, if H2A.Z nucleosomes are more sensitive to positive supercoiling of the DNA than H2A nucleosomes I expect less qPCR signal from H2A.Z-containing arrays compared to H2A-containing arrays at a given EtBr concentration.

Alternatively, EtBr-induced histone eviction can be measured by sucrose gradient centrifugation followed by SDS-PAGE and histone H3 Western analysis. If nucleosomes have dissociated from the DNA less H3 is expected in the chromatin fraction. These conditions will then be applied to H2A.Z or H2A nucleosome arrays. If H2A.Z nucleosomes are more sensitive to disassembly by positive supercoils, I expect to see less H3 in the chromatin fraction.

1.2.2. Using reverse gyrase to introduce positive supercoiling

Reverse gyrase is a unique ATP-dependent topoisomerase found in thermophiles that can introduce positive supercoils in circular DNA (Forterre et al., 1985). It is composed of two domains that resemble a topoisomerase IA and a SF2 helicase (Perugino et al., 2009). The enzyme is thought to have evolved to protect DNA from denaturation at high temperatures and

its enzymatic activity is optimal at 75˚C and functional at 55.0˚C (Kikuchi and Asai, 1984). Since nucleosomes are stable at 55˚C (Dyer et al., 2004) reverse gyrase can be used to introduce positive supercoils into the circular H2A.Z- or H2A-containing nucleosomal arrays and ask if they will disassemble differentially. Histone eviction will be analyzed as described for EtBr.

2. TFIID may be acting as a histone chaperone during H2A.Z eviction

One observation revealed by the H2A.Z qChIP-seq experiment is that the +1 nucleosomes that exhibited the strongest H2A.Z accumulation after TBP-FRB depletion are generally more enriched for TFIID (**Figure 2-11A** and **Figure 3-5A**). TFIID, which contains TBP, is one of the general transcription factors that binds the promoter during transcription initiation and begins formation of the PIC. This raises the possibility that TFIID may be playing a role in the PIC-dependent eviction of H2A.Z at +1 nucleosomal positions. However, the inability of purified TFIID complex to specifically bind and disrupt H2A.Z nucleosomes suggests that it is not sufficient to drive H2A.Z nucleosome disassembly (**Figures 3-5D** and **3-5E**). Therefore, TFIID may function as a histone chaperone to accept and/or donate histones during the assembly and disassembly of the +1 nucleosome. Indeed, when immobilized native TFIID complex was incubated with H2A-H2B and H2A.Z-H2B dimers and $(H3\text{-}H4)_2$ tetramers I observed that TFIID is capable of binding to all histone pairs indiscriminately (**Figure 3-5B**).

In addition to TBP, TFIID is comprised of 14 additional subunits called TBP-associating factors or Tafs, nine of which contain the histone specific histone fold domain (Papai et al., 2011). A previous study has demonstrated that recombinant histone fold domains of TFIID are

able to bind free histone monomers *in vitro* and some of the histone fold domain containing Tafs can form stable heterodimeric complexes, similar to histones (Hoffmann et al., 1996). In fact, analysis of the primary sequence of the Taf6, Taf9, Taf12, and Taf4 histone fold domains reveal a striking similarity to the canonical histones H4, H3, H2B, and H2A, respectively (Cler et al., 2009). In addition, the histone fold domains of Taf12 and Taf4 form a heterodimeric complex similar to the H2A-H2B dimer and the histone fold domains of Taf6 and Taf9 form a complex similar to the $(H3\text{-}H4)_2$ tetramer (Selleck et al., 2001). Furthermore, these Tafs can form an octameric complex *in vitro* suggesting the existence of a histone octamer-like structure within TFIID *in vivo* (Selleck et al., 2001). Therefore, I speculate that the Taf6-Taf9 complex could bind to H2A-Z-H2B and H2A-H2B dimers whereas the Taf12-Taf4 complex could bind to the $(H3\text{-}H4)_2$ tetramer.

To directly test the idea that the Taf pairs can bind histone pairs the recombinant proteins will be purified and checked if they can form a complex *in vitro*. It will be interesting to see if the different Taf pairs display a preference for specific histone pairs or if they act as general histone acceptors. In particular, it will be important to test if the Taf6-Taf9 complex exhibits a preference for H2A.Z-H2B dimers over H2A-H2B dimers. If it does, it suggests that TFIID could be acting as an H2A.Z chaperone during PIC-dependent disassembly of the +1 nucleosome, explaining the preferred eviction of H2A.Z at promoters.

3. A 'partial PIC' may remain bound at RP genes in *RPB1-FRB* that can catalyze eviction of H2A.Z

H2A.Z eviction was blocked at most +1 nucleosomes after the depletion of TBP or Rpb1. However, many ribosomal protein (RP) genes exhibited a different phenomenon in that the H2A.Z eviction defect associated with Rpb1 depletion is significantly less severe than for TBP depletion (compare **Figure 2-11B** and **Figure 2-12B**). One explanation for this discrepancy could be due to incomplete removal of PIC at RP gene promoters in the Rpb1 depletion mutant. The 'partial PIC' that is left behind after Rpb1 depletion may then be sufficient for catalyzing the eviction of the +1 H2A.Z nucleosome. Therefore, these genes provide us with the unique opportunity to understand what components of the PIC are important for driving the disassembly of +1 H2A.Z nucleosomes. Specifically, if I probe the composition of the PIC at RP genes after Rpb1 depletion we can narrow down what PIC components are required for evicting H2A.Z.

The yeast genome contains 137 RP genes, which encode 78 distinct ribosomal proteins, and are among the most highly transcribed genes (Warner, 1999). The expression of these genes is tightly regulated resulting in activation during growth and repression upon stress or starvation. Transcriptional regulation in RP genes utilizes a set of transcriptional activators and repressors that are distinct from other genes. For example, the transcription factor Rap1 (repressor activator protein 1) is bound to the majority of RP gene promoters and helps recruit the GTF TFIID (Layer et al., 2010; Lempiäinen and Shore, 2009; Papai et al., 2010). Even when RP genes are repressed, Rap1 remains bound at promoters but associates with different transcription factors and functions as a repressor instead. Therefore, due to its unique regulation and high expression it is possible that conditionally depleting Rpb1 and TBP for 60 minutes may lead to different promoter states. Whereas TBP depletion is still likely to result in complete disassembly of the

PIC, Rpb1 depletion may leave a 'partial PIC' bound at the promoter, which can continue to evict H2A.Z.

To test the hypothesis that a 'partial PIC' remains bound at RP genes in *RPB1-FRB*, ChIP can be performed on candidate PIC components before and after depletion of Rpb1 and occupancy probed using qPCR. It would be especially interesting to see if TFIID and TFIIH remain bound at RP gene promoters. If so, it would support the hypothesis that it is the unwinding of the DNA mediated by TFIIH during promoter melting that is providing the driving force for H2A.Z eviction, while TFIID facilitates the eviction process by behaving as a histone chaperone.

4. Concluding remarks

I have studied how the transcription machinery is involved in chromatin remodeling in and around the promoters of budding yeast. My data suggest that +1 nucleosomes that are assembled with H2A.Z are undergoing constitutive turnover at active and infrequently transcribed Pol II genes and components of the PIC are required for this turnover. I speculated that constitutive H2A.Z turnover is necessary to prime genes for activation, resulting in rapid gene induction under appropriate conditions (Santisteban et al., 2000; Venters et al., 2011; Zhang et al., 2005). Contrary to earlier studies I did not observe any significant change in H2A.Z levels upon inactivation of the remodeler INO80, which has previously been reported to catalyze H2A.Z eviction (Papamichos-Chronakis et al., 2011; Yen et al., 2012). It is possible that INO80 is responsible for removing H2A.Z at specific genes upon gene activation whereas constitutive

PIC-dependent turnover of H2A.Z is a more general phenomenon. I showed that nucleosomes containing H2A.Z are more labile than their H2A counterpart, which could be contributing to their preferred disassembly at the +1 position *in vivo*. However, because H2A.Z nucleosomes do not spontaneously disassemble *in vivo* when active processes are inhibited, H2A.Z eviction is expected to require an active ATP-dependent force. I hypothesize that TFIIH mediated DNA unwinding during transcription initiation provides that driving force and suggested experiments to test this hypothesis (**Figure 4-1**). Overall the incorporation of H2A.Z at +1 nucleosomes decreases the barrier chromatin imposes on the transcription process allowing the transcription machinery itself to catalyze removal of the +1 nucleosome, engage the TSS and transition to productive elongation.

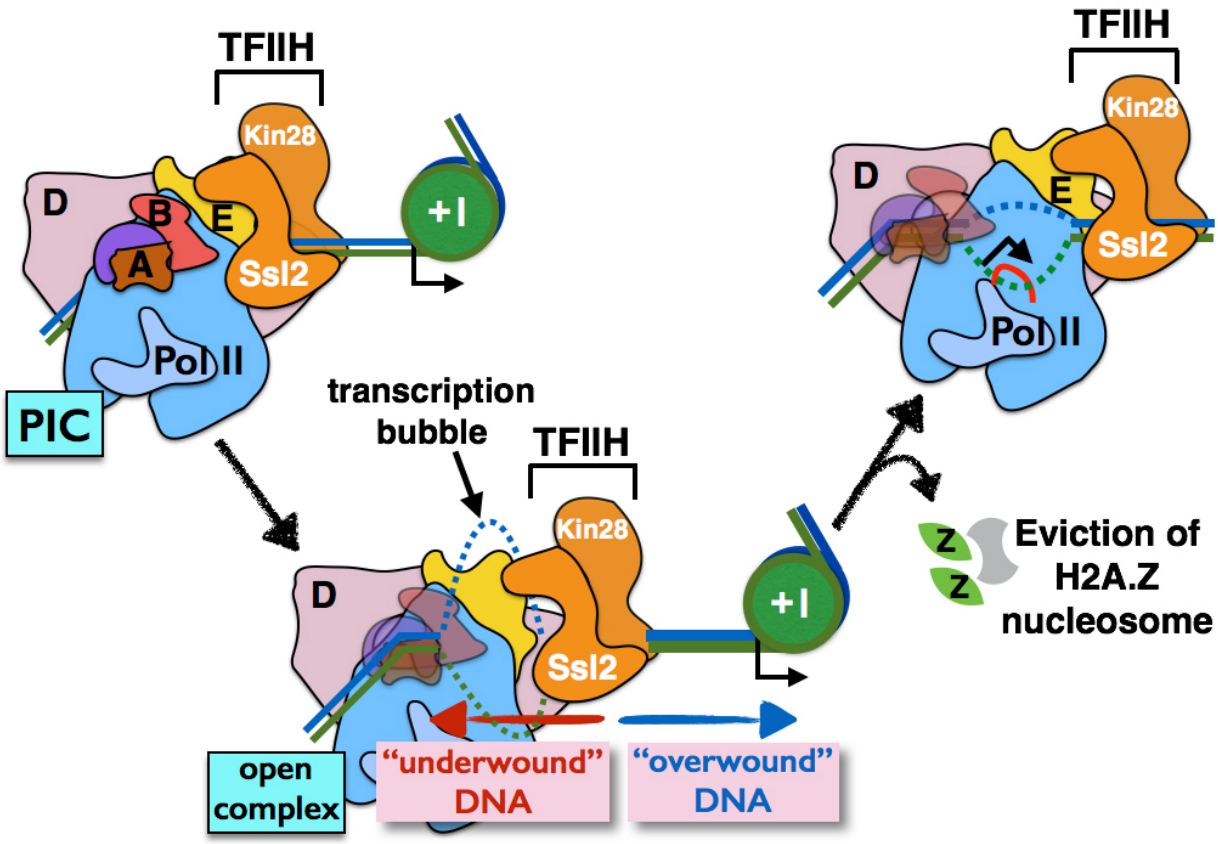

Figure 4-1. Proposed mechanism: TFIIH mediated DNA unwinding drives disassembly of +1 H2A.Z nucleosomes. The preinitiation complex (PIC) assembles upstream of the +1 nucleosome. During formation of the open complex, the activity of the Ssl2 translocase subunit of TFIIH drives the unwinding of the DNA duplex, which results in the formation of a single-stranded DNA structure called the 'transcription bubble'. Formation of the transcription bubbles causes the DNA upstream of TFIIH becomes to become "underwound" (indicated by *red arrow*) and the DNA downstream to become "overwound" (indicated by *blue arrow*). The overwound DNA will put a topological strain on +1 nucleosomes. The *blue* and *green lines* represent the template and coding strands of the promoter DNA, respectively. The *bent black arrows* indicate the transcription start site. *Green circles* represent the +1 H2A.Z nucleosome. *Green ovals* represent the H2A.Z-H2B dimers. When +1 nucleosomes contain H2A.Z, TFIIH mediated DNA unwinding will lead to eviction of the nucleosome from the promoter. D: TFIID; B: TFIIB; A: TFIIH; Pol II: RNA Polymerase II; E: TFIIE; PIC: preinitiation complex.

References

Abbott, D.W., Ivanova, V.S., Wang, X., Bonner, W.M., and Ausió, J. (2001). Characterization of the stability and folding of H2A.Z chromatin particles: implications for transcriptional activation. J. Biol. Chem. *276*, 41945–41949.

Adam, M., Robert, F., Larochelle, M., and Gaudreau, L. (2001). H2A.Z is required for global chromatin integrity and for recruitment of RNA polymerase II under specific conditions. Mol. Cell. Biol. *21*, 6270–6279.

Albert, I., Mavrich, T.N., Tomsho, L.P., Qi, J., Zanton, S.J., Schuster, S.C., and Pugh, B.F. (2007). Translational and rotational settings of H2A.Z nucleosomes across the Saccharomyces cerevisiae genome. Nature *446*, 572–576.

Allen, B.L., and Taatjes, D.J. (2015). The Mediator complex: a central integrator of transcription. Nat. Rev. Mol. Cell Biol. *16*, 155–166.

Almer, A., and Hörz, W. (1986). Nuclease hypersensitive regions with adjacent positioned nucleosomes mark the gene boundaries of the PHO5/PHO3 locus in yeast. EMBO J. *5*, 2681–2687.

Anderson, J.D., and Widom, J. (2001). Poly(dA-dT) promoter elements increase the equilibrium accessibility of nucleosomal DNA target sites. Mol. Cell. Biol. *21*, 3830–3839.

Ansari, S.A., Paul, E., Sommer, S., Lieleg, C., He, Q., Daly, A.Z., Rode, K.A., Barber, W.T., Ellis, L.C., Laporta, E., et al. (2014). Mediator, TATA-Binding Protein, and RNA Polymerase II contribute to low histone occupancy at active gene promoters in yeast. J. Biol. Chem.

Aparicio, O., Geisberg, J.V., Sekinger, E., Yang, A., Moqtaderi, Z., and Struhl, K. (2005). Chromatin immunoprecipitation for determining the association of proteins with specific genomic sequences in vivo. Curr. Protoc. Mol. Biol. Ed. Frederick M Ausubel Al *Chapter 21*, Unit 21.3.

Arents, G., Burlingame, R.W., Wang, B.C., Love, W.E., and Moudrianakis, E.N. (1991). The nucleosomal core histone octamer at 3.1 A resolution: a tripartite protein assembly and a left-handed superhelix. Proc. Natl. Acad. Sci. U. S. A. *88*, 10148–10152.

van Attikum, H., Fritsch, O., and Gasser, S.M. (2007). Distinct roles for SWR1 and INO80 chromatin remodeling complexes at chromosomal double-strand breaks. EMBO J. *26*, 4113–4125.

Badis, G., Chan, E.T., van Bakel, H., Pena-Castillo, L., Tillo, D., Tsui, K., Carlson, C.D., Gossett, A.J., Hasinoff, M.J., Warren, C.L., et al. (2008). A library of yeast transcription factor motifs reveals a widespread function for Rsc3 in targeting nucleosome exclusion at promoters. Mol. Cell *32*, 878–887.

Balcerski, J.S., and Pysh, E.S. (1976). Interaction of ethidium bromide with DNA: effect of LiCl and ethylene glycol. Nucleic Acids Res. *3*, 2401–2409.

Bannister, A.J., and Kouzarides, T. (2011). Regulation of chromatin by histone modifications. Cell Res. *21*, 381–395.

Barbaric, S., Luckenbach, T., Schmid, A., Blaschke, D., Hörz, W., and Korber, P. (2007). Redundancy of Chromatin Remodeling Pathways for the Induction of the Yeast PHO5 Promoter in Vivo. J. Biol. Chem. *282*, 27610–27621.

Basehoar, A.D., Zanton, S.J., and Pugh, B.F. (2004). Identification and distinct regulation of yeast TATA box-containing genes. Cell *116*, 699–709.

Belotserkovskaya, R., Oh, S., Bondarenko, V.A., Orphanides, G., Studitsky, V.M., and Reinberg, D. (2003). FACT facilitates transcription-dependent nucleosome alteration. Science *301*, 1090–1093.

Berretta, J., Pinskaya, M., and Morillon, A. (2008). A cryptic unstable transcript mediates transcriptional trans-silencing of the Ty1 retrotransposon in S. cerevisiae. Genes Dev. *22*, 615–626.

Bowman, G.D. (2010). Mechanisms of ATP-dependent nucleosome sliding. Curr. Opin. Struct. Biol. *20*, 73–81.

Brown, C.R., Mao, C., Falkovskaia, E., Law, J.K., and Boeger, H. (2011). In vivo role for the chromatin-remodeling enzyme SWI/SNF in the removal of promoter nucleosomes by disassembly rather than sliding. J. Biol. Chem. *286*, 40556–40565.

Bryant, G.O., Prabhu, V., Floer, M., Wang, X., Spagna, D., Schreiber, D., and Ptashne, M. (2008). Activator Control of Nucleosome Occupancy in Activation and Repression of Transcription. PLOS Biol *6*, e317.

Bumgarner, S.L., Neuert, G., Voight, B.F., Symbor-Nagrabska, A., Grisafi, P., van Oudenaarden, A., and Fink, G.R. (2012). Single-cell analysis reveals that noncoding RNAs contribute to clonal heterogeneity by modulating transcription factor recruitment. Mol. Cell *45*, 470–482.

Cairns, B.R. (2007). Chromatin remodeling: insights and intrigue from single-molecule studies. Nat. Struct. Mol. Biol. *14*, 989–996.

Cairns, B.R. (2009). The logic of chromatin architecture and remodelling at promoters. Nature *461*, 193–198.

Chambers, A.L., Ormerod, G., Durley, S.C., Sing, T.L., Brown, G.W., Kent, N.A., and Downs, J.A. (2012). The INO80 chromatin remodeling complex prevents polyploidy and maintains normal chromatin structure at centromeres. Genes Dev. *26*, 2590–2603.

Churchman, L.S., and Weissman, J.S. (2011). Nascent transcript sequencing visualizes transcription at nucleotide resolution. Nature *469*, 368–373.

Churchman, L.S., and Weissman, J.S. (2012). Native elongating transcript sequencing (NET-seq). Curr. Protoc. Mol. Biol. Ed. Frederick M Ausubel Al *Chapter 4*, Unit 4.14.1-17.

Clapier, C.R., and Cairns, B.R. (2009). The biology of chromatin remodeling complexes. Annu. Rev. Biochem. *78*, 273–304.

Clark, D.J., and Felsenfeld, G. (1992). A nucleosome core is transferred out of the path of a transcribing polymerase. Cell *71*, 11–22.

Cler, E., Papai, G., Schultz, P., and Davidson, I. (2009). Recent advances in understanding the structure and function of general transcription factor TFIID. Cell. Mol. Life Sci. CMLS *66*, 2123–2134.

Cormack, B.P., and Struhl, K. (1992). The TATA-binding protein is required for transcription by all three nuclear RNA polymerases in yeast cells. Cell *69*, 685–696.

Dhillon, N., Oki, M., Szyjka, S.J., Aparicio, O.M., and Kamakaka, R.T. (2006). H2A.Z functions to regulate progression through the cell cycle. Mol. Cell. Biol. *26*, 489–501.

Dion, M.F., Kaplan, T., Kim, M., Buratowski, S., Friedman, N., and Rando, O.J. (2007). Dynamics of replication-independent histone turnover in budding yeast. Science *315*, 1405–1408.

Drew, H.R., and Travers, A.A. (1985). DNA bending and its relation to nucleosome positioning. J. Mol. Biol. *186*, 773–790.

Dyer, P.N., Edayathumangalam, R.S., White, C.L., Bao, Y., Chakravarthy, S., Muthurajan, U.M., and Luger, K. (2004). Reconstitution of nucleosome core particles from recombinant histones and DNA. Methods Enzymol. *375*, 23–44.

Eaton, M.L., Galani, K., Kang, S., Bell, S.P., and MacAlpine, D.M. (2010). Conserved nucleosome positioning defines replication origins. Genes Dev. *24*, 748–753.

Egly, J.-M., and Coin, F. (2011). A history of TFIIH: two decades of molecular biology on a pivotal transcription/repair factor. DNA Repair *10*, 714–721.

Ehrensberger, A.H., and Kornberg, R.D. (2011). Isolation of an activator-dependent, promoter-specific chromatin remodeling factor. Proc. Natl. Acad. Sci. U. S. A. *108*, 10115–10120.

Eriksson, P.R., Ganguli, D., Nagarajavel, V., and Clark, D.J. (2012). Regulation of Histone Gene Expression in Budding Yeast. Genetics *191*, 7–20.

Fazal, F.M., Meng, C.A., Murakami, K., Kornberg, R.D., and Block, S.M. (2015). Real-time observation of the initiation of RNA polymerase II transcription. Nature *525*, 274–277.

Feaver, W.J., Svejstrup, J.Q., Henry, N.L., and Kornberg, R.D. (1994). Relationship of CDK-activating kinase and RNA polymerase II CTD kinase TFIIH/TFIIK. Cell *79*, 1103–1109.

Fishburn, J., Tomko, E., Galburt, E., and Hahn, S. (2015). Double-stranded DNA translocase activity of transcription factor TFIIH and the mechanism of RNA polymerase II open complex formation. Proc. Natl. Acad. Sci. *112*, 3961–3966.

Forterre, P., Mirambeau, G., Jaxel, C., Nadal, M., and Duguet, M. (1985). High positive supercoiling in vitro catalyzed by an ATP and polyethylene glycol-stimulated topoisomerase from Sulfolobus acidocaldarius. EMBO J. *4*, 2123–2128.

Ganguli, D., Chereji, R.V., Iben, J.R., Cole, H.A., and Clark, D.J. (2014). RSC-dependent constructive and destructive interference between opposing arrays of phased nucleosomes in yeast. Genome Res. *24*, 1637–1649.

Gibbons, B.J., Brignole, E.J., Azubel, M., Murakami, K., Voss, N.R., Bushnell, D.A., Asturias, F.J., and Kornberg, R.D. (2012). Subunit architecture of general transcription factor TFIIH. Proc. Natl. Acad. Sci. *109*, 1949–1954.

Gkikopoulos, T., Havas, K.M., Dewar, H., and Owen-Hughes, T. (2009). SWI/SNF and Asf1p Cooperate To Displace Histones during Induction of the Saccharomyces cerevisiae HO Promoter. Mol. Cell. Biol. *29*, 4057–4066.

Gkikopoulos, T., Schofield, P., Singh, V., Pinskaya, M., Mellor, J., Smolle, M., Workman, J.L., Barton, G.J., and Owen-Hughes, T. (2011). A role for Snf2-related nucleosome-spacing enzymes in genome-wide nucleosome organization. Science *333*, 1758–1760.

Grimaldi, Y., Ferrari, P., and Strubin, M. (2014). Independent RNA polymerase II preinitiation complex dynamics and nucleosome turnover at promoter sites in vivo. Genome Res. *24*, 117–124.

Grünberg, S., and Hahn, S. (2013). Structural insights into transcription initiation by RNA polymerase II. Trends Biochem. Sci. *38*, 603–611.

Grünberg, S., Warfield, L., and Hahn, S. (2012). Architecture of the RNA polymerase II preinitiation complex and mechanism of ATP-dependent promoter opening. Nat. Struct. Mol. Biol. *19*, 788–796.

Guillemette, B., Bataille, A.R., Gévry, N., Adam, M., Blanchette, M., Robert, F., and Gaudreau, L. (2005). Variant histone H2A.Z is globally localized to the promoters of inactive yeast genes and regulates nucleosome positioning. PLoS Biol. *3*, e384.

Gutiérrez, J.L., Chandy, M., Carrozza, M.J., and Workman, J.L. (2007). Activation domains drive nucleosome eviction by SWI/SNF. EMBO J. *26*, 730–740.

Hahn, S. (2004). Structure and mechanism of the RNA Polymerase II transcription machinery. Nat. Struct. Mol. Biol. *11*, 394–403.

Hahn, S., and Young, E.T. (2011). Transcriptional Regulation in Saccharomyces cerevisiae: Transcription Factor Regulation and Function, Mechanisms of Initiation, and Roles of Activators and Coactivators. Genetics *189*, 705–736.

Halley, J.E., Kaplan, T., Wang, A.Y., Kobor, M.S., and Rine, J. (2010). Roles for H2A.Z and its acetylation in GAL1 transcription and gene induction, but not GAL1-transcriptional memory. PLoS Biol. *8*, e1000401.

Han, M., and Grunstein, M. (1988). Nucleosome loss activates yeast downstream promoters in vivo. Cell *55*, 1137–1145.

Hartley, P.D., and Madhani, H.D. (2009). Mechanisms that specify promoter nucleosome location and identity. Cell *137*, 445–458.

Haruki, H., Nishikawa, J., and Laemmli, U.K. (2008). The anchor-away technique: rapid, conditional establishment of yeast mutant phenotypes. Mol. Cell *31*, 925–932.

Hayashi, M., and Harada, Y. (2007). Direct observation of the reversible unwinding of a single DNA molecule caused by the intercalation of ethidium bromide. Nucleic Acids Res. *35*, e125.

Heintzman, N.D., Stuart, R.K., Hon, G., Fu, Y., Ching, C.W., Hawkins, R.D., Barrera, L.O., Van Calcar, S., Qu, C., Ching, K.A., et al. (2007). Distinct and predictive chromatin signatures of transcriptional promoters and enhancers in the human genome. Nat. Genet. *39*, 311–318.

Hodges, C., Bintu, L., Lubkowska, L., Kashlev, M., and Bustamante, C. (2009). Nucleosomal fluctuations govern the transcription dynamics of RNA polymerase II. Science *325*, 626–628.

Hoffmann, A., Chiang, C.M., Oelgeschläger, T., Xie, X., Burley, S.K., Nakatani, Y., and Roeder, R.G. (1996). A histone octamer-like structure within TFIID. Nature *380*, 356–359.

Holstege, F.C., Fiedler, U., and Timmers, H.T. (1997). Three transitions in the RNA polymerase II transcription complex during initiation. EMBO J. *16*, 7468–7480.

Holstege, F.C., Jennings, E.G., Wyrick, J.J., Lee, T.I., Hengartner, C.J., Green, M.R., Golub, T.R., Lander, E.S., and Young, R.A. (1998). Dissecting the regulatory circuitry of a eukaryotic genome. Cell *95*, 717–728.

Hong, J., Feng, H., Wang, F., Ranjan, A., Chen, J., Jiang, J., Ghirlando, R., Xiao, T.S., Wu, C., and Bai, Y. (2014). The Catalytic Subunit of the SWR1 Remodeler Is a Histone Chaperone for the H2A.Z-H2B Dimer. Mol. Cell *53*, 498–505.

Horikoshi, N., Arimura, Y., Taguchi, H., and Kurumizaka, H. (2016). Crystal structures of heterotypic nucleosomes containing histones H2A.Z and H2A. Open Biol. *6*.

Hsin, J.-P., and Manley, J.L. (2012). The RNA polymerase II CTD coordinates transcription and RNA processing. Genes Dev. *26*, 2119–2137.

Hughes, A.L., and Rando, O.J. (2014). Mechanisms underlying nucleosome positioning in vivo. Annu. Rev. Biophys. *43*, 41–63.

Huh, W.-K., Falvo, J.V., Gerke, L.C., Carroll, A.S., Howson, R.W., Weissman, J.S., and O'Shea, E.K. (2003). Global analysis of protein localization in budding yeast. Nature *425*, 686–691.

Jeronimo, C., Watanabe, S., Kaplan, C.D., Peterson, C.L., and Robert, F. (2015). The Histone Chaperones FACT and Spt6 Restrict H2A.Z from Intragenic Locations. Mol. Cell *58*, 1113–1123.

Jiang, C., and Pugh, B.F. (2009a). Nucleosome positioning and gene regulation: advances through genomics. Nat. Rev. Genet. *10*, 161–172.

Jiang, C., and Pugh, B.F. (2009b). A compiled and systematic reference map of nucleosome positions across the Saccharomyces cerevisiae genome. Genome Biol. *10*, R109.

Jin, C., and Felsenfeld, G. (2007). Nucleosome stability mediated by histone variants H3.3 and H2A.Z. Genes Dev. *21*, 1519–1529.

Jin, C., Zang, C., Wei, G., Cui, K., Peng, W., Zhao, K., and Felsenfeld, G. (2009). H3.3/H2A.Z double variant-containing nucleosomes mark "nucleosome-free regions" of active promoters and other regulatory regions. Nat. Genet. *41*, 941–945.

Kanin, E.I., Kipp, R.T., Kung, C., Slattery, M., Viale, A., Hahn, S., Shokat, K.M., and Ansari, A.Z. (2007). Chemical inhibition of the TFIIH-associated kinase Cdk7/Kin28 does not impair global mRNA synthesis. Proc. Natl. Acad. Sci. *104*, 5812–5817.

Kaplan, C.D. (2003). Transcription Elongation Factors Repress Transcription Initiation from Cryptic Sites. Science *301*, 1096–1099.

Kaplan, N., Moore, I.K., Fondufe-Mittendorf, Y., Gossett, A.J., Tillo, D., Field, Y., LeProust, E.M., Hughes, T.R., Lieb, J.D., Widom, J., et al. (2009). The DNA-encoded nucleosome organization of a eukaryotic genome. Nature *458*, 362–366.

Kikuchi, A., and Asai, K. (1984). Reverse gyrase--a topoisomerase which introduces positive superhelical turns into DNA. Nature *309*, 677–681.

Kim, J.L., Nikolov, D.B., and Burley, S.K. (1993). Co-crystal structure of TBP recognizing the minor groove of a TATA element. Nature *365*, 520–527.

Kim, T.K., Ebright, R.H., and Reinberg, D. (2000). Mechanism of ATP-dependent promoter melting by transcription factor IIH. Science *288*, 1418–1422.

Knezetic, J.A., and Luse, D.S. (1986). The presence of nucleosomes on a DNA template prevents initiation by RNA polymerase II in vitro. Cell *45*, 95–104.

Kobor, M.S., Venkatasubrahmanyam, S., Meneghini, M.D., Gin, J.W., Jennings, J.L., Link, A.J., Madhani, H.D., and Rine, J. (2004). A protein complex containing the conserved Swi2/Snf2-related ATPase Swr1p deposits histone variant H2A.Z into euchromatin. PLoS Biol. *2*, E131.

Kouzarides, T. (2007). Chromatin modifications and their function. Cell *128*, 693–705.

Krogan, N.J., Keogh, M.-C., Datta, N., Sawa, C., Ryan, O.W., Ding, H., Haw, R.A., Pootoolal, J., Tong, A., Canadien, V., et al. (2003). A Snf2 family ATPase complex required for recruitment of the histone H2A variant Htz1. Mol. Cell *12*, 1565–1576.

Krogan, N.J., Baetz, K., Keogh, M.-C., Datta, N., Sawa, C., Kwok, T.C.Y., Thompson, N.J., Davey, M.G., Pootoolal, J., Hughes, T.R., et al. (2004). Regulation of chromosome stability by the histone H2A variant Htz1, the Swr1 chromatin remodeling complex, and the histone acetyltransferase NuA4. Proc. Natl. Acad. Sci. U. S. A. *101*, 13513–13518.

Kubik, S., Bruzzone, M.J., Jacquet, P., Falcone, J.-L., Rougemont, J., and Shore, D. (2015). Nucleosome Stability Distinguishes Two Different Promoter Types at All Protein-Coding Genes in Yeast. Mol. Cell *60*, 422–434.

Langmead, B., Trapnell, C., Pop, M., and Salzberg, S.L. (2009). Ultrafast and memory-efficient alignment of short DNA sequences to the human genome. Genome Biol. *10*, R25.

Layer, J.H., Miller, S.G., and Weil, P.A. (2010). Direct transactivator-transcription factor IID (TFIID) contacts drive yeast ribosomal protein gene transcription. J. Biol. Chem. *285*, 15489–15499.

Lee, W., Tillo, D., Bray, N., Morse, R.H., Davis, R.W., Hughes, T.R., and Nislow, C. (2007). A high-resolution atlas of nucleosome occupancy in yeast. Nat. Genet. *39*, 1235–1244.

Lempiäinen, H., and Shore, D. (2009). Growth control and ribosome biogenesis. Curr. Opin. Cell Biol. *21*, 855–863.

Li, B., Pattenden, S.G., Lee, D., Gutiérrez, J., Chen, J., Seidel, C., Gerton, J., and Workman, J.L. (2005). Preferential occupancy of histone variant H2AZ at inactive promoters influences local histone modifications and chromatin remodeling. Proc. Natl. Acad. Sci. U. S. A. *102*, 18385–18390.

Li, B., Carey, M., and Workman, J.L. (2007). The role of chromatin during transcription. Cell *128*, 707–719.

Lieleg, C., Krietenstein, N., Walker, M., and Korber, P. (2014). Nucleosome positioning in yeasts: methods, maps, and mechanisms. Chromosoma *124*, 131–151.

Lieleg, C., Krietenstein, N., Walker, M., and Korber, P. (2015). Nucleosome positioning in yeasts: methods, maps, and mechanisms. Chromosoma *124*, 131–151.

Lin, Y., Qi, Y., Lu, J., Pan, X., Yuan, D.S., Zhao, Y., Bader, J.S., and Boeke, J.D. (2008). A comprehensive synthetic genetic interaction network governing yeast histone acetylation and deacetylation. Genes Dev. *22*, 2062–2074.

Lipson, D., Raz, T., Kieu, A., Jones, D.R., Giladi, E., Thayer, E., Thompson, J.F., Letovsky, S., Milos, P., and Causey, M. (2009). Quantification of the yeast transcriptome by single-molecule sequencing. Nat. Biotechnol. *27*, 652–658.

Liu, C.L., Kaplan, T., Kim, M., Buratowski, S., Schreiber, S.L., Friedman, N., and Rando, O.J. (2005). Single-nucleosome mapping of histone modifications in S. cerevisiae. PLoS Biol. *3*, e328.

Liu, Y., Kung, C., Fishburn, J., Ansari, A.Z., Shokat, K.M., and Hahn, S. (2004). Two Cyclin-Dependent Kinases Promote RNA Polymerase II Transcription and Formation of the Scaffold Complex. Mol. Cell. Biol. *24*, 1721–1735.

Lohr, D., and Lopez, J. (1995). GAL4/GAL80-dependent Nucleosome Disruption/Deposition on the Upstream Regions of the Yeast GAL1-10 and GAL80 Genes. J. Biol. Chem. *270*, 27671–27678.

Longtine, M.S., McKenzie, A., Demarini, D.J., Shah, N.G., Wach, A., Brachat, A., Philippsen, P., and Pringle, J.R. (1998). Additional modules for versatile and economical PCR-based gene deletion and modification in Saccharomyces cerevisiae. Yeast Chichester Engl. *14*, 953–961.

Lopez, M.S., Kliegman, J.I., and Shokat, K.M. (2014). The logic and design of analog-sensitive kinases and their small molecule inhibitors. Methods Enzymol. *548*, 189–213.

Lorch, Y., LaPointe, J.W., and Kornberg, R.D. (1987). Nucleosomes inhibit the initiation of transcription but allow chain elongation with the displacement of histones. Cell *49*, 203–210.

Lorch, Y., Maier-Davis, B., and Kornberg, R.D. (2006). Chromatin remodeling by nucleosome disassembly in vitro. Proc. Natl. Acad. Sci. U. S. A. *103*, 3090–3093.

Lowary, P.T., and Widom, J. (1998). New DNA sequence rules for high affinity binding to histone octamer and sequence-directed nucleosome positioning. J. Mol. Biol. *276*, 19–42.

Luger, K. (2001). Nucleosomes: Structure and Function. In eLS, (John Wiley & Sons, Ltd), p.

Luger, K., Mäder, A.W., Richmond, R.K., Sargent, D.F., and Richmond, T.J. (1997). Crystal structure of the nucleosome core particle at 2.8 A resolution. Nature *389*, 251–260.

Luk, E., Vu, N.-D., Patteson, K., Mizuguchi, G., Wu, W.-H., Ranjan, A., Backus, J., Sen, S., Lewis, M., Bai, Y., et al. (2007). Chz1, a nuclear chaperone for histone H2AZ. Mol. Cell *25*, 357–368.

Luk, E., Ranjan, A., Fitzgerald, P.C., Mizuguchi, G., Huang, Y., Wei, D., and Wu, C. (2010). Stepwise histone replacement by SWR1 requires dual activation with histone H2A.Z and canonical nucleosome. Cell *143*, 725–736.

Marzluff, W.F., Gongidi, P., Woods, K.R., Jin, J., and Maltais, L.J. (2002). The human and mouse replication-dependent histone genes. Genomics *80*, 487–498.

Mavrich, T.N., Ioshikhes, I.P., Venters, B.J., Jiang, C., Tomsho, L.P., Qi, J., Schuster, S.C., Albert, I., and Pugh, B.F. (2008). A barrier nucleosome model for statistical positioning of nucleosomes throughout the yeast genome. Genome Res. *18*, 1073–1083.

McMurray, C.T., and van Holde, K.E. (1986). Binding of ethidium bromide causes dissociation of the nucleosome core particle. Proc. Natl. Acad. Sci. U. S. A. *83*, 8472–8476.

Meneghini, M.D., Wu, M., and Madhani, H.D. (2003). Conserved histone variant H2A.Z protects euchromatin from the ectopic spread of silent heterochromatin. Cell *112*, 725–736.

Miller, S.M., and Magasanik, B. (1991). Role of the complex upstream region of the GDH2 gene in nitrogen regulation of the NAD-linked glutamate dehydrogenase in Saccharomyces cerevisiae. Mol. Cell. Biol. *11*, 6229–6247.

Mizuguchi, G., Shen, X., Landry, J., Wu, W.-H., Sen, S., and Wu, C. (2004). ATP-driven exchange of histone H2AZ variant catalyzed by SWR1 chromatin remodeling complex. Science *303*, 343–348.

Murakami, K., Elmlund, H., Kalisman, N., Bushnell, D.A., Adams, C.M., Azubel, M., Elmlund, D., Levi-Kalisman, Y., Liu, X., Gibbons, B.J., et al. (2013). Architecture of an RNA polymerase II transcription pre-initiation complex. Science *342*, 1238724.

Narlikar, G.J., Sundaramoorthy, R., and Owen-Hughes, T. (2013). Mechanisms and Functions of ATP-Dependent Chromatin-Remodeling Enzymes. Cell *154*, 490–503.

Nathan, D., Ingvarsdottir, K., Sterner, D.E., Bylebyl, G.R., Dokmanovic, M., Dorsey, J.A., Whelan, K.A., Krsmanovic, M., Lane, W.S., Meluh, P.B., et al. (2006). Histone sumoylation is a negative regulator in Saccharomyces cerevisiae and shows dynamic interplay with positive-acting histone modifications. Genes Dev. *20*, 966–976.

Neumann, H., Hancock, S.M., Buning, R., Routh, A., Chapman, L., Somers, J., Owen-Hughes, T., van Noort, J., Rhodes, D., and Chin, J.W. (2009). A Method for Genetically Installing Site-Specific Acetylation in Recombinant Histones Defines the Effects of H3 K56 Acetylation. Mol. Cell *36*, 153–163.

Newman, J.R.S., Ghaemmaghami, S., Ihmels, J., Breslow, D.K., Noble, M., DeRisi, J.L., and Weissman, J.S. (2006). Single-cell proteomic analysis of S. cerevisiae reveals the architecture of biological noise. Nature *441*, 840–846.

Nishimura, K., and Kanemaki, M.T. (2014). Rapid Depletion of Budding Yeast Proteins via the Fusion of an Auxin-Inducible Degron (AID). Curr. Protoc. Cell Biol. *64*, 20.9.1-16.

Ocampo, J., Chereji, R.V., Eriksson, P.R., and Clark, D.J. (2016). The ISW1 and CHD1 ATP-dependent chromatin remodelers compete to set nucleosome spacing in vivo. Nucleic Acids Res. *44*, 4625–4635.

Papai, G., Tripathi, M.K., Ruhlmann, C., Layer, J.H., Weil, P.A., and Schultz, P. (2010). TFIIA and the transactivator Rap1 cooperate to commit TFIID for transcription initiation. Nature *465*, 956–960.

Papai, G., Weil, P.A., and Schultz, P. (2011). New insights into the function of transcription factor TFIID from recent structural studies. Curr. Opin. Genet. Dev. *21*, 219–224.

Papamichos-Chronakis, M., Krebs, J.E., and Peterson, C.L. (2006). Interplay between Ino80 and Swr1 chromatin remodeling enzymes regulates cell cycle checkpoint adaptation in response to DNA damage. Genes Dev. *20*, 2437–2449.

Papamichos-Chronakis, M., Watanabe, S., Rando, O.J., and Peterson, C.L. (2011). Global regulation of H2A.Z localization by the INO80 chromatin-remodeling enzyme is essential for genome integrity. Cell *144*, 200–213.

Park, Y.-J., Dyer, P.N., Tremethick, D.J., and Luger, K. (2004). A new fluorescence resonance energy transfer approach demonstrates that the histone variant H2AZ stabilizes the histone octamer within the nucleosome. J. Biol. Chem. *279*, 24274–24282.

Parnell, T.J., Huff, J.T., and Cairns, B.R. (2008). RSC regulates nucleosome positioning at Pol II genes and density at Pol III genes. EMBO J. *27*, 100–110.

Perugino, G., Valenti, A., D'amaro, A., Rossi, M., and Ciaramella, M. (2009). Reverse gyrase and genome stability in hyperthermophilic organisms. Biochem. Soc. Trans. *37*, 69–73.

Pradhan, S.K., Xue, Y., and Carey, M.F. (2015). Fragile Nucleosomes Influence Pol II Promoter Function. Mol. Cell *60*, 342–343.

Quackenbush, J. (2002). Microarray data normalization and transformation. Nat. Genet. *32 Suppl*, 496–501.

Quinlan, A.R. (2014). BEDTools: The Swiss-Army Tool for Genome Feature Analysis. Curr. Protoc. Bioinforma. Ed. Board Andreas Baxevanis Al *47*, 11.12.1-34.

Raisner, R.M., Hartley, P.D., Meneghini, M.D., Bao, M.Z., Liu, C.L., Schreiber, S.L., Rando, O.J., and Madhani, H.D. (2005). Histone variant H2A.Z marks the 5' ends of both active and inactive genes in euchromatin. Cell *123*, 233–248.

Ramachandran, S., Zentner, G.E., and Henikoff, S. (2015). Asymmetric nucleosomes flank promoters in the budding yeast genome. Genome Res. *25*, 381–390.

Rando, O.J., and Chang, H.Y. (2009). Genome-wide views of chromatin structure. Annu. Rev. Biochem. *78*, 245–271.

Rando, O.J., and Winston, F. (2012). Chromatin and transcription in yeast. Genetics *190*, 351–387.

Ranjan, A., Mizuguchi, G., FitzGerald, P.C., Wei, D., Wang, F., Huang, Y., Luk, E., Woodcock, C.L., and Wu, C. (2013). Nucleosome-free region dominates histone acetylation in targeting SWR1 to promoters for H2A.Z replacement. Cell *154*, 1232–1245.

Ranjan, A., Wang, F., Mizuguchi, G., Wei, D., Huang, Y., and Wu, C. (2015). H2A histone-fold and DNA elements in nucleosome activate SWR1-mediated H2A.Z replacement in budding yeast. eLife *4*, e06845.

Reinke, H., and Hörz, W. (2003). Histones are first hyperacetylated and then lose contact with the activated PHO5 promoter. Mol. Cell *11*, 1599–1607.

Reja, R., Vinayachandran, V., Ghosh, S., and Pugh, B.F. (2015). Molecular mechanisms of ribosomal protein gene coregulation. Genes Dev. *29*, 1942–1954.

Rhee, H.S., and Pugh, B.F. (2012). Genome-wide structure and organization of eukaryotic pre-initiation complexes. Nature *483*, 295–301.

Rhee, H.S., Bataille, A.R., Zhang, L., and Pugh, B.F. (2014). Subnucleosomal Structures and Nucleosome Asymmetry across a Genome. Cell *159*, 1377–1388.

Rosonina, E., Yurko, N., Li, W., Hoque, M., Tian, B., and Manley, J.L. (2014). Threonine-4 of the budding yeast RNAP II CTD couples transcription with Htz1-mediated chromatin remodeling. Proc. Natl. Acad. Sci. U. S. A. *111*, 11924–11931.

Rudnizky, S., Bavly, A., Malik, O., Pnueli, L., Melamed, P., and Kaplan, A. (2016). H2A.Z controls the stability and mobility of nucleosomes to regulate expression of the LH genes. Nat. Commun. *7*, 12958.

Rufiange, A., Jacques, P.-E., Bhat, W., Robert, F., and Nourani, A. (2007). Genome-wide replication-independent histone H3 exchange occurs predominantly at promoters and implicates H3 K56 acetylation and Asf1. Mol. Cell *27*, 393–405.

Saha, A., Wittmeyer, J., and Cairns, B.R. (2006). Mechanisms for nucleosome movement by ATP-dependent chromatin remodeling complexes. Results Probl. Cell Differ. *41*, 127–148.

Sainsbury, S., Bernecky, C., and Cramer, P. (2015). Structural basis of transcription initiation by RNA polymerase II. Nat. Rev. Mol. Cell Biol. *16*, 129–143.

Sanders, S.L., Garbett, K.A., and Weil, P.A. (2002). Molecular characterization of Saccharomyces cerevisiae TFIID. Mol. Cell. Biol. *22*, 6000–6013.

Santisteban, M.S., Kalashnikova, T., and Smith, M.M. (2000). Histone H2A.Z Regulates Transcription and Is Partially Redundant with Nucleosome Remodeling Complexes. Cell *103*, 411–422.

Santisteban, M.S., Hang, M., and Smith, M.M. (2011). Histone variant H2A.Z and RNA polymerase II transcription elongation. Mol. Cell. Biol. *31*, 1848–1860.

Saravanan, M., Wuerges, J., Bose, D., McCormack, E.A., Cook, N.J., Zhang, X., and Wigley, D.B. (2012). Interactions between the nucleosome histone core and Arp8 in the INO80 chromatin remodeling complex. Proc. Natl. Acad. Sci. U. S. A. *109*, 20883–20888.

Schones, D.E., Cui, K., Cuddapah, S., Roh, T.-Y., Barski, A., Wang, Z., Wei, G., and Zhao, K. (2008). Dynamic regulation of nucleosome positioning in the human genome. Cell *132*, 887–898.

Schramm, L., and Hernandez, N. (2002). Recruitment of RNA polymerase III to its target promoters. Genes Dev. *16*, 2593–2620.

Schultz, M.C., Reeder, R.H., and Hahn, S. (1992). Variants of the TATA-binding protein can distinguish subsets of RNA polymerase I, II, and III promoters. Cell *69*, 697–702.

Segal, E., and Widom, J. (2009). Poly(dA:dT) Tracts: Major Determinants of Nucleosome Organization. Curr. Opin. Struct. Biol. *19*, 65–71.

Selleck, W., Howley, R., Fang, Q., Podolny, V., Fried, M.G., Buratowski, S., and Tan, S. (2001). A histone fold TAF octamer within the yeast TFIID transcriptional coactivator. Nat. Struct. Biol. *8*, 695–700.

Shen, X., Ranallo, R., Choi, E., and Wu, C. (2003). Involvement of actin-related proteins in ATP-dependent chromatin remodeling. Mol. Cell *12*, 147–155.

Straka, C., and Hörz, W. (1991). A functional role for nucleosomes in the repression of a yeast promoter. EMBO J. *10*, 361–368.

Talbert, P.B., and Henikoff, S. (2010). Histone variants--ancient wrap artists of the epigenome. Nat. Rev. Mol. Cell Biol. *11*, 264–275.

Thambirajah, A.A., Dryhurst, D., Ishibashi, T., Li, A., Maffey, A.H., and Ausió, J. (2006). H2A.Z stabilizes chromatin in a way that is dependent on core histone acetylation. J. Biol. Chem. *281*, 20036–20044.

Unnikrishnan, A., Gafken, P.R., and Tsukiyama, T. (2010). Dynamic changes in histone acetylation regulate origins of DNA replication. Nat. Struct. Mol. Biol. *17*, 430–437.

Venkatesh, S., and Workman, J.L. (2015). Histone exchange, chromatin structure and the regulation of transcription. Nat. Rev. Mol. Cell Biol. *16*, 178–189.

Venters, B.J., and Pugh, B.F. (2009). A canonical promoter organization of the transcription machinery and its regulators in the Saccharomyces genome. Genome Res. *19*, 360–371.

Venters, B.J., Wachi, S., Mavrich, T.N., Andersen, B.E., Jena, P., Sinnamon, A.J., Jain, P., Rolleri, N.S., Jiang, C., Hemeryck-Walsh, C., et al. (2011). A comprehensive genomic binding map of gene and chromatin regulatory proteins in Saccharomyces. Mol. Cell *41*, 480–492.

Wan, Y., Saleem, R.A., Ratushny, A.V., Roda, O., Smith, J.J., Lin, C.-H., Chiang, J.-H., and Aitchison, J.D. (2009). Role of the Histone Variant H2A.Z/Htz1p in TBP Recruitment, Chromatin Dynamics, and Regulated Expression of Oleate-Responsive Genes. Mol. Cell. Biol. *29*, 2346–2358.

Wang, F., Ranjan, A., Wei, D., and Wu, C. (2016). Comment on "A histone acetylation switch regulates H2A.Z deposition by the SWR-C remodeling enzyme." Science *353*, 358.

Wang, W., Carey, M., and Gralla, J.D. (1992). Polymerase II promoter activation: closed complex formation and ATP-driven start site opening. Science *255*, 450–453.

Warner, J.R. (1999). The economics of ribosome biosynthesis in yeast. Trends Biochem. Sci. *24*, 437–440.

Weber, C.M., and Henikoff, S. (2014). Histone variants: dynamic punctuation in transcription. Genes Dev. *28*, 672–682.

Weber, C.M., Ramachandran, S., and Henikoff, S. (2014). Nucleosomes Are Context-Specific, H2A.Z-Modulated Barriers to RNA Polymerase. Mol. Cell *53*, 819–830.

Weiner, A., Hughes, A., Yassour, M., Rando, O.J., and Friedman, N. (2010). High-resolution nucleosome mapping reveals transcription-dependent promoter packaging. Genome Res. *20*, 90–100.

Weitao, T., Nordström, K., and Dasgupta, S. (2000). Escherichia coli cell cycle control genes affect chromosome superhelicity. EMBO Rep. *1*, 494–499.

van Werven, F.J., Neuert, G., Hendrick, N., Lardenois, A., Buratowski, S., van Oudenaarden, A., Primig, M., and Amon, A. (2012). Transcription of two long noncoding RNAs mediates mating-type control of gametogenesis in budding yeast. Cell *150*, 1170–1181.

West, M.H., and Bonner, W.M. (1980). Histone 2B can be modified by the attachment of ubiquitin. Nucleic Acids Res. *8*, 4671–4680.

Whitehouse, I., Rando, O.J., Delrow, J., and Tsukiyama, T. (2007). Chromatin remodelling at promoters suppresses antisense transcription. Nature *450*, 1031–1035.

Williamson, P., and Felsenfeld, G. (1978). Transcription of histone-covered T7 DNA by Escherichia coli RNA polymerase. Biochemistry (Mosc.) *17*, 5695–5705.

Wong, K.H., Jin, Y., and Struhl, K. (2014). TFIIH Phosphorylation of the Pol II CTD Stimulates Mediator Dissociation from the Preinitiation Complex and Promoter Escape. Mol. Cell *54*, 601–612.

Wu, C. (1980). The 5′ ends of Drosophila heat shock genes in chromatin are hypersensitive to DNase I. Nature *286*, 854–860.

Wu, W.-H., Alami, S., Luk, E., Wu, C.-H., Sen, S., Mizuguchi, G., Wei, D., and Wu, C. (2005). Swc2 is a widely conserved H2AZ-binding module essential for ATP-dependent histone exchange. Nat. Struct. Mol. Biol. *12*, 1064–1071.

Xi, Y., Yao, J., Chen, R., Li, W., and He, X. (2011). Nucleosome fragility reveals novel functional states of chromatin and poises genes for activation. Genome Res. *21*, 718–724.

Xu, Z., Wei, W., Gagneur, J., Perocchi, F., Clauder-Münster, S., Camblong, J., Guffanti, E., Stutz, F., Huber, W., and Steinmetz, L.M. (2009). Bidirectional promoters generate pervasive transcription in yeast. Nature *457*, 1033–1037.

Yao, W., King, D.A., Beckwith, S.L., Gowans, G.J., Yen, K., Zhou, C., and Morrison, A.J. (2016). The INO80 Complex Requires the Arp5-Ies6 Subcomplex for Chromatin Remodeling and Metabolic Regulation. Mol. Cell. Biol. *36*, 979–991.

Yen, K., Vinayachandran, V., Batta, K., Koerber, R.T., and Pugh, B.F. (2012). Genome-wide nucleosome specificity and directionality of chromatin remodelers. Cell *149*, 1461–1473.

Yen, K., Vinayachandran, V., and Pugh, B.F. (2013). SWR-C and INO80 chromatin remodelers recognize nucleosome-free regions near +1 nucleosomes. Cell *154*, 1246–1256.

Yoshida, T., Shimada, K., Oma, Y., Kalck, V., Akimura, K., Taddei, A., Iwahashi, H., Kugou, K., Ohta, K., Gasser, S.M., et al. (2010). Actin-related protein Arp6 influences H2A.Z-dependent and -independent gene expression and links ribosomal protein genes to nuclear pores. PLoS Genet. *6*, e1000910.

Yuan, G.-C., Liu, Y.-J., Dion, M.F., Slack, M.D., Wu, L.F., Altschuler, S.J., and Rando, O.J. (2005). Genome-scale identification of nucleosome positions in S. cerevisiae. Science *309*, 626–630.

Yudkovsky, N., Ranish, J.A., and Hahn, S. (2000). A transcription reinitiation intermediate that is stabilized by activator. Nature *408*, 225–229.

Zanton, S.J., and Pugh, B.F. (2006). Full and partial genome-wide assembly and disassembly of the yeast transcription machinery in response to heat shock. Genes Dev. *20*, 2250–2265.

Zhang, Z., and Pugh, B.F. (2011). High-resolution genome-wide mapping of the primary structure of chromatin. Cell *144*, 175–186.

Zhang, H., Roberts, D.N., and Cairns, B.R. (2005). Genome-wide dynamics of Htz1, a histone H2A variant that poises repressed/basal promoters for activation through histone loss. Cell *123*, 219–231.

Zhang, Z., Wippo, C.J., Wal, M., Ward, E., Korber, P., and Pugh, B.F. (2011). A packing mechanism for nucleosome organization reconstituted across a eukaryotic genome. Science *332*, 977–980.

Zlatanova, J., and Thakar, A. (2008). H2A.Z: view from the top. Struct. Lond. Engl. 1993 *16*, 166–179.